# EVALUATION OF PASSIVE CAPILLARY WICK SAMPLERS FOR MEASURING DEEP INFILTRATION IN THE JEMEZ RIVER BASIN CRITICAL ZONE OBSERVATORY

by

Ben Krisanto Yap Paras



A Thesis Submitted to the Faculty of the

DEPARTMENT OF HYDROLOGY AND ATMOSPHERIC SCIENCES

In Partial Fulfillment of the Requirements
For the Degree of

MASTER OF SCIENCE

In the Graduate College

THE UNIVERSITY OF ARIZONA

2 0 1 7

## STATEMENT BY AUTHOR

This thesis titled *Evaluation of Passive Capillary Wick Samplers for Measuring Deep Infiltration in the Jemez River Basin Critical Zone Observatory* prepared by *Ben Krisanto Yap Paras* has been submitted in partial fulfillment of requirements for a master's degree at the University of Arizona and is deposited in the University Library to be made available to borrowers under rules of the Library.

Brief quotations from this thesis are allowable without special permission, provided that accurate acknowledgment of source is made. Requests for permission for extended quotation from or reproduction of this manuscript in whole or in part may be granted by the head of the major department or the Dean of the Graduate College when in his or her judgment the proposed use of the material is in the interests of scholarship. In all other instances, however, permission must be obtained from the author.

SIGNED: _____

Ben Krisanto Yap Paras

APPROVAL BY THESIS DIRECTOR

This thesis has been approved on the date shown below:

_____ *August 21, 2017*

*Paul Ferré* Date

*Professor, Hydrology and Atmospheric Sciences*

**ACKNOWLEDGEMENTS**

Logistical support and/or data were provided by the NSF-supported Jemez River Basin and Santa Catalina Mountains Critical Zone Observatory EAR-0724958 and EAR-1331408. This thesis was made possible through the funding of these research groups.

I would like to thank all the students, alumni, staff, and faculty of the Hydrology and Water Resources Department as I've always felt welcome and accommodated throughout my time here. I am very thankful for the camaraderie and friendships I have experienced. Thank you Jon Chorover and Jennifer McIntosh for not only being part of my thesis committee, but also giving me the opportunity to work with you guys and the CZO. I truly am grateful for all the educational experiences I've had because of the CZO (even the physically demanding ones). I also appreciate all my friends and colleagues at Montgomery & Associates for giving me the work flexibility needed to finish this thesis and for adopting me as one of their own.

Special mention goes Hoshin Gupta and Olivia Hanson for being the first two people who helped me get my bearings when applying to be a student of the department in 2013. They connected me with Ty Ferré who became my mentor and, more importantly, great friend. I cannot express enough gratitude for Ty for accepting me as his student and for helping me find my direction in life. I hope to keep up the musical jams sessions we've enjoyed together.

I owe the deepest gratitude to my family. Thank you Elana, my sister, for being the hilarious ball of energy you are for keeping my laughs up in tough times. Ashley, your love and support has kept me sane and happy throughout this roller coaster experience. My life is and will continue to be far richer with you in it. Mamu and Papu, words cannot express how thankful I am for all sacrifices you have made for us. I would not be the person I am today without your unwavering love and support.

**TABLE OF CONTENTS**

**LIST OF FIGURES**

**LIST OF FIGURES CONTINUED**

**LIST OF FIGURES CONTINUED**

**ABSTRACT**

Passive capillary wick samplers (PCAPs) are primarily used to sample water from the vadose zone. PCAPs use fiberglass wicks to form a hanging water column that exerts suction on the surrounding soil. Although PCAPs have been used to estimate soil water flux, the accuracy with which PCAPs can estimate flux comes into question due to over/undersampling caused by this applied flux. I used numerical models to explore the effects of a PCAP on flow through the vadose zone. Specifically, I used a two-dimensional axisymmetric flow model of a PCAP embedded in a medium based on HYDRUS (Simunek et al., 2009). Both steady-state and transient conditions were simulated through the application of various precipitation rates and periods across several soil textures. In this study, I examine soil hydraulic properties, across the soil texture triangle, subject to a range of precipitation events. Results show that the PCAP does over/underestimate water flux. The degree of error is quantified by defining a capture efficiency, which is the ratio of the flux into the plate and the flux that would occur at the same depth with no PCAP present. Higher fluxes and longer time periods resulted in increased convergence of flux into the PCAP, while lower fluxes and shorter durations resulted in divergence of flux from the PCAP. The goal of the study is to understand the behavior of PCAPs under different conditions and to use that knowledge to interpret field measurements in the Jemez River Basin Critical Zone Observatory.

# 1 INTRODUCTION

Measurement of water flux in the vadose zone is critical for characterizing processes ranging from water management to contaminant transport. Unsaturated water flow measurements are difficult to collect because flow rates through the vadose zone span many orders of magnitude. Currently, there are various available methods for measuring flux in the vadose zone: soil core sampling, porous suction cups, pan lysimeters, constant-tension lysimeters, equilibrium tension plate lysimeters, and passive capillary wick samplers (PCAPs). Any instrumentation installed in the ground becomes a disruptor of flow, which could cause convergence or divergence (Gee, 2004).

Method selection depends on project setting, goals, and logistics. Soil core sampling is an efficient method because measurements can be replicated easily at different depths. However, soil core sampling is a destructive method, so repeated measurements are not possible at the same location. Porous suction cup samplers are used by the Environmental Protection Agency to characterize leachate because of lower costs and easier installation, but they are unable to estimate flux due to having unknown soil sample volumes (England, 1974). Pan lysimeters are coarse material-filled pans that collect flux under a zero-tension boundary condition, but they will underestimate flux because of negative tension in the soil under unsaturated conditions (Zhu, 2002). Constant-tension lysimeters are similar to pan lysimeters, but have an applied constant suction. Inaccuracies are still present with the constant-tension lysimeters depending on the soil and flux conditions. Equilibrium tension plate lysimeters are an improvement to both pan and constant-tension lysimeters because they match the tension of the soil to the vacuum applied to the sampler. However, high implementation cost and maintenance makes equilibrium tension plate lysimeters logistically difficult to use (Masarik et al, 2004).

PCAPs offer better estimates of actual water fluxes compared to alternative field methods (Gee et al., 2002; Louie et al., 2000) because they capture flow in both saturated and unsaturated conditions (Boll et al, 1992). PCAPs form a hanging water column that applies suction through the use of braided fiberglass wicks. PCAPs are recommended because they have been shown in field and laboratory settings to perform better than other samplers for measuring water drainage, leachate, and flux (Brahy et al., 2002; Brandi-Dohrn et al., 1996; Holder et al., 1991; Knutson and Selker, 1996; Poletika et al., 1992; Zhu et al., 2002). The Critical Zone Observatory (CZO) in the Jemez River Basin primarily uses PCAPs at their field sites to measure water flux.

The CZO in the Jemez River Basin is one of six environmental interdisciplinary observatories funded by the National Science Foundation to study critical zone interactions. The critical zone encompasses biological, geological, chemical, and hydrological processes from the top of the tree canopy to the bedrock. The CZO in the Jemez River Basin is using PCAPs to measure water flux. However, previous numerical (Gee et al., 2004; Louie et al., 2000; Mertens et al., 2007; Rimmer et al., 1995) and field analysis (Gee et al., 2004, Jabro et al., 2008) demonstrate that PCAPs are still susceptible to overestimation and underestimation of flux depending on the precipitation event and the soil conditions. The objective of this thesis is to quantify which conditions give rise to PCAP inaccuracy and to discuss other potential factors affecting PCAP capture not covered by the studies mentioned. This will be used to improve interpretation of PCAP measurements across the CZO.

The research question is addressed through the following steps:

1. Develop a numerical groundwater flow model for PCAP capture in a homogeneous porous medium using HYDRUS (2D/3D) software;

2. Explore PCAP capture behavior during steady-state infiltration by varying soil type and flux;
3. Analyze transient and steady-state capture during and after a precipitation event;
4. Quantify capture efficiencies for steady-state and transient conditions;
5. Compare HYDRUS-predicted and field-measured capture efficiency for conditions observed at the CZO in the Jemez River Basin
6. Revisit interpretations of subsurface flux from PCAP measurements at the CZO in the Jemez River Basin

# 2 THEORY

A model-driven analysis of PCAPs requires an understanding of water flow in variably saturated porous media subject to a variety of boundary conditions. The theoretical background of water flow in one and two dimensions under various conditions is summarized in the following sections. How PCAPs work is elaborated upon thereafter.

## 2.1 WATER FLOW

### 2.1.1 Saturated Water Flow

A comprehensive characterization of flow through the vadose zone requires consideration of dimensionality, heterogeneity, and complex transient boundary conditions. One of the simpler cases of water flow is one-dimensional vertical, steady-state, saturated water flow in a homogeneous medium. This is governed by Darcy's law:

$$q = \frac{Q}{A} = \frac{dS}{dt} = -K\frac{dH}{dL} \tag{2.1}$$

Based on Darcy's law, the water flux is directly proportional to the hydraulic head gradient. Hydraulic head [L] is the potential energy per unit weight of the fluid and is the summation of both elevation and pressure heads:

$$H = z + \psi \tag{2.2}$$

Hydraulic conductivity [L/T] is the proportionality constant that represents the magnitude of flux per unit hydraulic head gradient. It is dependent on various properties of the medium through which the water travels. Under unsaturated conditions, the equation becomes non-linear as hydraulic conductivity varies with the degree of saturation. Hydraulic conductivity is also dependent on the distribution of soil textures within the medium. The distribution of soil textures can be generalized as either homogeneous (uniform) or heterogeneous (non-uniform). Water

flow is described as undergoing steady-state conditions if there is no variation in water storage with time. A special steady-state condition, the hydrostatic condition, arises when there is no water flow in the system. The relationship described in Eq. 2.1 can be visualized for a 100 cm long one-dimensional column undergoing steady-state flow in a homogeneous medium with a pressure head of 50 cm at the top boundary and a bottom boundary pressure head of 0 cm (Figure 2.1). A similar column with a top pressure head of -100 cm would result in no-flow conditions because the hydraulic head becomes a constant (Figure 2.2). When the pressure head at the top of the same column is set to 0 cm, the hydraulic head gradient is -1 cm/cm and the hydraulic head is equal to the elevation head (Figure 2.3).

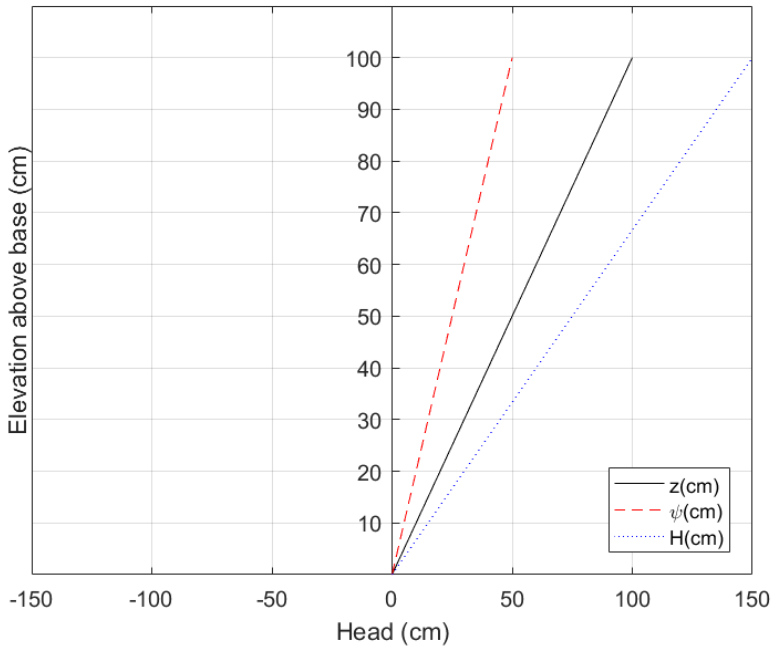


Figure 2.1. A homogeneous medium-filled column undergoing steady-state downward flow with the elevation datum at the base. The column has a top boundary pressure head of 50 cm and a bottom pressure head of 0 cm.

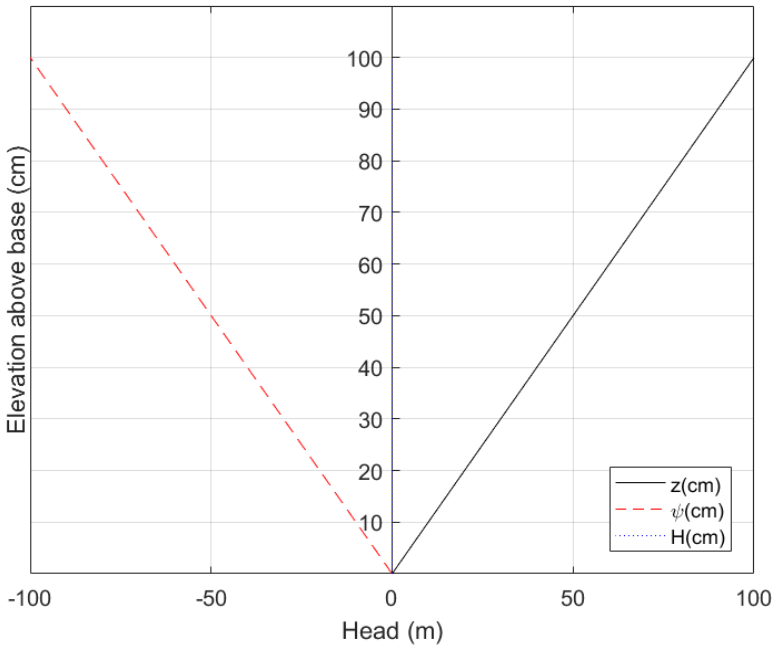


Figure 2.2. A homogeneous medium-filled column under hydrostatic conditions with the datum elevation at the base. The column has a top boundary pressure head of -100 cm and bottom boundary pressure head of 0 cm.

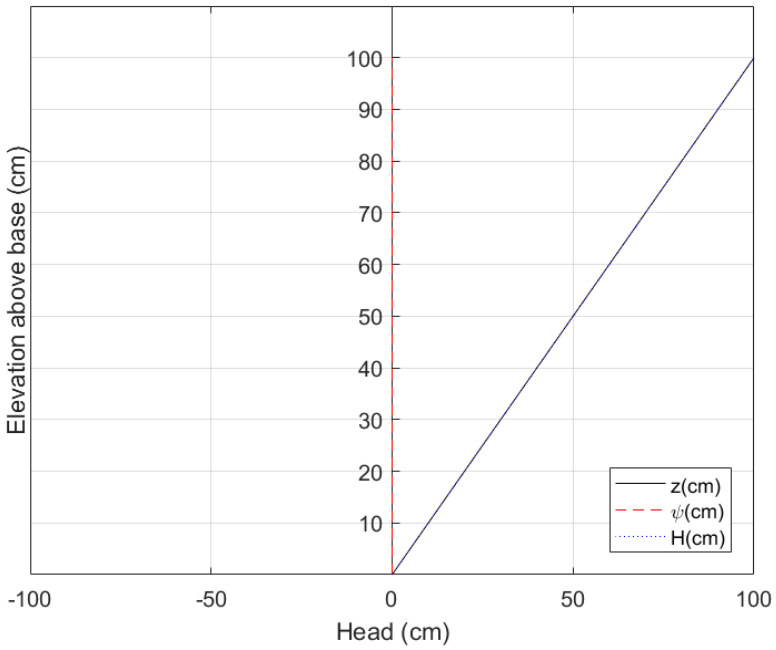


Figure 2.3. A homogeneous medium-filled column undergoing unit gradient flow with elevation datum at the base. The column has top and bottom pressure heads of 0 cm.

A hydraulic head gradient of -1 cm/cm represents a condition known as a unit gradient condition. Under saturated conditions, unit gradient flow is achieved when the flux through the system is equal to the saturated hydraulic conductivity of the medium.

In two dimensions, the saturated water flow equation becomes the diffusion equation for both heterogeneous and homogenous soils:

$$\nabla \bullet \left(\overline{\overline{K}} \nabla H\right) = S_s \frac{\partial H}{\partial t} \tag{2.3}$$

The diffusion equation has a saturated hydraulic conductivity tensor [L/T], $\overline{\overline{K}} = \begin{bmatrix} K_x & 0 \\ 0 & K_z \end{bmatrix}$ and includes a specific storage term. The specific storage, $S_s$ [$L^{-1}$], of the medium is the volume of water released per unit volume of porous medium per unit decrease in hydraulic head. Physically, $S_s$ combines two storage mechanisms related to expansion of water or the medium. This is written as:

$$S_s = \rho g(\alpha + n\beta) \tag{2.4}$$

where ρ is the density of water [$ML^{-3}$], $g$ is gravitational acceleration [$LT^{-2}$], $\alpha$ is the compressibility of the medium [$LT^2M^{-1}$], $n$ is the porosity [-], and $\beta$ is the compressibility of the fluid [$LT^2M^{-1}$] (Freeze and Cherry, 1979). Flow in two dimensions follows similar behaviors as flow in one dimension; flow travels from higher energy potential to a lower energy potential. Anisotropy is the ratio of hydraulic conductivity in the two principle directions $\left(a = \frac{K_x}{K_z}\right)$. An anisotropy value of one describes an isotropic medium, which is assumed throughout this study to reduce complexity.

### 2.1.2 Unsaturated Water Flow

Unsaturated flow in multiple directions is described by the Richards' equation:

$$\nabla \bullet \left( \overline{\overline{K}}(\psi) \nabla H \right) = \frac{\partial \theta}{\partial t} \tag{2.5}$$

Hydraulic conductivity becomes a non-linear function of water content and pressure head under unsaturated conditions. The Richards' equation can be represented in a pressure head form:

$$\nabla \bullet \left( \overline{\overline{K}}(\psi) \nabla H \right) = C(\psi) \frac{\partial \psi}{\partial t} \tag{2.6}$$

$$C(\psi) = \frac{\partial \theta}{\partial \psi} \tag{2.7}$$

Water capacity [$L^{-1}$] ($C(\psi)$) is the change of water content per unit change of pressure head. When the pressure head is greater than the air entry pressure, the soil is saturated and the water capacity is zero. The Richards' equation can also be written in a water content form:

$$\theta = \theta_r + (\theta_s - \theta_r)\left(1 + |\alpha\psi|^n\right)^{-m} \tag{2.8}$$

Finally, the necessary constitutive relationships have several forms. I chose to relate the hydraulic conductivity to the pressure head through the van Genuchten-Mualem model (van Genuchten, 1980; Mualem, 1976) and the piecewise form of hydraulic conductivity:

$$\overline{\overline{K}} = \begin{cases} \overline{\overline{K}}(\psi) & \psi < \psi_{ae} \\ \overline{\overline{K}}_s & \psi \geq \psi_{ae} \end{cases} \tag{2.9}$$

$$Se = \frac{\theta - \theta_r}{\theta_s - \theta_r} = \begin{cases} \left(1 + |\alpha\psi|^n\right)^{-m} & \psi < \psi_{ae} \\ 1 & \psi \geq \psi_{ae} \end{cases} \tag{2.10}$$

$$m = 1 - \frac{1}{n} \tag{2.11}$$

There is a discontinuity when the pressure head exceeds the air-entry pressure $(\psi_{ae})$, above which $K = K_s$. $m$ and $n$ are soil-specific constants. Hydraulic conductivity is then written as the following with respect to effective saturation and then pressure head:

$$K = K_s S_e^{\frac{1}{2}} \left[ 1 - \left( 1 - S_e^{\frac{1}{m}} \right)^m \right]^2 \tag{2.11}$$

$$K = K_s \left( 1 + |\alpha\psi|^n \right)^{\frac{-m}{2}} \left[ 1 - \left( 1 - \left( 1 + |\alpha\psi|^n \right)^{-1} \right) \right]^2 \tag{2.12}$$

van Genuchten soil characteristic curves based on the parameters $\alpha$, $m$, and $n$ are shown for the key soils considered here on Figures 2.4 and 2.5.

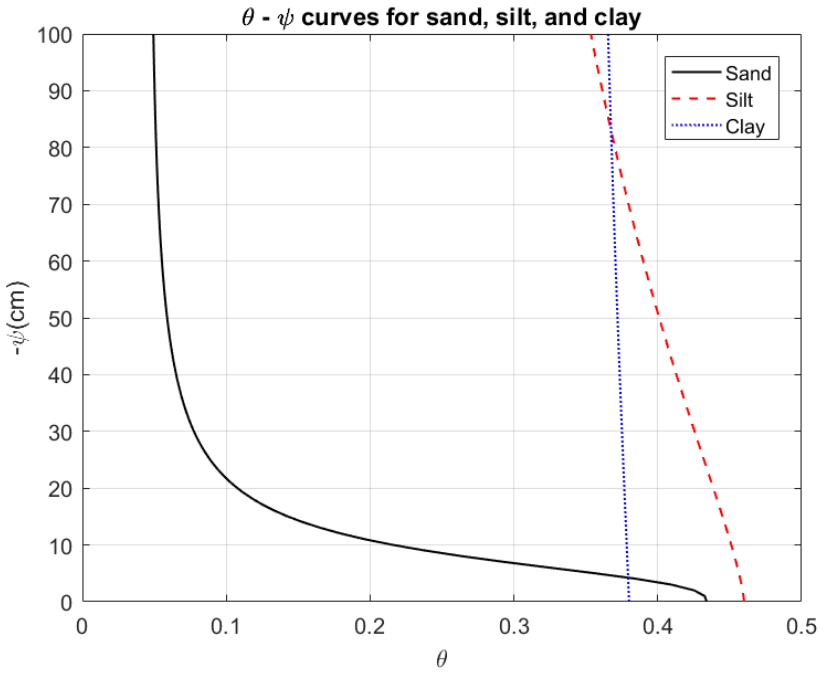


Figure 2.4. Soil characteristic curves relating water content and pressure head for sand, silt, and clay for their respective van Genuchten parameters of $\alpha$, $m$, and $n$ (Table 2.1).

**Table 2.1 van Genuchten parameter list to generate Figure 2.4**

| Soil Type | Saturated Hydraulic Conductivity (cm/day) | Water Content | | van Genuchten Parameters | |
|---|---|---|---|---|---|
| | | residual | saturated | alpha | n |
| Sand | 712.8 | 0.045 | 0.434 | 0.145 | 2.68 |
| Silt | 6 | 0.034 | 0.46 | 0.016 | 1.37 |
| Clay | 4.8 | 0.068 | 0.38 | 0.008 | 1.09 |

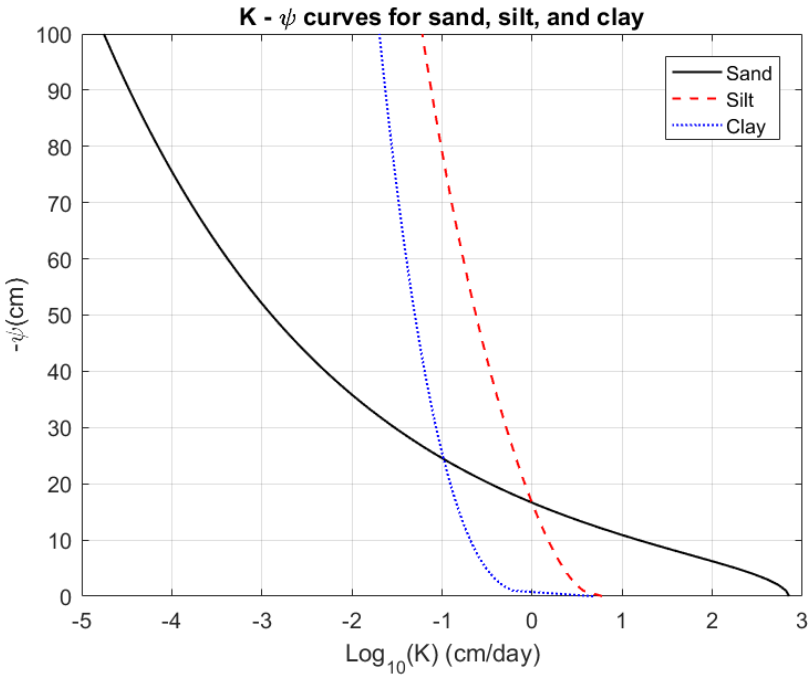


Figure 2.5. Unsaturated hydraulic conductivity plots for sand, silt, and clay in log scale.

Hydraulic conductivity values span many orders of magnitude depending on the degree of saturation. Under saturated conditions ($\psi >= 0$), sand has the largest hydraulic conductivity followed by silt and then clay. For many negative pressure head conditions, water can move more easily through silt and clay compared to sand. Specifically, from Figure 2.5, silt and clay have a higher hydraulic conductivity than sand at pressure heads smaller than -25 cm. A one-dimensional example of how unsaturated conditions affect flow can be visualized using plots for a one-dimensional sand column undergoing steady-state flow with a top boundary pressure head of -50 cm and a bottom boundary pressure head of 0 cm (Figure 2.6). The head gradient is higher at the top of the column because it is drier, therefore less conductive, there. An example of unit gradient conditions for unsaturated conditions is shown in Figure 2.7. Because the pressure head is constant throughout, the water content and hydraulic conductivity are also constant, leading to a constant gradient of -1 cm/cm.

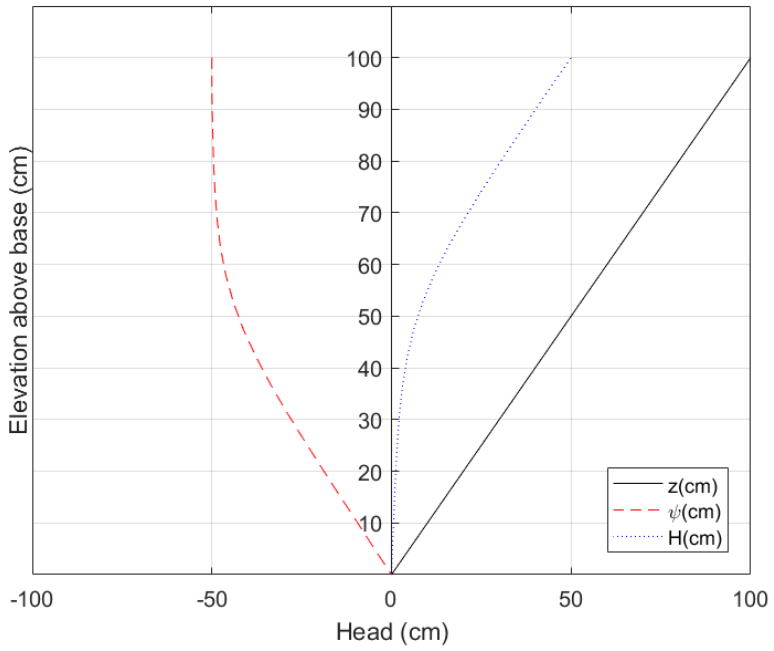


Figure 2.6. A sand-filled column undergoing steady-state downward flow under unsaturated conditions with the elevation datum at the base. Top pressure head is -50 cm and the bottom pressure head is 0 cm.

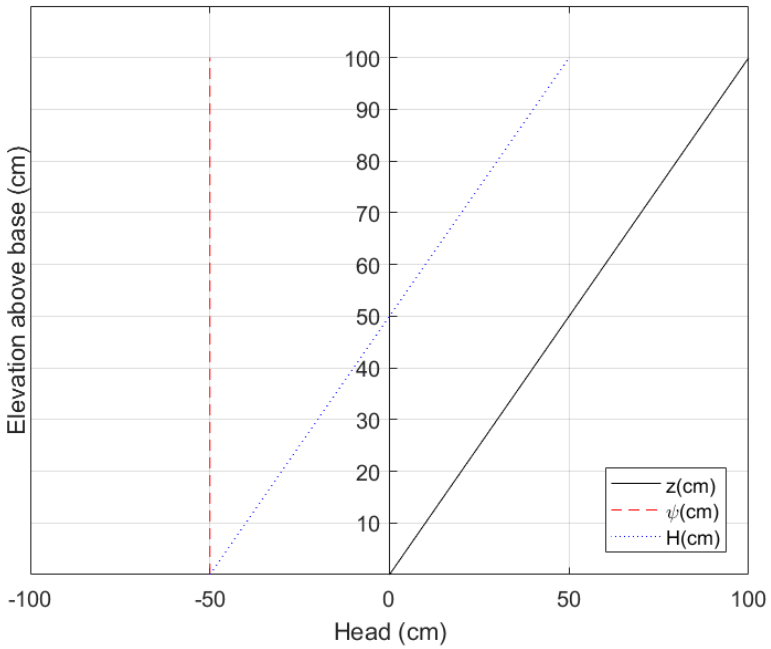


Figure 2.7. A sand-filled column undergoing unit gradient flow under unsaturated conditions with elevation datum at the base. Both pressure heads are set at -50 cm.

Although both unsaturated and saturated conditions can give rise to steady-state, unit gradient flow, the magnitude of flux will be lower for unsaturated conditions because the hydraulic conductivity for a sand at -50 cm of pressure head is six orders of magnitude smaller than the saturated hydraulic conductivity at 0 cm of pressure head (Figure 2.5). Unit gradient flux is equal to the unsaturated conductivity at the water content established under the applied conditions.

### 2.1.3 Infiltration

Strictly defined, infiltration is the flux of water across the ground surface. Flow through the vadose zone (unsaturated zone) is defined as percolation. This study will use the term 'infiltration' to represent both infiltration and percolation. Infiltration has implications in topics including contaminant transport, irrigation, and groundwater recharge. When a constant flux

greater than the saturated hydraulic conductivity of the soil is applied at the ground surface, the water will pond and infiltrate. Excess ponded water will flow overland. The depth of the wetting front as a function of time depends on the texture of the medium, initial pressure head condition (or water content), and rate of applied flux. Infiltration at a constant rate will eventually result in a unit gradient condition if water can drain freely at depth. If the infiltration rate is equal to the saturated hydraulic conductivity, the pressure head will be zero everywhere. For an applied flux lower than the saturated hydraulic conductivity, the pressure head of the medium will increase until the hydraulic conductivity at that pressure head is equal to the applied flux. That is, a unit gradient condition with a negative gauge pressure head indicates flow lower than the saturated hydraulic conductivity.

I used a numerical solution of Richards' equation to visualize water content and pressure head profiles in soils with different hydraulic properties during infiltration and drainage. The following discussion of infiltration is supplemented with simulation results from HYDRUS-1D, a simulator of one-dimensional water, mass, and heat transport in variably saturated media (Simunek et al., 2009). HYDRUS-1D solves the Richards' equation through numerical iteration for a selected set of boundary conditions and soil properties. For the following illustrative examples, soil properties for sand, silt, loam, and clay have been defined within HYDRUS-1D using the included ROSETTA software that estimates soil properties with pedotransfer functions (Shaap et al., 2001).

Consider infiltration under a constant flux into a drained sand with an initial water pressure of -100 cm. The profiles for water content and pressure head will proceed through the medium, establishing a relatively sharp wetting front because the lower hydraulic conductivity of the drier soil (Figure 2.8) prevents water from advancing beyond the wetting front. The rate of

advance of the wetting front will depend on the prescribed flux (Figure 2.9). In the case that the saturated hydraulic conductivity of the sand is either increased or decreased by a factor of 10 (other parameters unchanged), the wetting front will travel further in the sand with the larger saturated hydraulic conductivity because it can transmit water more easily at lower pressure heads and, therefore, lower water contents (Figure 2.10). That is, less water is held in storage to achieve the necessary degree of saturation, leaving more water to reach deeper depths. When the applied flux is less than the saturated hydraulic conductivity, finer soils can advance the wetting front farther than the coarser soils (Figure 2.11). Finer soils generally have a higher hydraulic conductivity at lower pressure heads compared to coarser soils (Figure 2.4). In the case of limited duration infiltration and drainage (Figure 2.12), once the infiltration has been halted, the water content will continually decrease behind the wetting front, even though the wetting front continues to advance to greater depths. As the medium above the wetting front drains, its hydraulic conductivity will decrease. Assuming an approximate unit gradient condition above the wetting front, this leads to a steadily decreasing flux across the wetting front through time. This, in turn, leads to a decrease in the rate of advance of the wetting front with time.

a)

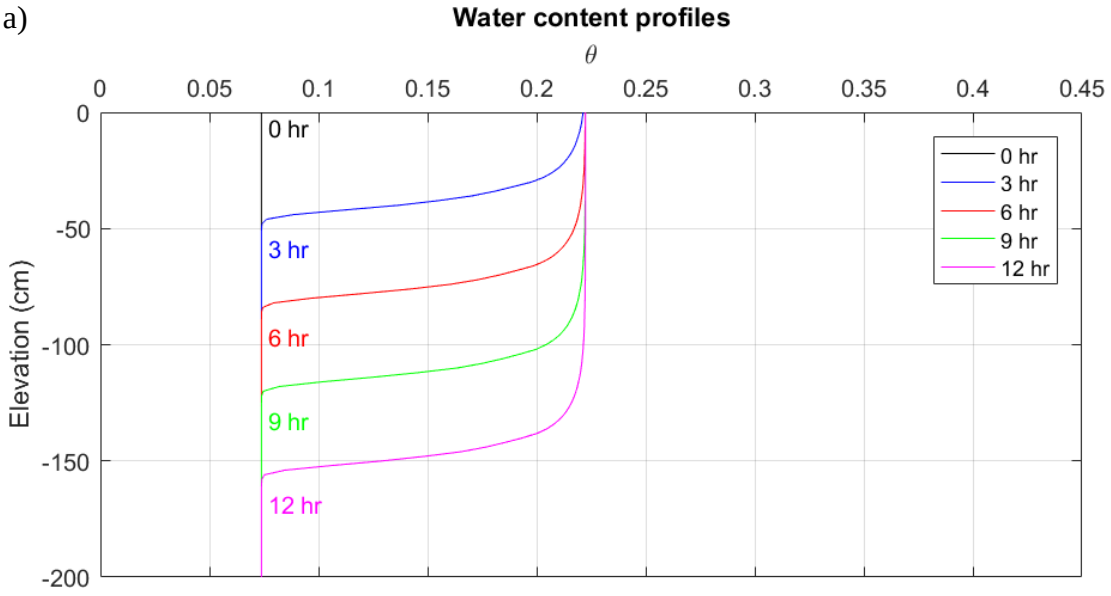


b)

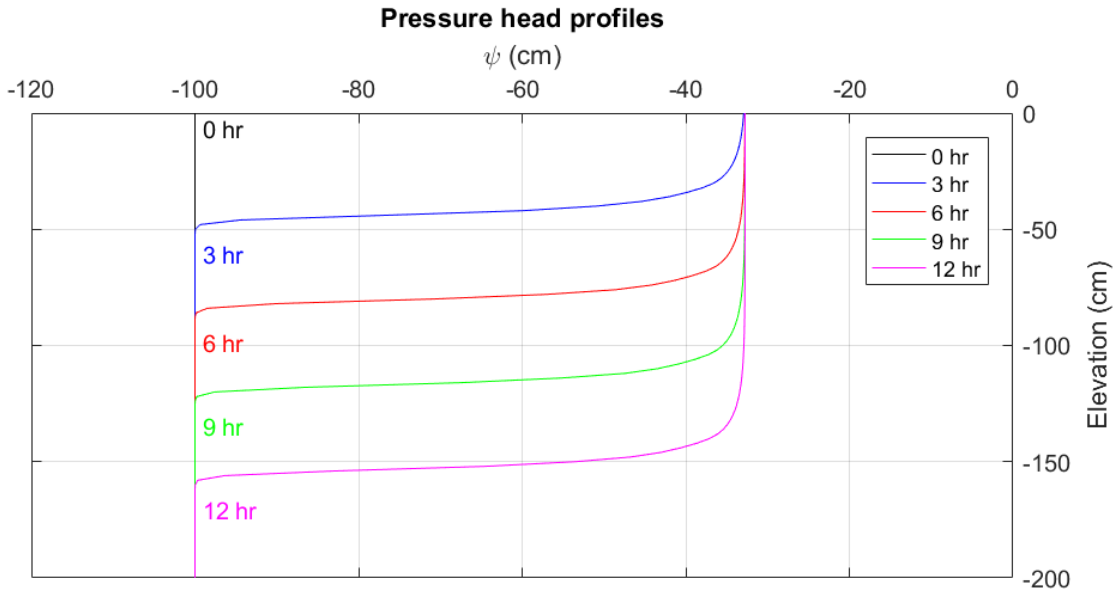


Figure 2.8. a) Water content and b) pressure head profiles for 0, 3, 6, 9, and 12 hours of infiltration into a drained sand at a constant flux of 43.2 cm/day.

a)

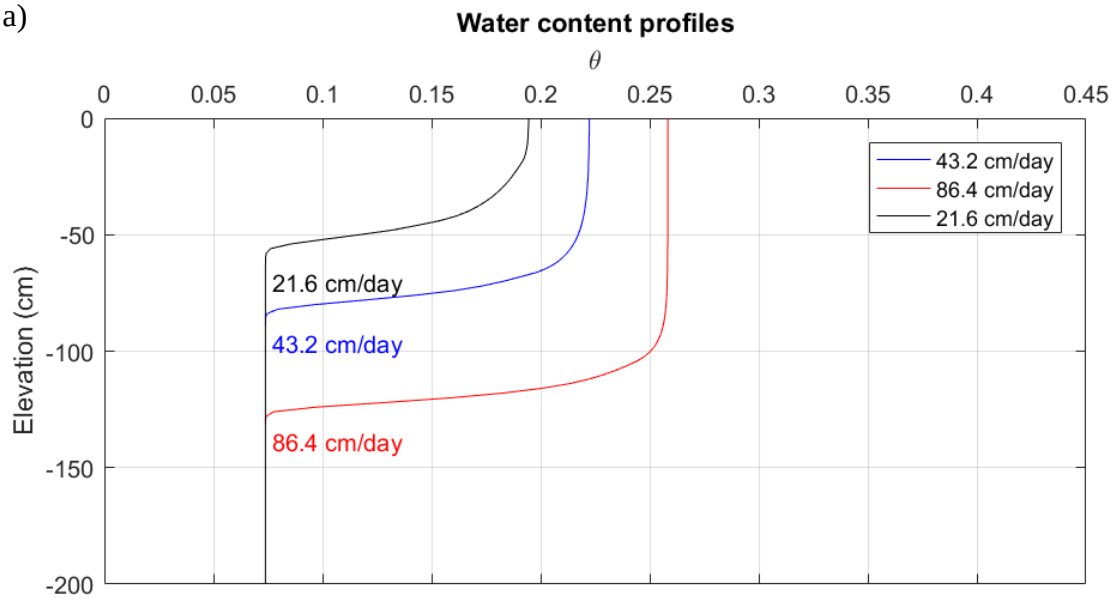


b)

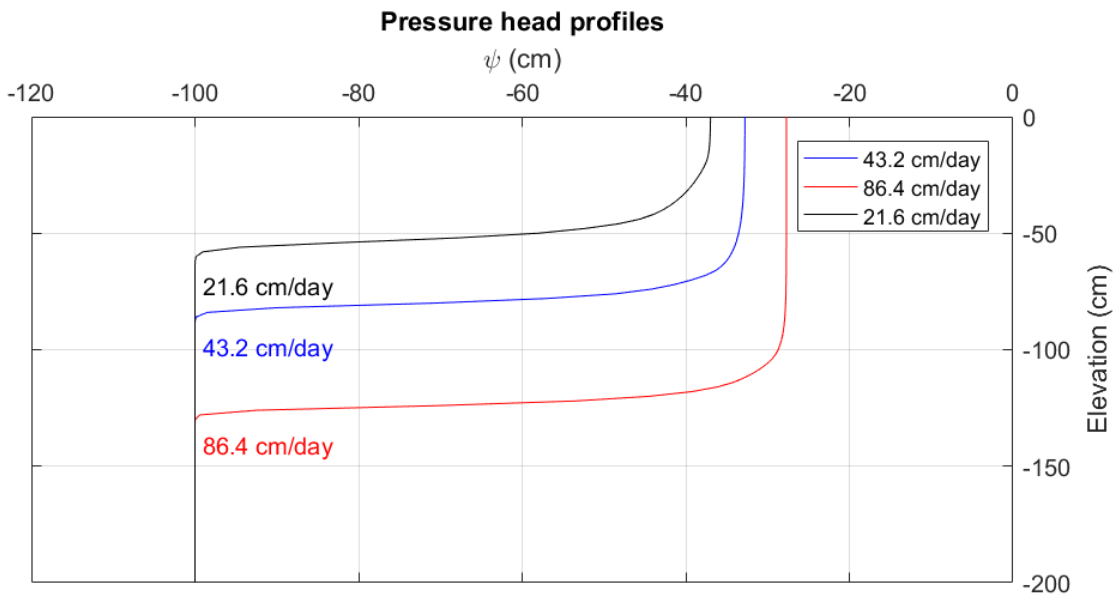


Figure 2.9. a) Water content and b) pressure head profiles after 6 hours of infiltration through a drained sand at 21.6, 43.2, and 86.4 cm/day.

a)

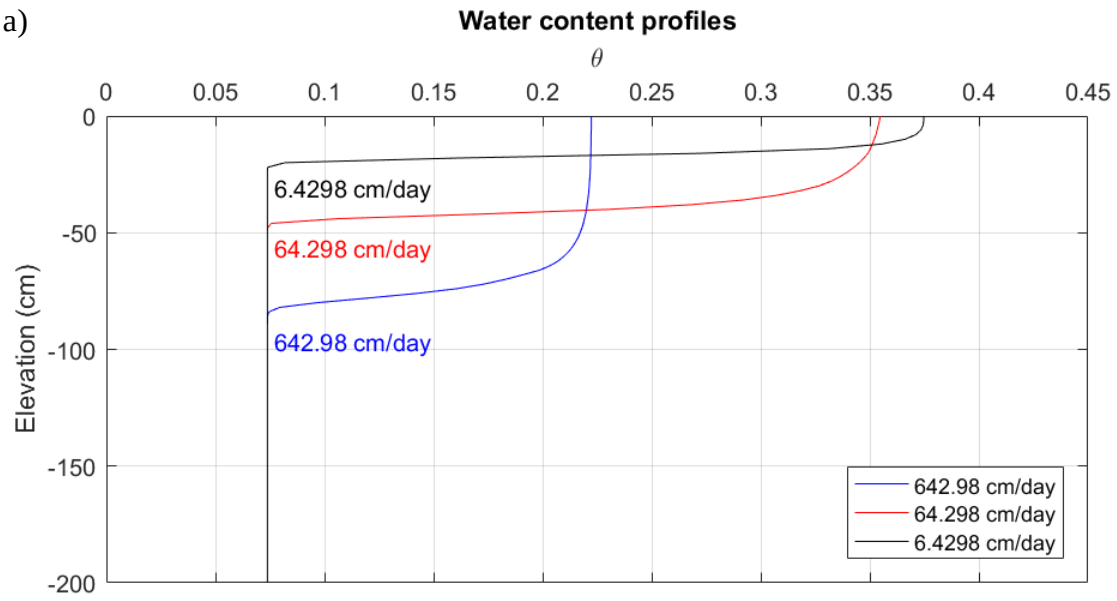


b)

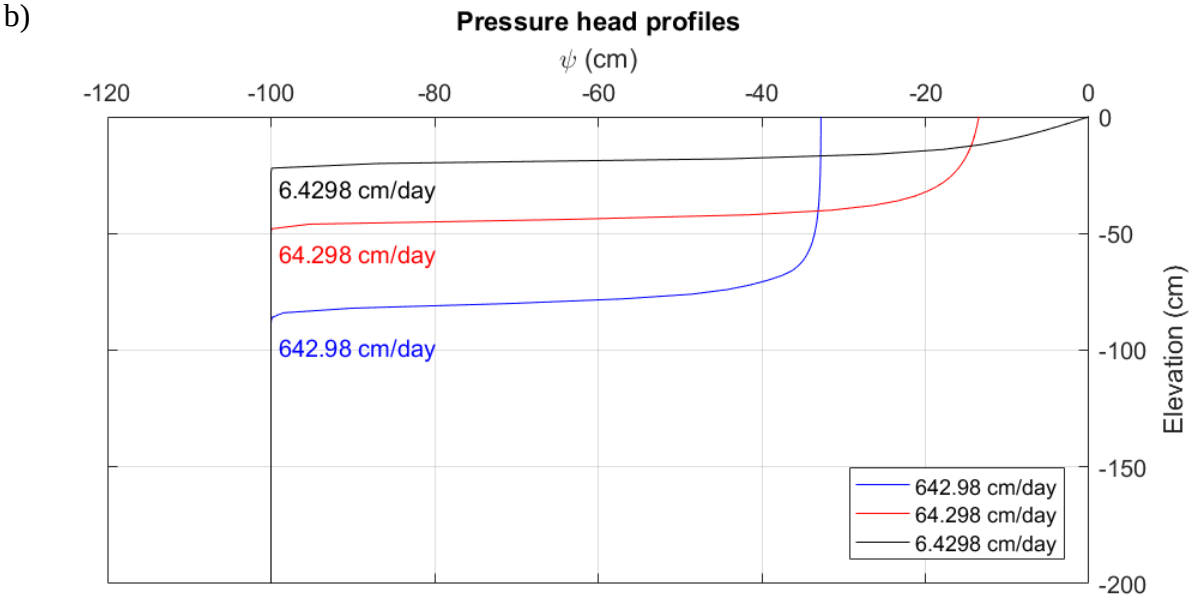


Figure 2.10. a) Water content and b) pressure head profiles after 6 hours of infiltration through a drained sand at 43.2 cm/day with varied saturated hydraulic conductivities of 6.43, 64.30, and 640.00 cm/day.

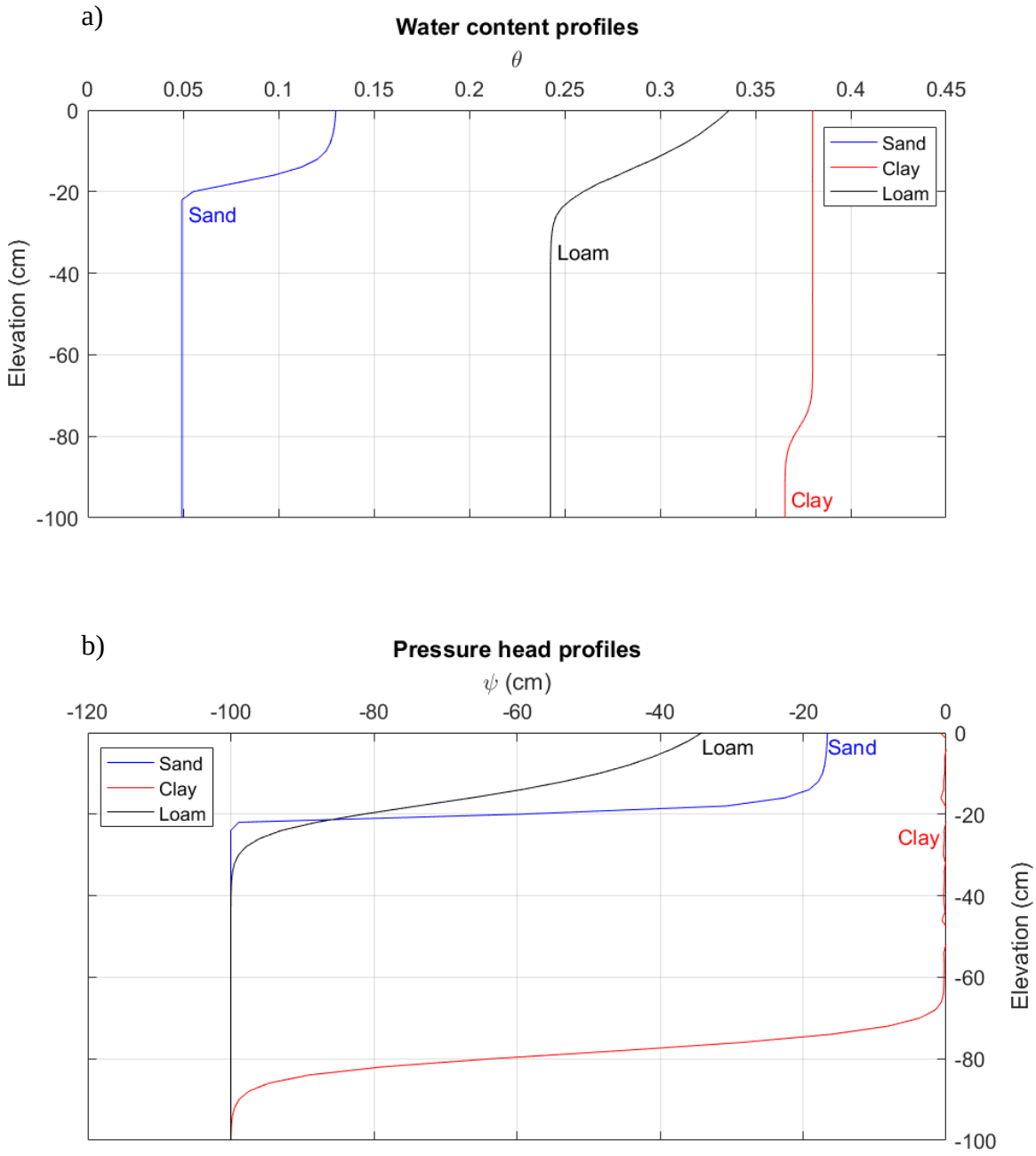


Figure 2.11. a) Water content and b) pressure head profiles after 24 hours of infiltration through a sand, clay, and loam at 1.3 cm/day.

a)

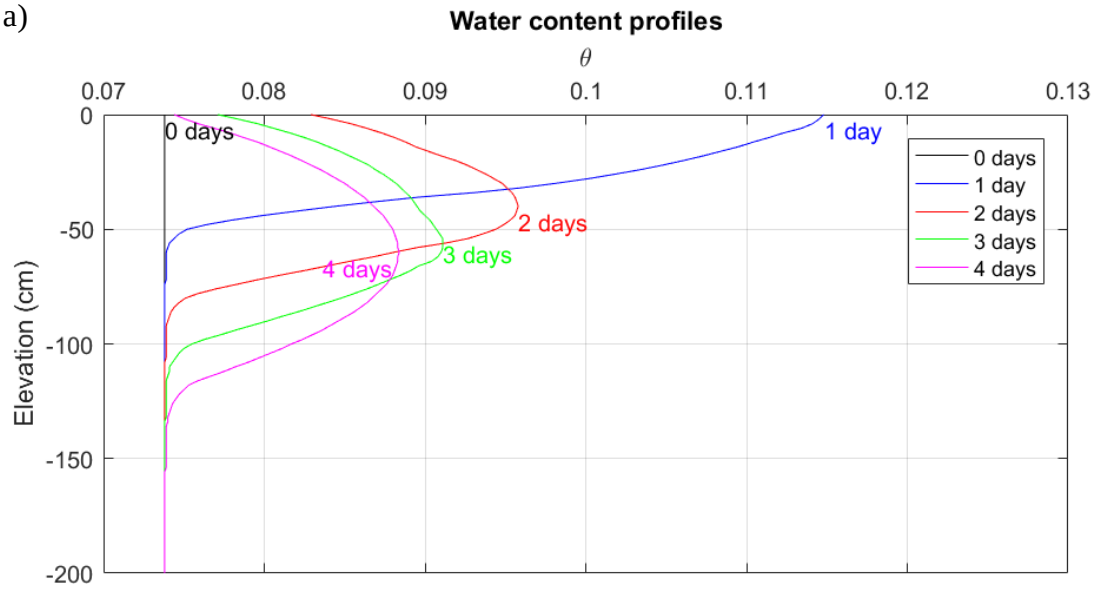


b)

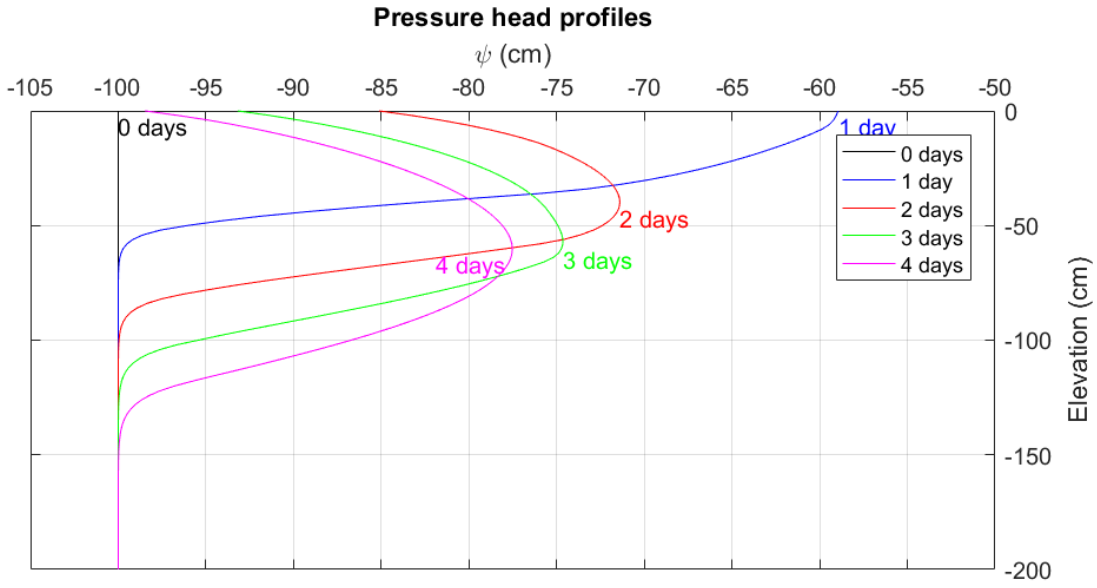


Figure 2.12. a) Water content and b) pressure head profiles after 1 day of infiltration at 1.3 cm/day followed by 3 days of drainage through a sand.

## 2.2 PASSIVE CAPILLARY WICK SAMPLERS (PCAPS)

PCAPs (Figure 2.13) collect water by using wicks, usually fiberglass, to form a hanging water column. The wicks are splayed out on the plate such that any water that comes into contact gets drawn into the tube via the braided wick. The saturated hydraulic conductivity of the wicks is sufficiently high to allow the collected water to drain to the collection chamber without being impeded by the wick. The contents of the collection tank are then pumped out at the end of each desired sampling period. Water flux could be measured directly by placing a transducer at the base of the collection tank (Gee, 2004).

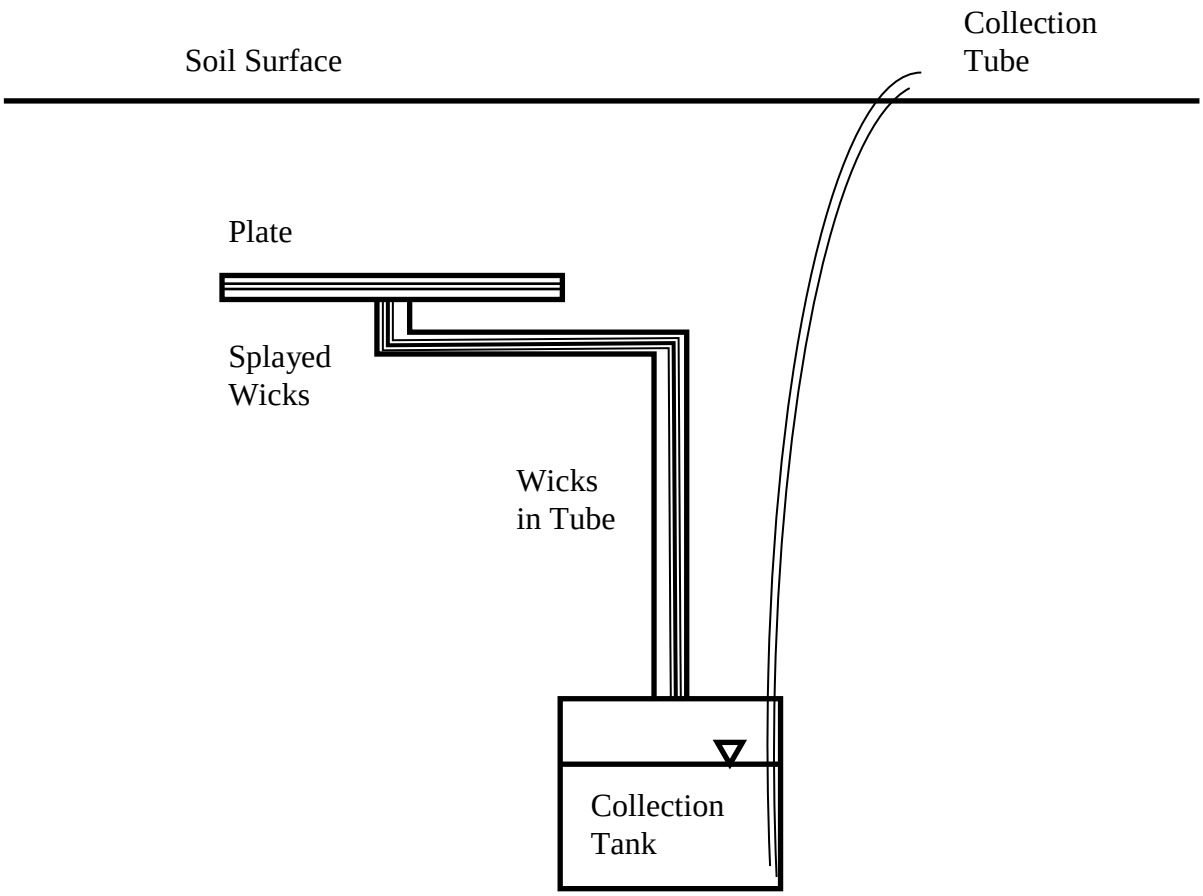


Figure 2.13. Schematic diagram of a PCAP used at the CZO site.

An important assumption in the simplification of PCAP capture for this study is that there is a negative constant pressure head boundary along the top of the PCAP plate equal to the length of the hanging water column. This is assumed to maintain a zero pressure head boundary condition at the bottom end of the wick. The carboy where the wicks drain the captured flux is assumed to be perfectly sealed, which means that the pressure head where the wicks end above the water level is equal to atmospheric pressure ($\psi = 0$). For example, the constant pressure head along the plate would be -30 cm if the vertical length of the tube is 30 cm. If the wetting front above the plate has a pressure head greater (less negative) than -30 cm, then water would converge towards the PCAP (Figure 2.14 a)). Pressure heads less than -30 would result in divergent flow away from the PCAP (Figure 2.14 b)). The degree of divergence or convergence depends on the difference between the pressure at the PCAP boundary and the pressure in the soil. The hydraulic conductivity of the medium at the water content achieved also constrains the degree of convergence or divergence.

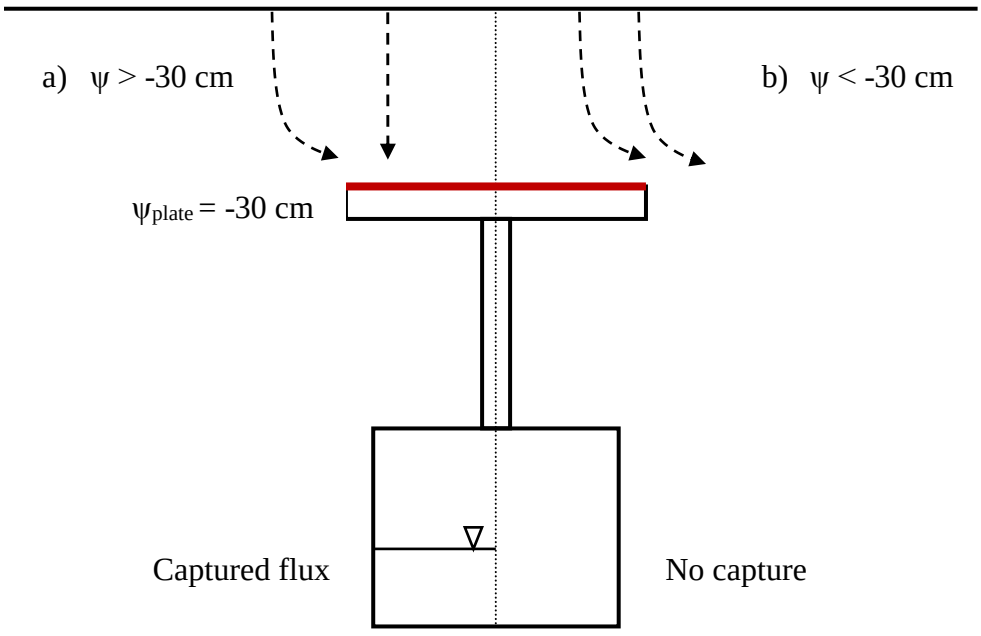


Figure 2.14. Flow lines from infiltration at pressure heads greater than or less than -30 cm showing a) convergence and b) divergence near the PCAP.

The assumption of constant pressure head at the top of the PCAP has been demonstrated analytically in a study from Rimmer (1995) in which a steady-state, one-dimensional, mathematical solution was developed to determine the pressure head profiles due to the wick-soil interface. Rimmer showed pressure head distributions from plotting his analytical solution while using actual wick sampler parameters and soil hydraulic characteristics. His results reveal a constant pressure head above the wick sampler. He also observed that soil moisture just above the wick sampler was drier at lower fluxes and wetter at larger fluxes, implying occurrence of convergence/divergence when the pressure head just above the wick sampler was lower/higher than that of the surrounding soil. The purpose of this study is to explore convergence and divergence and attempt to predict the magnitude of these effects on a wick-sampler before it is placed in the vadose zone.

# 3 METHODOLOGY

## 3.1 COMPARISON CRITERIA

Capture efficiencies are used commonly to evaluate the performance of flux-measuring instruments like PCAPs (Zhu, 2002). Capture efficiencies describe how much flux the PCAP has measured compared to the actual flux through the medium. This comparison can be made most easily for steady-state conditions; but, it is also possible to examine the time series of capture efficiency for transient analysis. PCAPs were used for measuring infiltration at the CZO site. The objective of this study was to determine the likely magnitudes of errors in those estimated fluxes.

The capture efficiency for the PCAP under steady-state conditions is defined as:

$$C_e = \frac{q_{PCAP}}{q_{top}} \tag{3.1}$$

where $q_{top}$ is the background flux through the soil and $q_{PCAP}$ is the flux into the PCAP. Models simulated steady-state conditions, identified by constant pressure heads throughout the domain through time. A capture efficiency less than one implies that the PCAP has underestimated the actual flux (divergence). A capture efficiency greater than one means that the PCAP has overestimated the actual flux (convergence). A capture efficiency of one means that the PCAP-measured flux is equal to the actual flux.

## 3.2 HYDRUS

The HYDRUS software package is an iterative numerical solution of the Richards' equation for variably saturated flow and the advection-dispersion equation for solute and heat transport (Simunek et al., 2005). Model structure including initial conditions, boundary conditions, soil model, layer composition, and convergence criteria are specified in input text files. The input text files can be modified manually or via the included graphical user interface. HYDRUS stores the results of each simulation in output text files from which results can be analyzed. Simulations can be performed in one, two, or three dimensions with the two available packages, HYDRUS-1D and HYDRUS (2D/3D). This study used both packages of HYDRUS and the included GUIs for steady-state and transient analysis. The computing software package MATLAB (MathWorks Inc., 2016) was used to modify the input files and analyze the output files. HYDRUS allows for efficient analysis of flow in a PCAP-implemented medium across different soils and conditions.

HYDRUS solves the Richards' equation by using linear finite difference and finite element schemes for one dimension and multiple dimensions, respectively. Assuming that water vapor and thermal gradients are negligible, the modified Richards' equation solved by HYDRUS is:

$$\frac{\partial \theta}{\partial t} = \frac{\partial}{\partial x}\left[K\left(\frac{\partial h}{\partial x} + \cos\alpha\right)\right] - S \tag{3.2}$$

where $\theta$ is the volumetric water content [$L^3L^{-3}$], $t$ is time [T], $x$ is the positive upward coordinate [L], $K$ is the unsaturated hydraulic conductivity [$LT^{-1}$], $h$ is the water pressure head [L], α is the angle between the flow direction and the vertical axis, and $S$ is a sink term [$L^3L^{-3}T^{-1}$] . The unsaturated hydraulic conductivity K is a function of saturated [$LT^{-1}$] and relative hydraulic conductivity [dimensionless]:

$$K(h,x) = K_s(x)K_r(h,x) \tag{3.3}$$

The multidimensional versions of Eq. (2.2) and (2.3) solved by the HYDRUS (2D/3D) package is:

$$\frac{\partial\theta}{\partial t} = \frac{\partial}{\partial x_i}\left[K\left(K_{ij}^A\frac{\partial h}{\partial x_j} + K_{iz}^A\right)\right] - S \tag{3.4}$$

$$K(h,x,y,z) = K_s(x,y,z)K_r(h,x,y,z) \tag{3.5}$$

where $K_{ij}^A$ is the anisotropy tensor and the subscripts $i$ and $j$ represent the $x$, $y$, or $z$ coordinates depending on the number of dimensions. All other terms in Eq. (3.4) and Eq. (3.5) are the same as Eq. (3.2) and Eq. (3.3).

In the one-dimensional case, HYDRUS begins numerically solving the above equations by discretizing the soil profile into N-1 adjacent elements which all end with a node for a total of N nodes. The discretization resolution is specified by the user in the input text file. Equations that describe pressure head or water content are solved iteratively at each time step until convergence is attained on all the nodes within a user-specified tolerance. The multidimensional case employs a similar process, but with nodes extending to two- or three-dimensional spaces.

Information on the initial and boundary conditions of water content or pressure head are required a priori for HYDRUS to solve the modified Richards' equations described previously (Eq 3.4). The boundary conditions that HYDRUS can implement include constant pressure head or flux, atmospheric-controlled with precipitation and evaporation, variable pressure head or

flux, horizontal drains, seepage face, deep drainage, free drainage, and no-flow boundaries. Initial and boundary conditions are specified by the user in the input text files. This study uses pressure heads for initial conditions and a mix of free drainage, constant pressure head, no-flow boundaries, and precipitation for variable fluxes for boundary conditions.

HYDRUS has several constitutive relations available for modeling soil hydraulic properties. The model used to represent soil hydraulic properties is important because it determines the behavior of flow under unsaturated conditions. The relative hydraulic conductivity function (Eq. 3.3) that determines hydraulic conductivity is dependent on the soil analytical model. The widely accepted van Genucthen model (van Genuchten, 1980) is used in this study for having a more consistent predictive accuracy compared to the other models (Nandagiri and Prasad, 1996).

Many van Genucthen soil parameters can be defined using the ROSETTA pedotransfer function software package, which is included in HYDRUS. ROSETTA (Schaap et al., 2001) is a hierarchical program that uses soil texture and other information, as available, to define soil hydraulic parameters. Soil textures are usually defined by the relative proportions of soil particle sizes: sand, silt, and clay. The soil texture triangle (Figure 3.1) adopted by the United States Department of Agriculture (USDA) is one of the most common tools to visualize soil textures (Davis and Bennet, 1927). The texture triangle delineates 12 different soil classes based on their sand, silt, and clay percentages. Assuming that soils within each class behave similarly (Twarakavi et al, 2010), averaging hydraulic properties for soils within each class would generate representative parameter values (Table 3.1). This study used sand, silt, and clay percentages throughout the texture triangle to simulate flow in a variety of soil types.

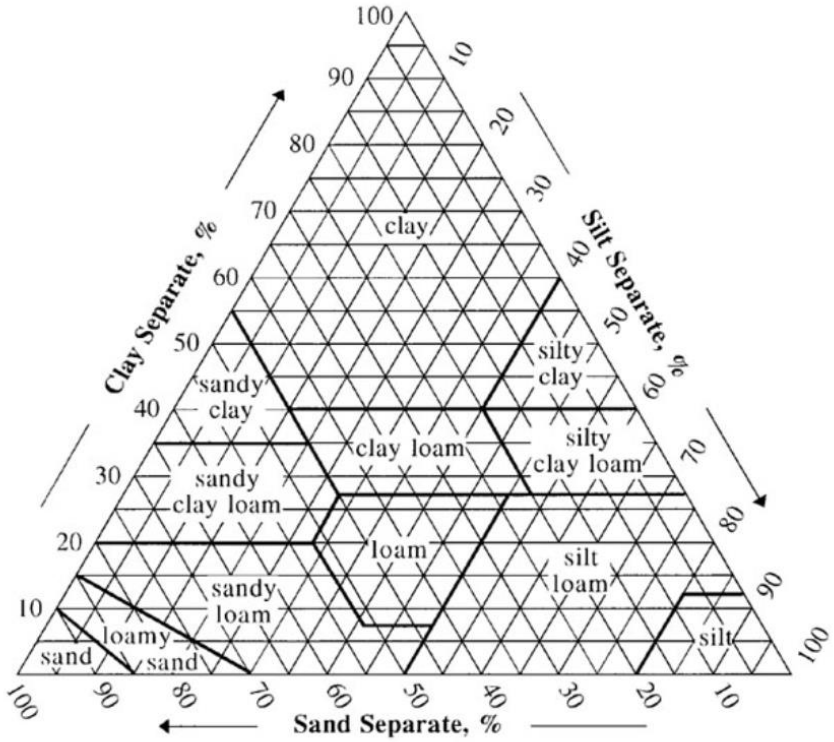


Figure 3.1. USDA soil texture triangle.

**Table 3.1.** Soil class van Genuchten hydraulic parameters with approximate sand, silt, and clay percentages.

| | $\theta_r$ | $\theta_s$ | α (1/cm) | n | Ks (cm/day) | L | Sand % | Silt % | Clay % |
|---|---|---|---|---|---|---|---|---|---|
| **Sand** | 0.045 | 0.43 | 0.145 | 2.68 | 712.8 | 0.5 | 94.0 | 6.0 | 0.0 |
| **Loamy Sand** | 0.057 | 0.41 | 0.124 | 2.28 | 350.2 | 0.5 | 86.0 | 14.0 | 0.0 |
| **Sandy Loam** | 0.065 | 0.41 | 0.075 | 1.89 | 106.1 | 0.5 | 82.0 | 18.0 | 0.0 |
| **Loam** | 0.078 | 0.43 | 0.036 | 1.56 | 24.96 | 0.5 | 54.0 | 10.0 | 36.0 |
| **Silt** | 0.034 | 0.46 | 0.016 | 1.37 | 6 | 0.5 | 54.0 | 40.0 | 6.0 |
| **Silt Loam** | 0.067 | 0.45 | 0.02 | 1.41 | 10.8 | 0.5 | 50.0 | 26.0 | 24.0 |
| **Sandy Clay Loam** | 0.1 | 0.39 | 0.059 | 1.48 | 31.44 | 0.5 | 44.0 | 2.0 | 54.0 |
| **Clay Loam** | 0.095 | 0.41 | 0.019 | 1.31 | 6.24 | 0.5 | 26.0 | 26.0 | 48.0 |
| **Silty Clay Loam** | 0.089 | 0.43 | 0.01 | 1.23 | 1.68 | 0.5 | 20.0 | 44.0 | 36.0 |
| **Sandy Clay** | 0.1 | 0.38 | 0.027 | 1.23 | 2.88 | 0.5 | 32.0 | 0.0 | 68.0 |
| **Silty Clay** | 0.07 | 0.36 | 0.005 | 1.09 | 0.48 | 0.5 | 26.0 | 52.0 | 22.0 |
| **Clay** | 0.068 | 0.38 | 0.008 | 1.09 | 4.8 | 0.5 | 34.0 | 44.0 | 22.0 |

### 3.3 HYDRUS PCAP MODEL

The PCAP model used for this study (Figure 3.3) was developed with the HYDRUS (2D/3D) software package (Simunek et al., 2012). The approximate dimensions (Table 3.2) of the PCAPs installed at the CZO site (Figure 3.2) were used for the tube and the carboy. Actual dimensions were used for the PCAP plate.

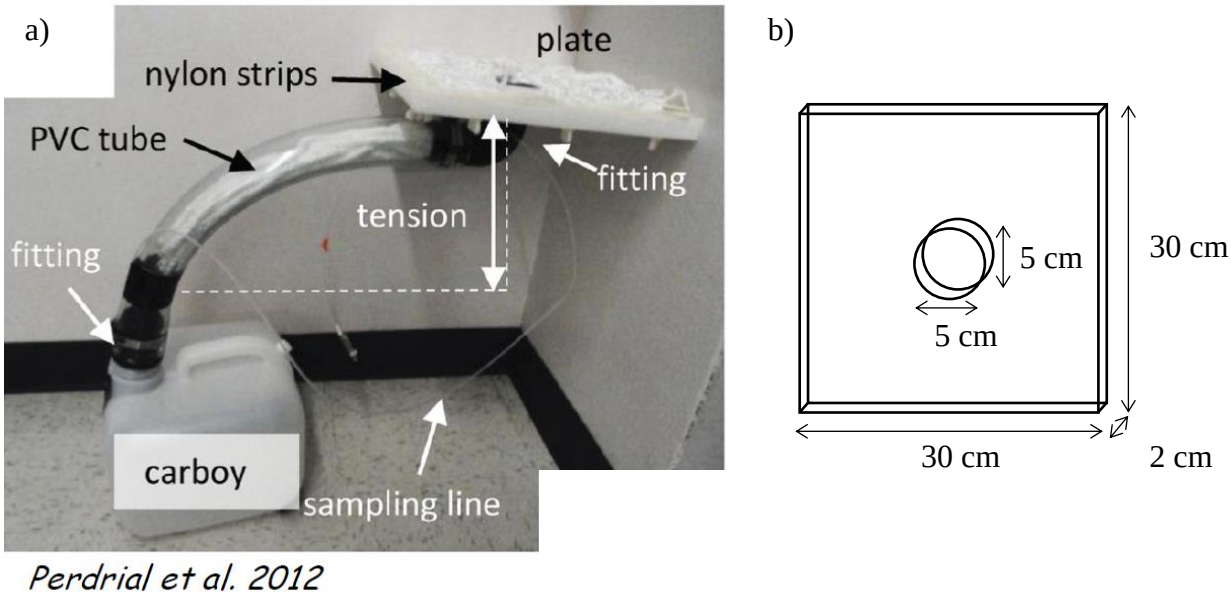


Figure 3.2. (a) Photo PCAP components and (b) plate schematic with actual dimensions.

**Table 3.2.** Dimensions of PCAP used in model. Plate dimensions are exact, while the rest are approximate.

| Part | Length (cm) | Width (cm) | Depth (cm) |
|---|---|---|---|
| Plate | 30 | 30 | 2 |
| Tube | 5 | 5 | 30 (bent) |
| Carboy | 30 | 30 | 30 |

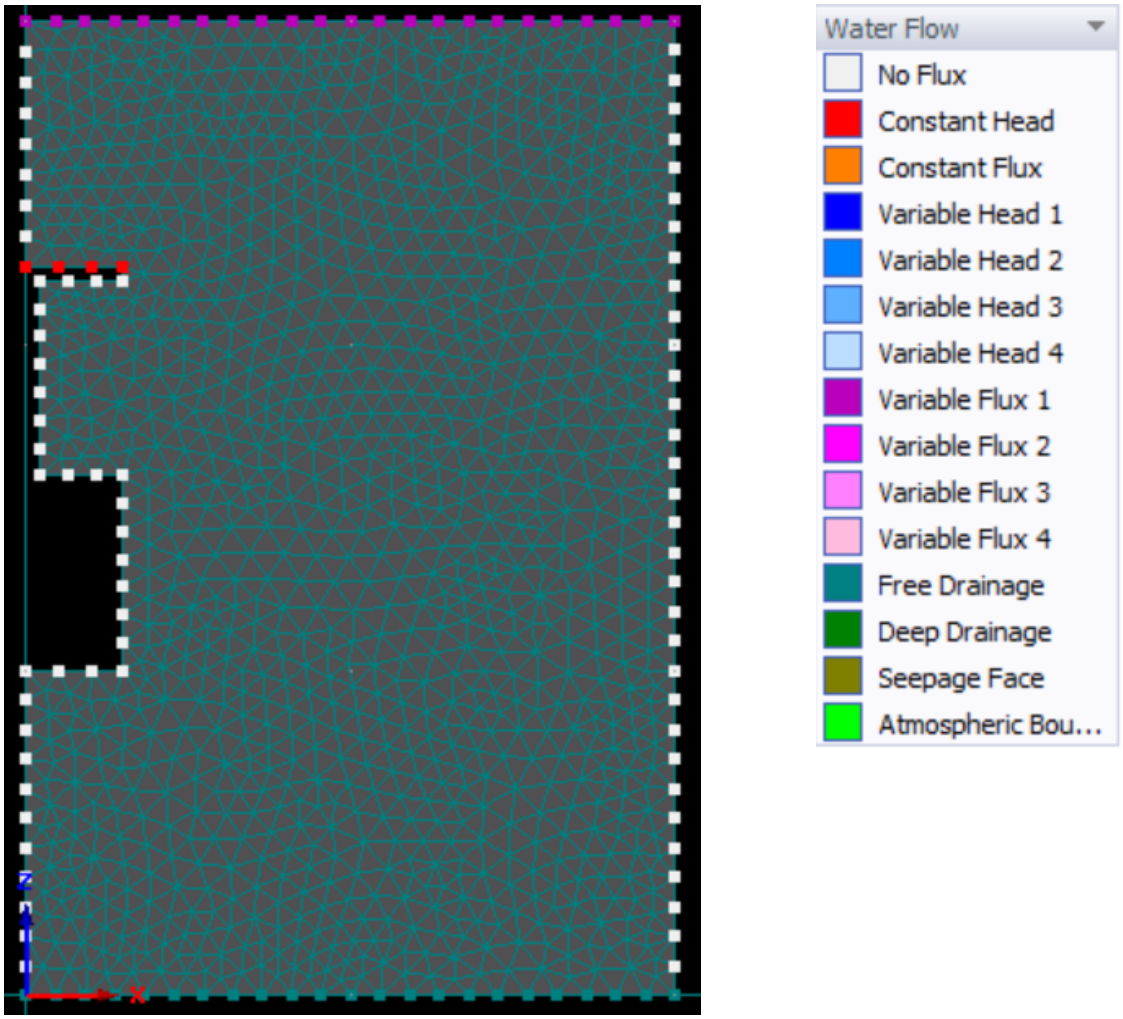


Figure 3.3. A 100 cm by 150 cm HYDRUS (2D/3D) 2D axisymmetric model of a PCAP with variable flux (top), free drainage (bottom), no-flux (left and right), and constant head (top of PCAP plate) boundary conditions. The default HYDRUS finite element mesh parameters of 10 cm target size, stretching factor of 1 in the x-direction, and a minimum of 15 points on curved boundaries are used to generate a mesh of 2133 elements and 1129 nodes.

Water capture by PCAP is modeled as an infiltration process using a two-dimensional axisymmetric system measuring 100 cm in the x-direction and 150 cm in the z-direction. The axis of symmetry is rotated around the z-axis through the center of the PCAP, representing the cylindrical design of the instrument. The dimensions of the PCAP within the model are approximated from actual specifications of PCAPs used at the CZO site (Table 3.2). PCAPs are

generally installed at depths close to 10 cm, 30 cm, and 60 cm below the surface at the CZO site. A single, representative location of 38 cm below the surface was selected for the model as it falls within the range of depths. The finite element mesh was generated with the default settings in HYDRUS for a total of 1129 nodes. The model has a variable flux boundary condition at the surface to represent infiltration from precipitation events. No-flow boundary conditions are assigned to the PCAP tube, carboy, plate sides, and along the left and right extents of the model domain. The carboy is sealed at the bottom and open to the atmosphere, so it will have a water pressure head of 0 cm at the open water surface and at the bottom of the wick. A constant pressure head of -30 cm is assigned along the top of the PCAP plate because of the 30 cm tube extending from the plate into the carboy. The wicks in the tube do no extend below the water surface in the carboy. PCAPs are placed in the vadose zone, so the water table is assumed to be much deeper than the modeled domain; the bottom of the domain can be represented as a free drainage or a unit vertical gradient boundary. Initial conditions of either a constant -30 cm pressure head or hydrostatic conditions with 0 cm pressure head at the bottom of the domain are used depending on the investigation scenario. The constant pressure head of -30 cm allows pressure head equilibrium to be achieved quickly. Iteration criteria for convergence is left as the HYDRUS default values. The variables that are adjusted for each simulation of the model are the flux rates with the respective durations at the top of the domain and the soil type that represent the homogeneous media.

### 3.4 INVESTIGATION SCENARIOS

Precipitation events at the CZO site produce varying periods of infiltration and drainage depending on the soil composition, precipitation intensity, and precipitation duration. This study

used different combinations of the three sections of a generalized precipitation event (Figure 3.4) to drive a model-based analysis. The first investigation scenario explores constant infiltration (Figure 3.4, section (2)) under steady-state conditions. The second investigation scenario extends the first by simulating infiltration that goes from hydrostatic to transient and then steady-state conditions followed by drainage (Figure 3.4, section (2), and (3)). The third scenario is similar to the second except that infiltration occurs for a fixed time and does not reach steady-state before drainage begins. The first three scenarios build upon each other to explore PCAP capture behavior under a variety of flow conditions using a small subset of soil types (Table 3.1). The last scenario uses the same conditions as the third scenario, but examines soils across the USDA soil texture triangle.

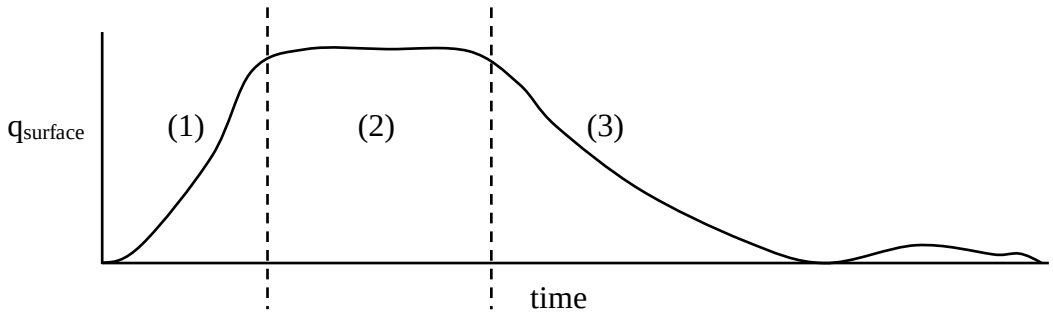


Figure 3.4. Surface flux profile from a typical precipitation event (Hursh and Brater, 1941) showing increasing infiltration (1), constant infiltration (2), and drainage (3).

Simulations of the PCAP involving constant infiltration (Figure 3.4, section (2)) provide the clearest visualization and quantification of convergence or divergence. Simulated top boundary conditions were set to fluxes equal to the hydraulic conductivity for a given soil at pressure heads from 0, -5, -10, -15, -20, -25, and -30 cm. Different fluxes can be applied to different soils with this set of pressure heads because hydraulic conductivity at any given

pressure head varies across soils. These pressures allow for the simulation of precipitation at rates lower than the saturated hydraulic conductivity, avoiding ponding or surface runoff altogether. Initial conditions throughout the domain were set to -30 cm of pressure head to allow a more rapid establishment of steady-state conditions. The initial conditions have no effect on the analyzed results because this investigation is only interested in fluxes under steady-state conditions. Simulations ended when the pressure head distribution remained constant at every location in the domain through time. One simulation was performed for each of the soil categories referenced in Table 3.1 for a total of twelve simulations.

All further investigation scenarios use one day of hydrostatic conditions before applying an infiltration and drainage process. However, the hydrostatic condition used is not a true hydrostatic condition because of the -30 cm pressure head boundary condition from the PCAP. A true hydrostatic condition would generate a linear pressure head profile with depth. The PCAP introduces a rapid pressure head increase nearing the PCAP boundary (38 cm) and a rapid decrease below the PCAP boundary before resuming a gradual linear increase like a normal hydrostatic condition (Figure 3.5). Hydrostatic conditions referenced throughout this study are actually pseudo-hydrostatic, but will still be referenced as hydrostatic for simplicity.

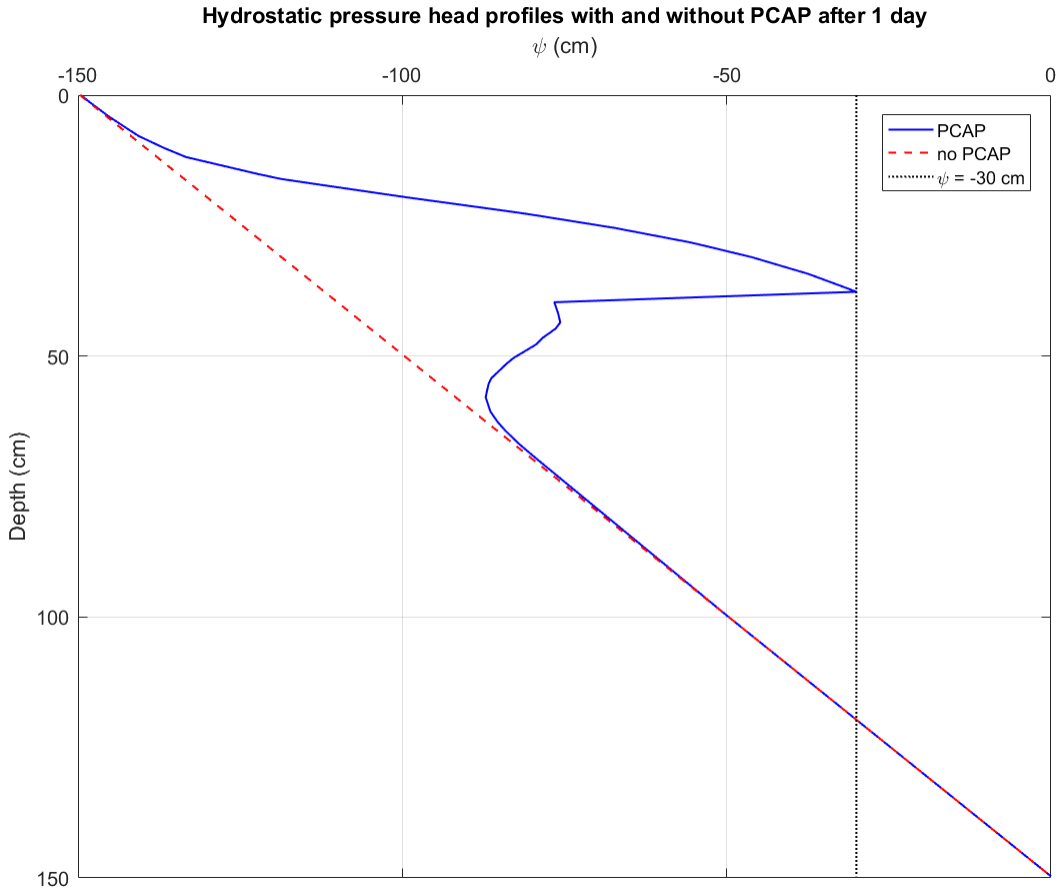


Figure 3.5. Hydrostatic pressure head profiles after one day through a medium without a PCAP and a medium with a PCAP. Pressure head profiles with depth are taken through the middle of the PCAP and at a location 70 cm to the right of the PCAP from a HYDRUS simulation based on Figure 3.3.

The second investigation scenario adds a transient process to see how the capture efficiency of the PCAP varies with time throughout a precipitation event. Initial conditions are set to hydrostatic with 0 cm of pressure head at the bottom of the domain. A constant flux is applied after one day of hydrostatic conditions. Once steady-state has been reached, the flux at the top of the domain is set to zero; the rest of the simulation represents a drainage process. Drainage is simulated for the same amount of time that was required for the infiltration phase to reach steady-state. Simulations did not necessarily reach hydrostatic conditions during the simulated

drainage period. The constant fluxes used are the same as those used in investigation scenario one.

The third scenario builds on the second by simulating flux pulses that are not necessarily long enough in duration to achieve steady-state flow throughout the domain. The flux pulses are simulated for 5, 10, 15, 20, 25, and 30 days for each flux used in the last two scenarios for a total of 36 simulations per soil. Only sand, loam, and clay soils were simulated using the hydraulic parameters from Table 3.1. This set of simulations explores the variation of PCAP capture efficiency in transient conditions as a function of flux duration, flux strength, and soil type.

The objective of the fourth investigation scenario is to determine whether a PCAP in different soils will over- or underestimate the actual flux over the course of a transient event. This investigation starts like investigation three, with one day under hydrostatic conditions followed by a four-day flux pulse and then drainage. The flux needed to produce a capture efficiency of one can be determined iteratively by performing many HYDRUS simulations. The determined flux is then plotted on to the USDA texture triangle. Any flux higher than the plotted value would result in overestimation by the PCAP, while any flux lower would be underestimated. For this investigation, the fluxes needed for a capture efficiency of one for a four-day pulse is determined iteratively across the USDA texture triangle in 10% increments of percent sand, silt and clay, resulting in 66 different soils (Figure 3.1). The soils between the 10% increments were interpolated using the nearest-neighbor scheme and then plotted onto the triangle for full coverage. This results in a lookup triangle that shows the flux needed for a capture efficiency of one for a four-day pulse. A MATLAB script was coded to simulate many models of HYDRUS to generate the lookup triangle. This investigation can be repeated for

different capture efficiencies as well as different pulse lengths to produce more lookup triangles that will aid in capture efficiency estimation.

### 3.5 CAPTURE EFFICIENCY ESTIMATION

The methodology presented previously focuses on determining capture efficiency for various conditions. Capture efficiency allows us to determine the captured flux compared to the actual flux if given a soil type, flux, and flux duration. This can be useful as a forecasting tool to predict which flux events can be captured by the PCAP. Weaker infiltration events will be underestimated, while higher flux events will be overestimated because weaker infiltration events will generate lower maximum pressure heads at depth (Figures 2.10 and 2.12). Water is captured by the PCAP only when pressure heads at depth exceed the pressure head threshold of the PCAP plate. If an infiltration event is stronger (higher flux and longer duration,) it will generate higher pressure heads at depth, therefore, more of the water will be subject to capture, which would yield a higher capture efficiency. Given a soil type and captured flux, the actual flux could be determined iteratively, but this is beyond the scope of this study. Lookup triangles for capture efficiencies of 0.5, 1.0, 1.5, and 2.0 with pulse durations of 2, 4, and 6 days are generated for a total of 12 different conditions. The data points from the 12 lookup triangles are composed of pulse durations, fluxes, and the resulting capture efficiencies. Interpolation can be performed on the data points if soil composition, pulse duration, or flux rate are different than those simulated.

Consider an example of interpolation for the capture efficiency of a silty clay soil with a 10% sand, 50% silt, and 40% clay composition undergoing a flux of 6 cm/day for a pulse duration of 3 days (Figure 3.6).The 12 data points are pulled from all 12 lookup triangles for the soil composition of 10% sand, 50% silt, and 40% clay. The 3-day pulse duration and the flux rate of 6 cm/day form the query point of (3, 6) which falls within one of the triangles in the surface. Linear interpolation is applied at the query point using the points in the surrounding triangle.

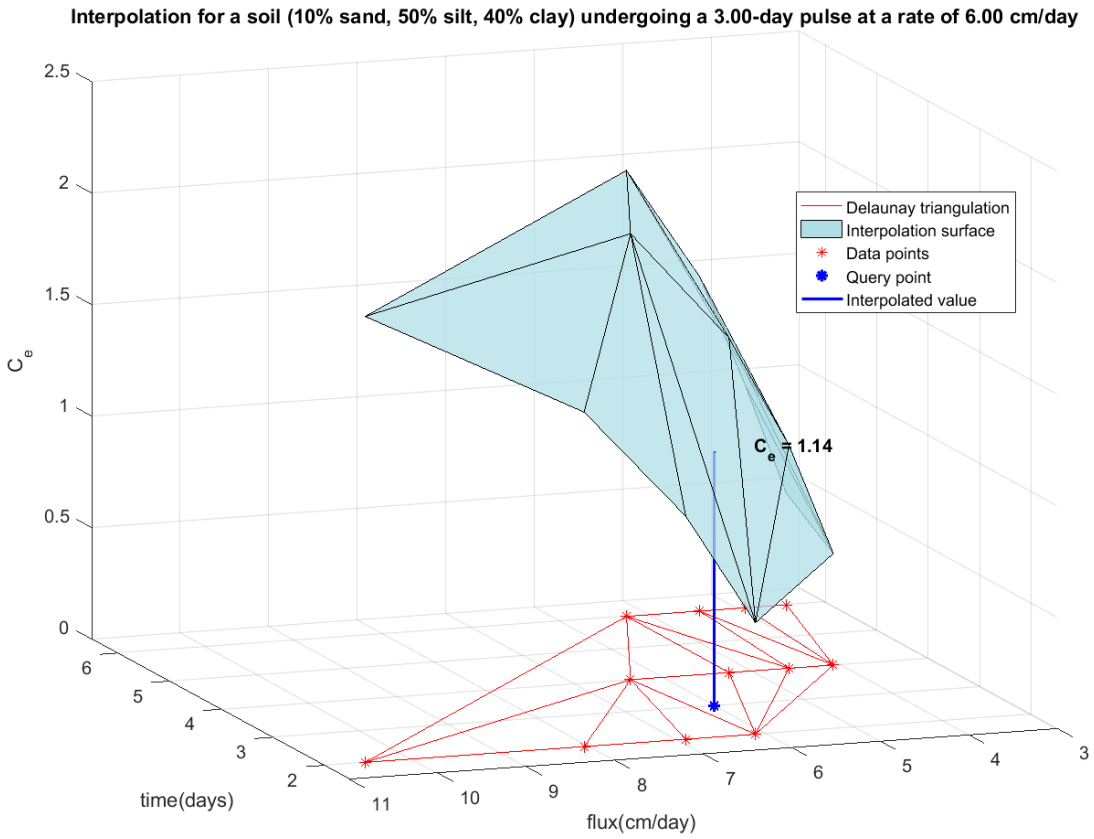


Figure 3.6. Interpolation of capture efficiency for a silty clay soil undergoing a flux of 6 cm/day for a pulse duration of 3 days.

The method used is Delaunay triangulation interpolation. Delaunay triangulation generates a surface from a set of points with the property that no point within the set falls inside the circumcircle of any triangle in the surface (Lee and Schachter, 1980). The circumcircle of a

triangle is a unique circle than intersects each point of the triangle (Figure 3.7). Delaunay triangulation interpolation works by creating the Delaunay triangulation from the set of points, generating an interpolation surface by lifting the vertices of the data points to the corresponding values, and then evaluating the query point on the interpolation surface. The evaluation of the query point involves locating the triangle that encompasses it in the triangulation before applying an interpolation method.

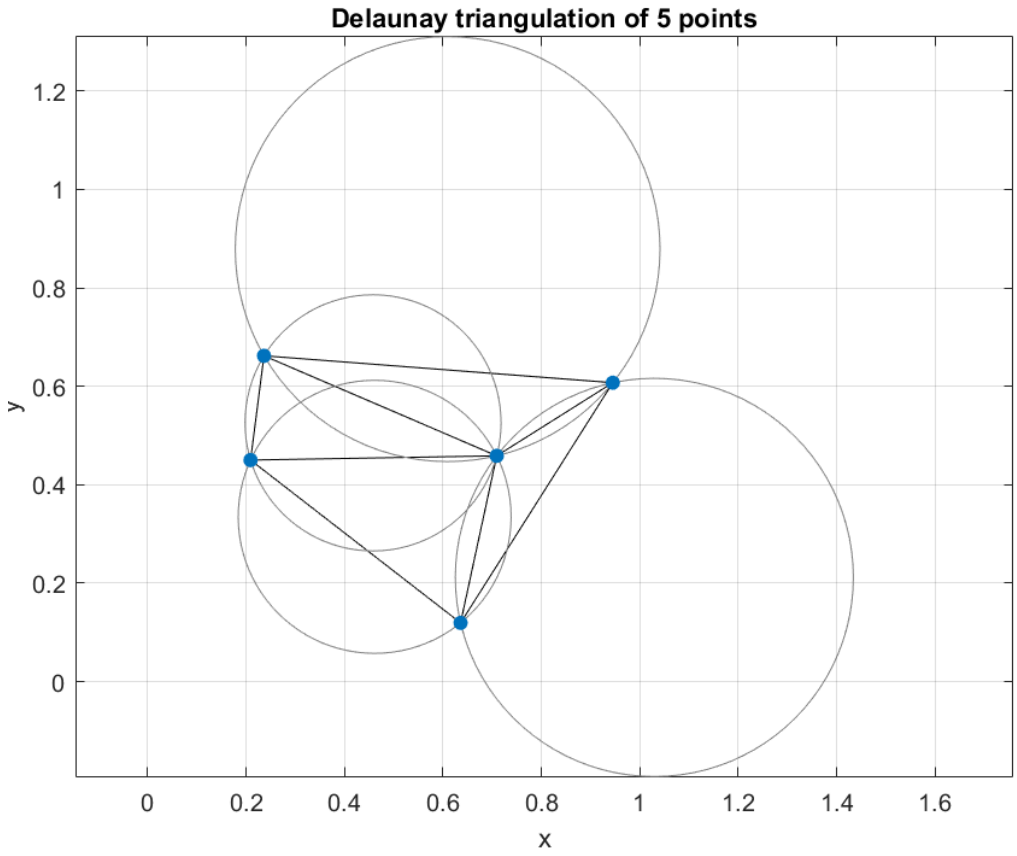


Figure 3.7. Delaunay triangulation of 5 random points showing the circumcircles for each triangle

Query points based on pulse duration and flux rate do not always fall within a triangle or a triangulation surface. Consider a similar example of interpolation for the capture efficiency of a

silty clay soil with a 10% sand, 50% silt, and 40% clay composition undergoing a flux of 6 cm/day, but instead for a pulse duration of 4 days (Figure 3.8). The query point (4, 6) directly falls on a line in between two triangles. Linear interpolation is then applied using the two points that form the line on which that query point lies.

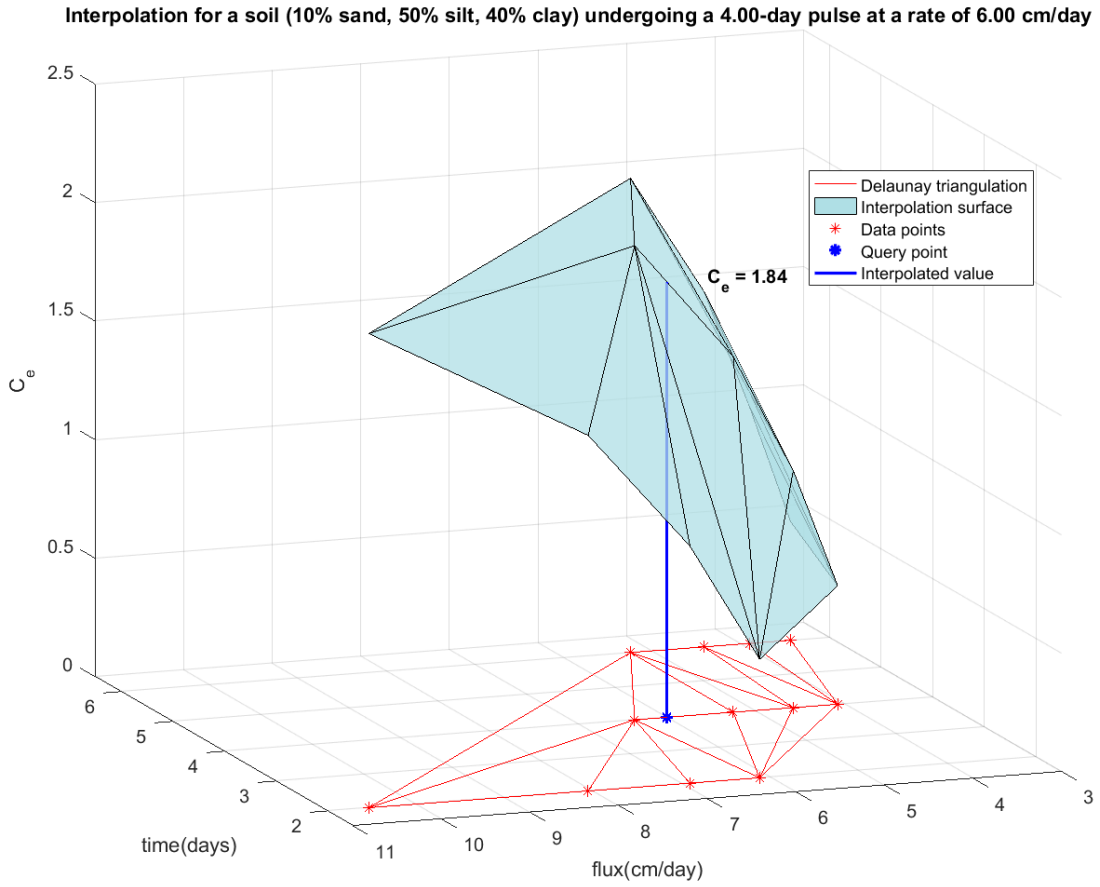


Figure 3.8. Interpolation of capture efficiency for a silty clay soil undergoing a flux of 6 cm/day for a pulse duration of 4 days.

If the query point is not encompassed by the triangulation surface, a nearest neighbor interpolation is performed and the capture efficiency is defined as a limiting value of either 0.5 or 2.0 depending on which corner of the surface the query point is closest to. Consider the same interpolation for a flux rate of 6 cm/day for 4 days, but for sandy soil with a composition of 90%

sand, 0% silt, and 10% (Figure 3.9). The query point (4, 6) for the sandy soil has a pulse duration that falls in range of the pulse durations in the data, but has a flux that is much smaller than the minimum flux of the data points, so the capture efficiency defaults to 0.5.

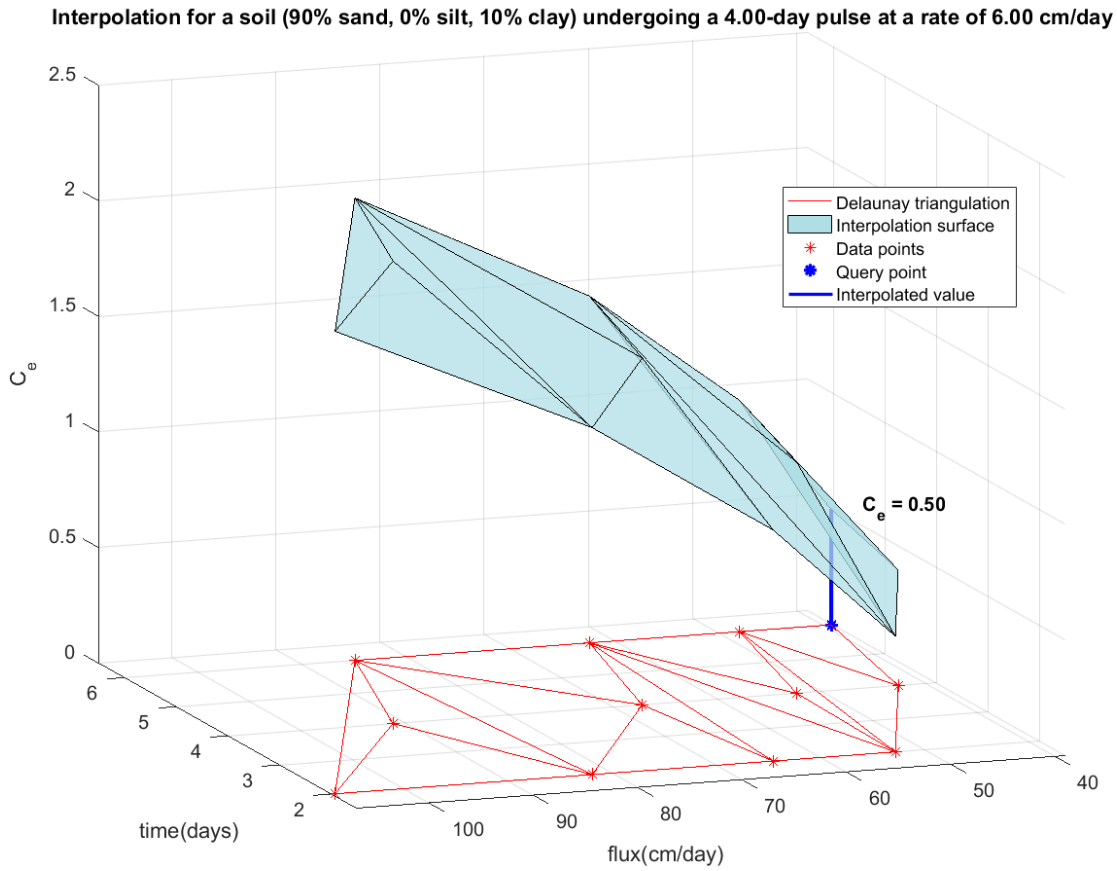


Figure 3.9. Interpolation of capture efficiency for a sandy soil undergoing a flux of 6 cm/day for a pulse duration of 4 days. Query point is outside the minimum of the triangulation range.

Now consider a sandy clay soil with a composition of 30% sand, 10% silt, and 60% clay (Figure 3.10). The same query point (4, 6) has a pulse duration in range of the data points, but the flux is greater than the maximum flux in the data. In this case, the capture efficiency defaults to 2.0. The default capture efficiencies of 0.5 and 2.0 are selected because they are the maximum and minimum values generated from the limited set of lookup triangles

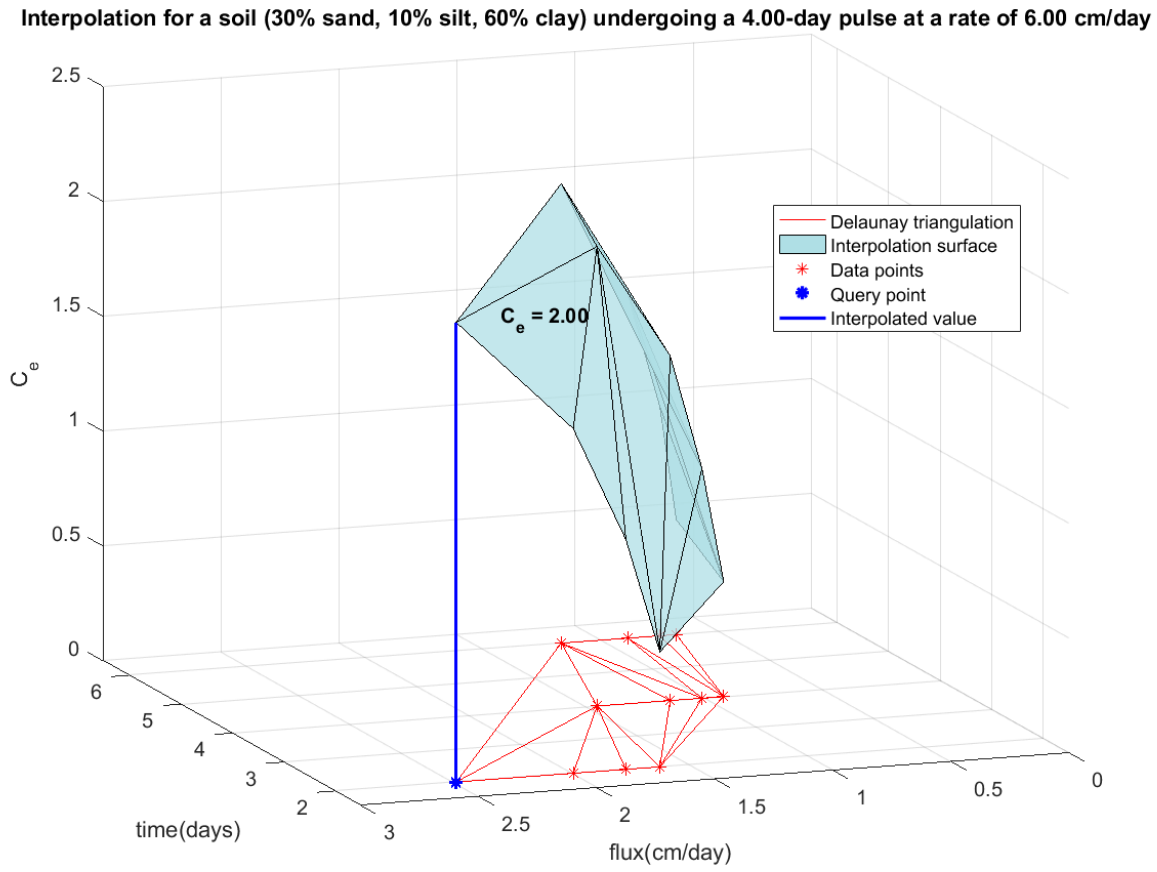


Figure 3.10. Interpolation of capture efficiency for a sandy clay soil undergoing a flux of 6 cm/day for a pulse duration of 4 days. Query point is outside the maximum of the triangulation range.

To test the performance of interpolation, I compared capture efficiency values determined by interpolation with those based on HYDRUS simulations directly. The metric for performance is the difference between the interpolated capture efficiency with a HYDRUS-based capture efficiency (Eq. 3.6):

$$C_{e\ interpolated} - C_{e\ HYDRUS} = error \tag{3.6}$$

HYDRUS capture efficiency is obtained by running a simulation with the same parameters of pulse duration, flux, and soil type. I want to select pulse duration and flux rate pairs that are encompassed by the Delaunay triangulation surface for the most number of soils in the lookup

triangle. A pulse duration of 4 days is selected because it falls between the minimum and the maximum pulse durations (2 and 6 days) used in this study. Flux rates of 2, 4, 6, and 10 cm/day are selected as test fluxes because they fall in range of the data for 15, 14, 10, and 8 different soils, respectively, on the 4-day lookup triangles (Figure 3.11).

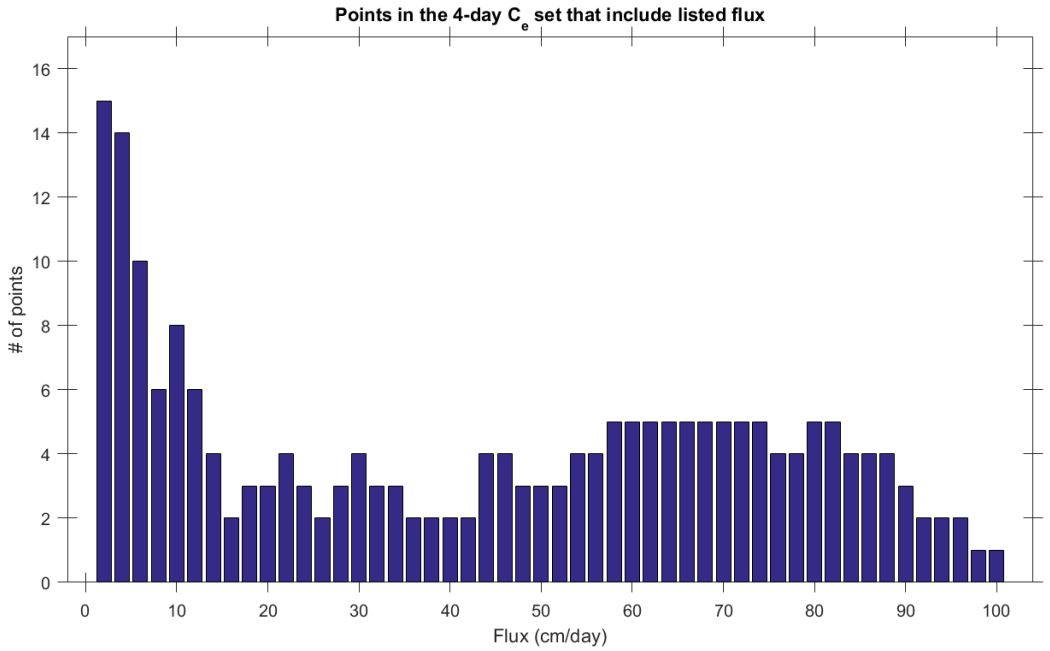


Figure 3.11. Number of points or soils in the 4-day pulse lookup triangle sets that encompass the specified flux

Error can be visualized on the texture triangle like the flux lookup triangles generated previously. Error triangles are produced by calculating the differences between the capture efficiencies from interpolations and HYDRUS simulations. This is performed across the soils on the texture triangle in 10% increments for a total of 66 different comparisons. A nearest-neighbor interpolation is then used to fill in the rest of each triangle. Four error triangles are produced based on the selected pulse duration and flux rates described previously to evaluate interpolation across different conditions. One example of an error triangle is shown for illustration (Figure 3.12). All four triangles are discussed in a later section.

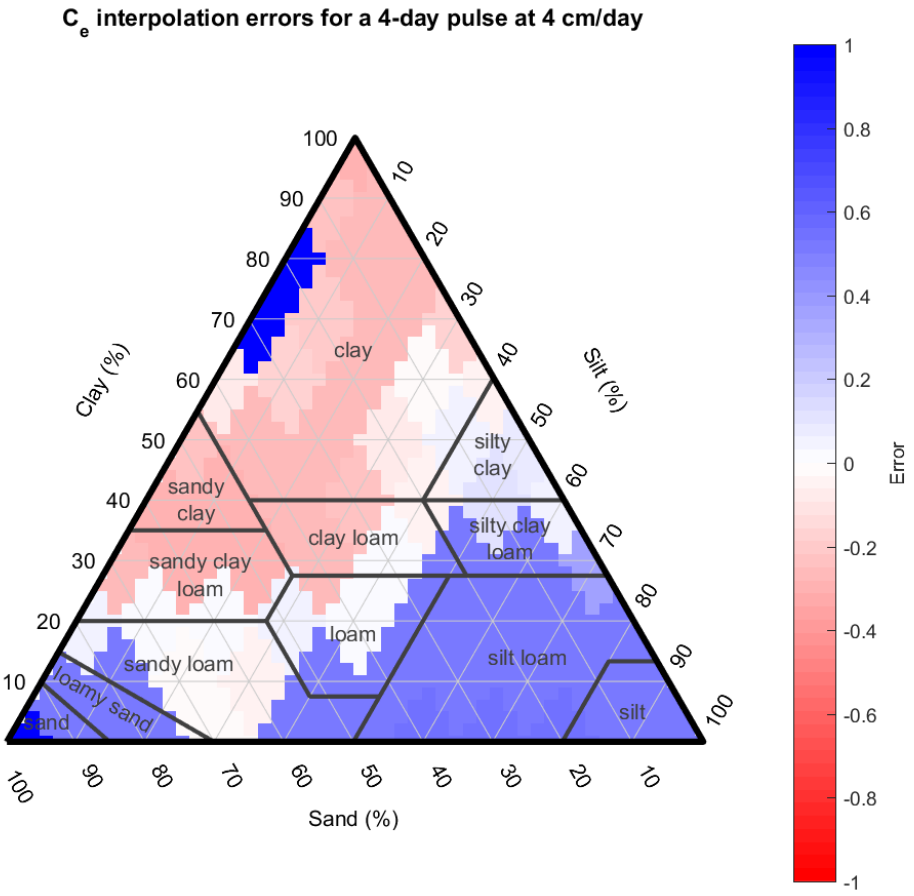


Figure 3.12. An example error triangle generated from the query point formed from a 4-day pulse with a 4 cm/day rate.

## 4 RESULTS AND ANALYSIS

The objective of this study is to perform a model-based analysis of PCAP capture efficiency of the PCAPs and to interpret field measurements at the CZO site. Numerical analysis is presented in the following sections. Analysis of field measurements is presented in the last section. The first set of figures shows the general behavior of PCAP capture within a loam soil. The figures that follow correspond to each investigation scenario described in the previous sections.

## 4.1 PCAP CAPTURE

The first step in the analysis was to see if convergence or divergence occurs for the simplest conditions. The fluxes used the initial simulations are 9.67, 3.21, 0.91, and 0.26 cm/day. This set of fluxes corresponds to unsaturated hydraulic conductivities for a loam at the pressure heads of -5, -15, -30, and -50 cm. Fluxes greater or less than the unsaturated hydraulic conductivity at -30 cm would converge or diverge, respectively, due to the -30 cm constant pressure head boundary condition at the PCAP. Larger differences in pressure heads between the ground surface and the -30 cm boundary at the PCAP resulted in more pronounced convergence or divergence. The simulation results for fluxes 9.67 cm/day (Figure 4.1, a)) and 3.21 cm/day (Figure 4.1, b)) show the flow lines converging toward the plate. The fluxes of 9.67 cm/day and 3.21 cm/day for a loam corresponds to the unsaturated hydraulic conductivity at -5 and -15 cm of pressure head. The gradient is larger for the higher flux, corresponding to -5 cm of pressure head, than for the lower flux associated with -15 cm of pressure head. Therefore, there is more convergence for the higher flux. Neither convergence nor divergence occurs for the simulation with the flux set to the unsaturated hydraulic conductivity at -30 cm of pressure head (Figure 4.1, c)) because there is no pressure head gradient as expected.

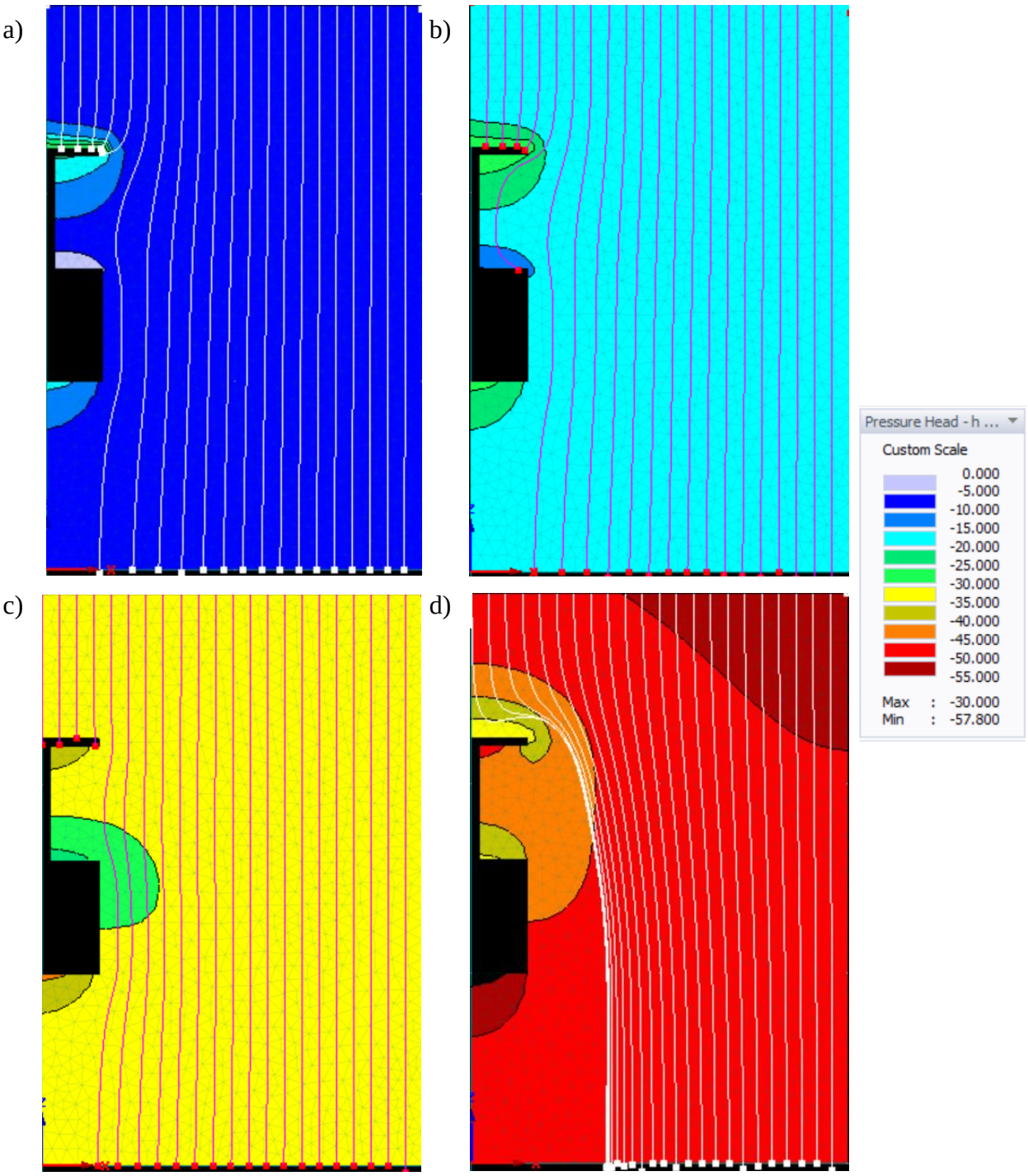


Figure 4.1. HYDRUS (2D/3D) flowline and pressure head results of PCAP capture for a loam soil going through steady-state infiltration at constant fluxes equal to unsaturated hydraulic conductivities at a) -5, b) -15, c) -30, and d) -50 cm of pressure head.

Divergence occurs for the simulation with the flux set to the unsaturated hydraulic conductivity at -50 cm of pressure head (Figure 4.1, d)) because the PCAP plate is maintained at a higher pressure head than the soil under these conditions.

## 4.2 STEADY-STATE INFILTRATION

Investigation scenario one extends the initial analysis of PCAP capture (Figure 4.1) by repeating the simulations across all of the soils in Table 3.1. Based on the results for investigation scenario one (Figure 4.2), the PCAP generally overestimates flux (capture efficiencies are greater than one). The capture efficiency gets smaller as the prescribed flux decreases (pressure head in the soil becomes more negative). At very low fluxes, the PCAP rejects flux, represented by capture efficiencies less than one. Coarser textures (e.g. sand) yielded lower capture efficiencies. Simulations with finer textures (e.g. clays) led to larger capture efficiencies. Coarser soils have a larger hydraulic conductivity than finer soils for pressure heads from -5 cm to about -25 cm (Figure 2.5), so the PCAP head boundary has less impact on the incoming flux (capture efficiency is smaller). However, for pressure heads less than -25 cm, coarser soils have larger capture efficiencies because finer soils have larger hydraulic conductivities at pressure heads smaller than -25 cm. Larger capture efficiencies were produced by simulations that included higher fluxes and coarser soils. Lower fluxes and finer soils led to smaller capture efficiencies. The first investigation implies that flux strength and soil texture directly impact the magnitude of capture efficiency under steady-state conditions.

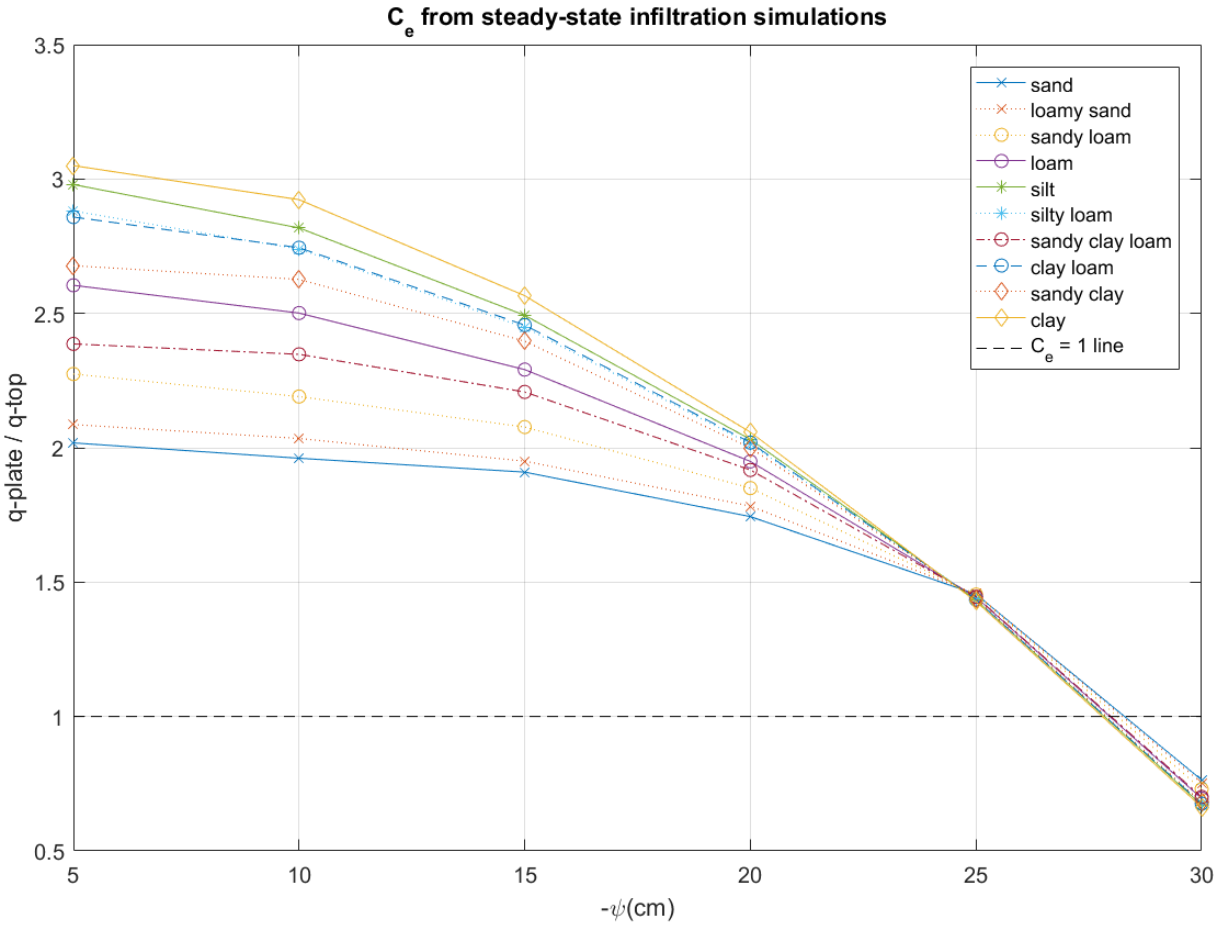


Figure 4.2. $C_e$ for steady-state infiltration simulations for each soil in Table 3.1. Silty clay loam and silty clay soils are not included because their simulations did not converge.

## 4.3 TRANSIENT AND STEADY-STATE INFILTRATION WITH DRAINAGE

The results of investigation scenario one give a general idea of PCAP capture behavior under steady-state conditions. Investigation scenario two is more representative of actual precipitation events because it includes both infiltration and drainage throughout a transient event. Capture efficiencies for the rest of the simulations in this study are calculated using cumulative fluxes, defined as:

$$C_e = \int_0^{\infty} \frac{q_{PCAP}(t)}{q_{obs\_node}(t)}\, dt \tag{4.1}$$

Cumulative fluxes must be compared at the same spatial location because this study is interested in exploring how the PCAP affects flux within a medium. A separate one-dimensional model of the same specifications as the two-dimension axisymmetric model was developed in HYDRUS-1D. An observation point was placed at the same location as the top of the PCAP from the HYDRUS (2D/3D) model. The cumulative flux through the PCAP in the HYDRUS (2D/3D) model is compared to the cumulative flux through the observation node in the HYDRUS-1D model in each simulation to account for the time delay of flux between the ground surface and the PCAP under transient conditions.

The inclusion of transient processes with infiltration and drainage results in time-varying pressure heads throughout the medium. Consider PCAP capture through a loam soil, initially under one day of hydrostatic conditions with 0 cm of pressure head at the bottom of the domain, that experiences five days of infiltration at 9.67 cm/day ($\psi$ = -5 cm) followed by five days of drainage (Figure 4.3). For a loam soil, the unsaturated hydraulic conductivity at -5 cm of pressure head is equal to 9.67 cm/day. After the first day of hydrostatic conditions, infiltration begins and the pressure head at the ground surface increases to -5 cm of pressure head. The applied flux is large enough for the ground surface pressure head to build up to -5 cm in the five-day infiltration period. The pressure head just above the PCAP has a slight delay after infiltration begins before increasing to a pressure head less than -5 cm of pressure head. The pressure head just above the PCAP does not reach to -5 cm because of the -30 cm pressure head boundary at the PCAP. The pressure heads then remain constant for the duration of infiltration. When drainage begins on the sixth day, the pressure heads at the ground surface and above the PCAP begin to decline. The pressure head above the PCAP declines at a slower rate because the water between the plate and the surface has yet to drain.

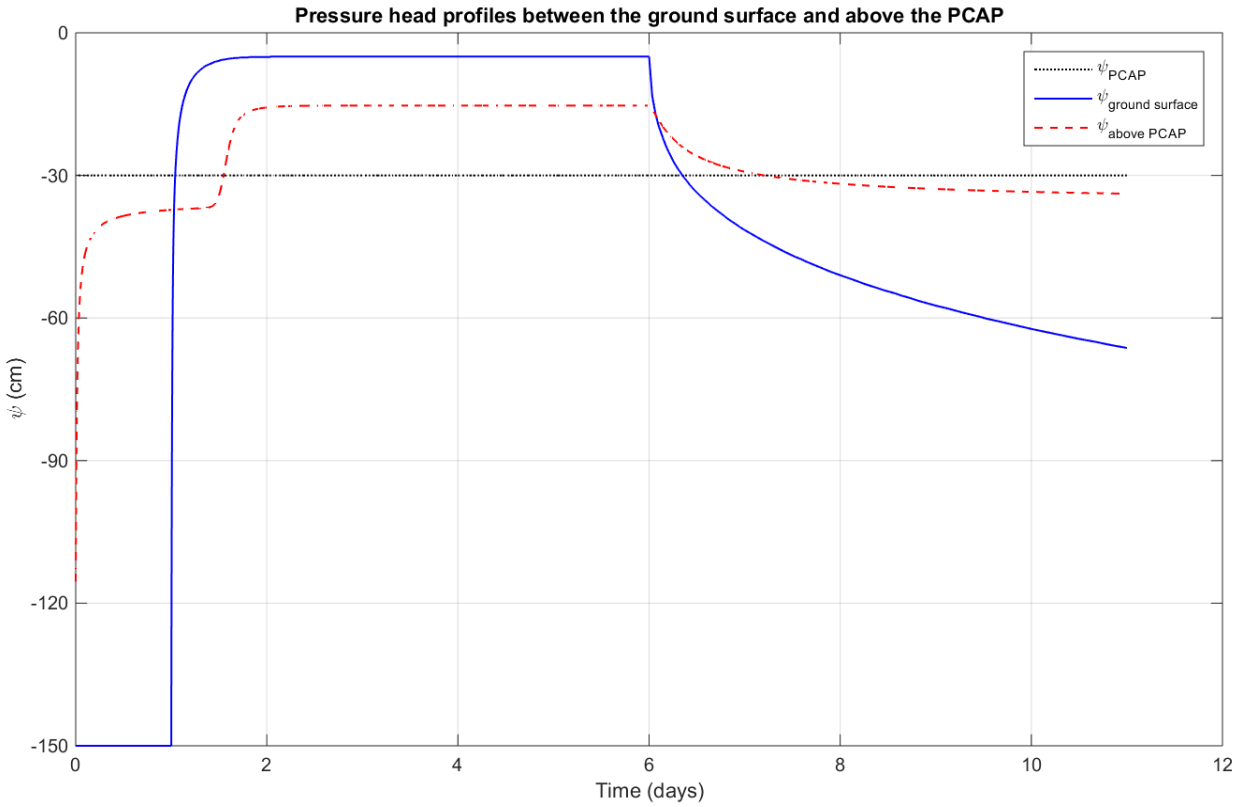


Figure 4.3. Pressure head profiles for a loam soil initially under hydrostatic conditions for 1 day before undergoing infiltration from a 5-day flux at a rate of 9.67 cm/day (ψ = -5 cm) followed by drainage for 5 days. Profiles correspond to the pressure head at the PCAP (black), ground surface (blue), and just above the PCAP (red).

The capture efficiencies of investigation scenario two (Figure 4.5) are generally smaller than those of investigation scenario one (Figure 4.2). The inclusion of transient conditions in the second investigation yielded smaller capture efficiencies because the captured flux varied in time with the maximum occurring during steady-state flow (Figure 4.4). However, this difference only falls in the range of 0.65% to 6.87%. The differences in capture efficiencies between the scenarios depend on how gravity-dominated flow through the soil is. As a soil saturates from infiltration, gravity progressively becomes the dominant force driving water movement. Certain soils are described to be more gravity-dominated than others if they can transmit water more easily when gravity becomes the main force in the infiltration process. Silt is the least gravity-

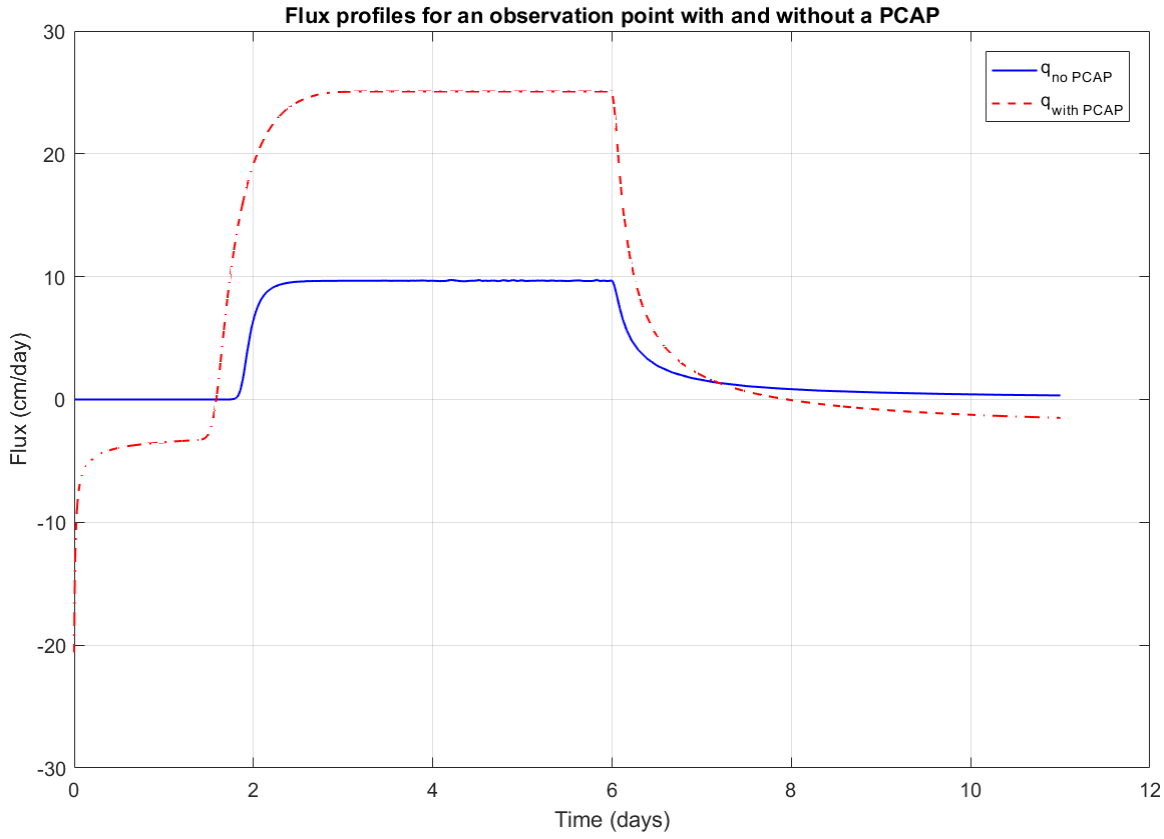


Figure 4.4. Flux profiles for a loam soil initially under hydrostatic conditions for 1 day before undergoing infiltration from a 5-day flux at a rate of 9.67 cm/day ($\psi$ = -5 cm) followed by drainage for 5 days at an observation point located 38 cm below the surface.

dominated soil in investigation two; it has the largest difference in capture efficiencies. Simulations with sand (more gravity-dominated) led to no difference in capture efficiencies. Fluxes at pressure heads less than -30 cm were not simulated for this investigation because the PCAP would not have captured any flux.

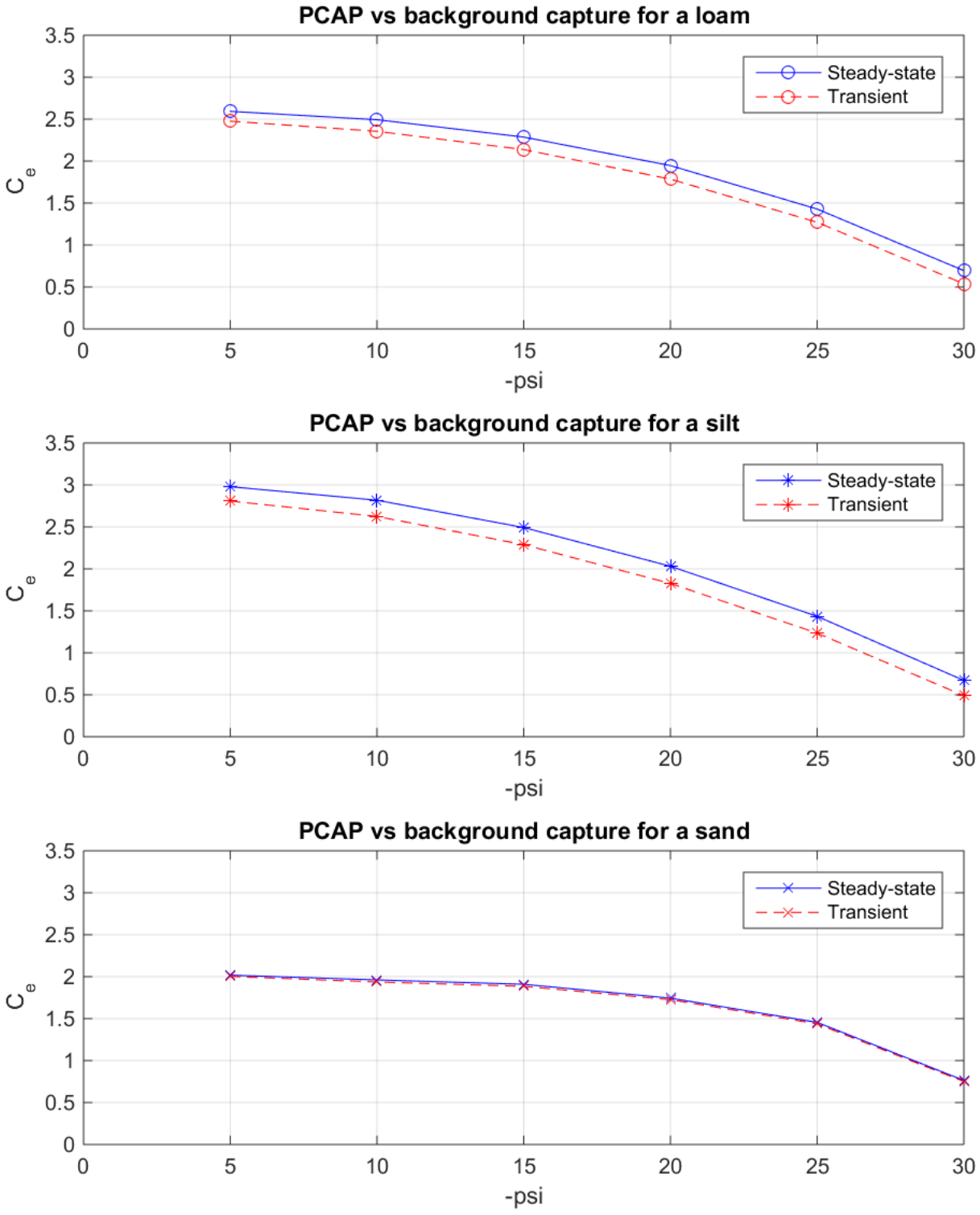


Figure 4.5. Investigation one (steady-state) and investigation two (transient) comparisons of $C_e$ for loam, silt, and sand.

## 4.4 TRANSIENT-ONLY INFILTRATION WITH DRAINAGE

Investigation scenario two may be more representative of actual PCAP capture scenarios, but infiltration doesn't always reach a steady-state condition before proceeding to the drainage phase of the event. Precipitation events can send infiltration pulses that don't reach steady-state prior to drainage. Investigation scenario three explores the effects of different infiltration pulse lengths on capture efficiency.

The introduction of pulse periods for infiltration results in lower capture efficiencies for some of the simulated fluxes. The pressure head at the ground surface needs a sufficient amount of time to build up to pressure head at the applied flux. Lack of pressure head buildup at the ground surface leads to less pressure head above the PCAP throughout the infiltration and drainage event, which leads to smaller capture efficiencies.

Consider PCAP capture similar through a loam soil, initially under one day of hydrostatic conditions with 0 cm of pressure head at the bottom of the domain, that undergoes five days of infiltration at 1.33 cm/day ($\psi$ = -25 cm) followed by five days of drainage (Figure 4.6). Infiltration begins after the first day and the pressure head builds up immediately at the ground surface and then above the PCAP after a slight delay. The pressure heads keep building for the duration of the pulse before stopping at day six. The five-day infiltration at 1.33 cm/day does not give the pressure head enough time to reach -25 cm at depth. The pressure head just above the PCAP spends a small amount of time at -30 cm of pressure head. This leads to no pressure head gradient to the PCAP because of the -30 cm pressure head boundary. No flux gets captured even though the applied flux was greater than -30 cm of pressure head. The five-day infiltration period is insufficient for a flux of 1.33 cm/day, but larger fluxes such as the previously simulated 9.67 cm/day (Figure 4.3) are not affected by the shorter infiltration periods. If the flux of 1.33 cm/day

were to be applied for a longer duration than the five-day infiltration period, flux may actually get captured. This is because the pressure head at depth is dependent on the duration of applied flux (Figure 2.8). Given enough time, the pressure head at depth will approach the pressure head of the applied flux at the surface, which would yield higher capture efficiency.

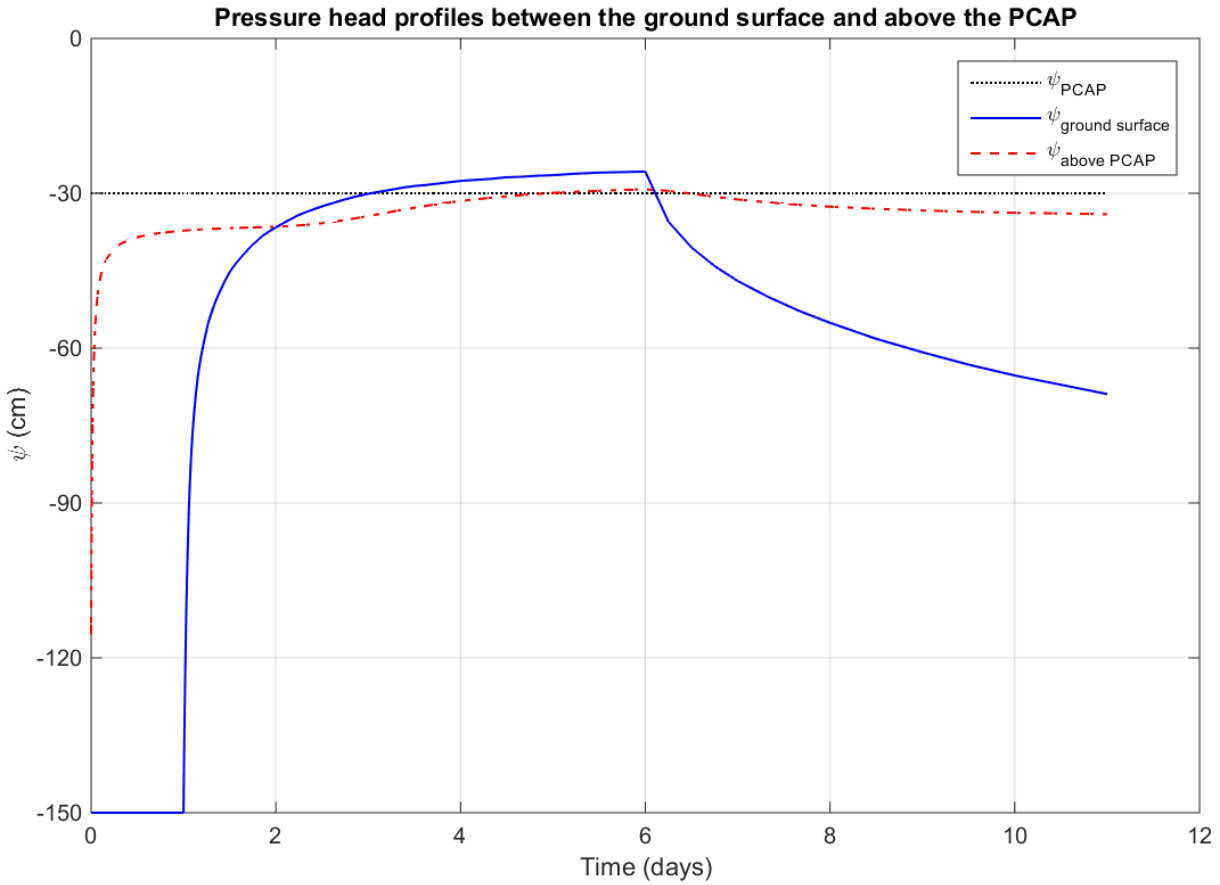


Figure 4.6. Pressure head profiles for a loam soil initially under hydrostatic conditions for 1 day before undergoing infiltration from a 5-day flux at a rate of 1.33 cm/day (ψ = -25 cm) followed by drainage for 5 days. Profiles correspond to the pressure head at the PCAP (black), ground surface (blue), and just above the PCAP (red).

The results of investigation scenario three (Figure 4.7) show that capture efficiencies greater than one tend to occur at larger fluxes with longer durations. Smaller fluxes with shorter durations led to capture efficiencies less than one. Mixed combinations of flux strength and duration led yielded capture efficiencies that either overestimate or underestimate. The results in

the third investigation remain consistent with the first two investigations with respect to the effects of flux strength and soil type. Higher fluxes and coarser soils still led to larger capture efficiency. Smaller capture efficiencies still resulted from lower fluxes and finer soils. Longer pulse durations generally yielded larger capture efficiencies. Some of the simulations yielded capture efficiency values near or at zero, especially those with short pulse durations and lower fluxes. Comparisons to steady-state capture efficiencies (Figure 4.5) also remained consistent for this investigation (Figure 4.8) with sand, loam, and silt yielding the least to most error, respectively. Simulations for fluxes associated with pressure heads less than -30 cm were not performed because their resulting capture efficiencies would be zero, even for steady-state conditions.

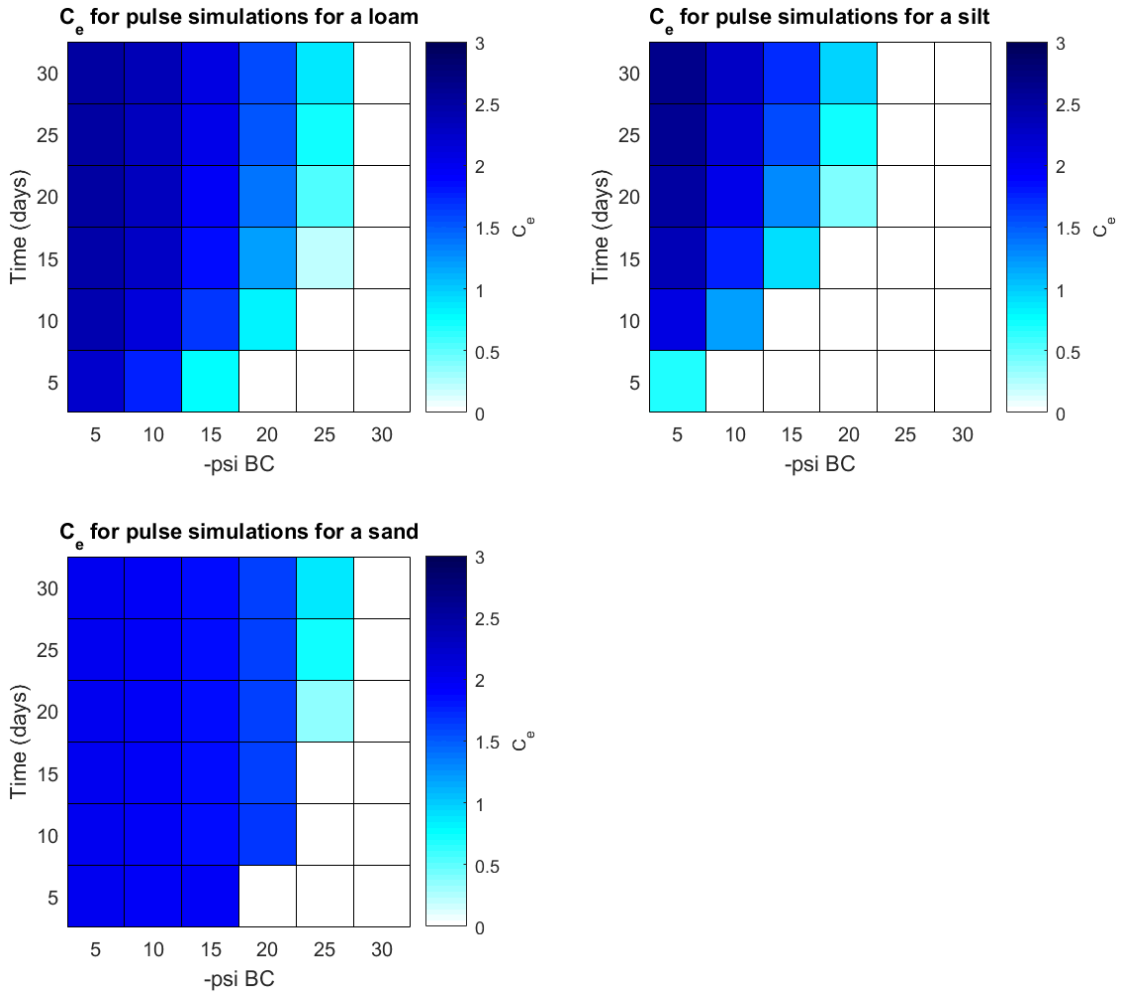


Figure 4.7. $C_e$ for transient flux pulses for a loam, silt and sand at fluxes equal to unsaturated conductivity at pressure heads at -5, -10, -15, -20, -25, and -30 cm for infiltration durations of 5, 10, 15, 20, 25, and 30 days.

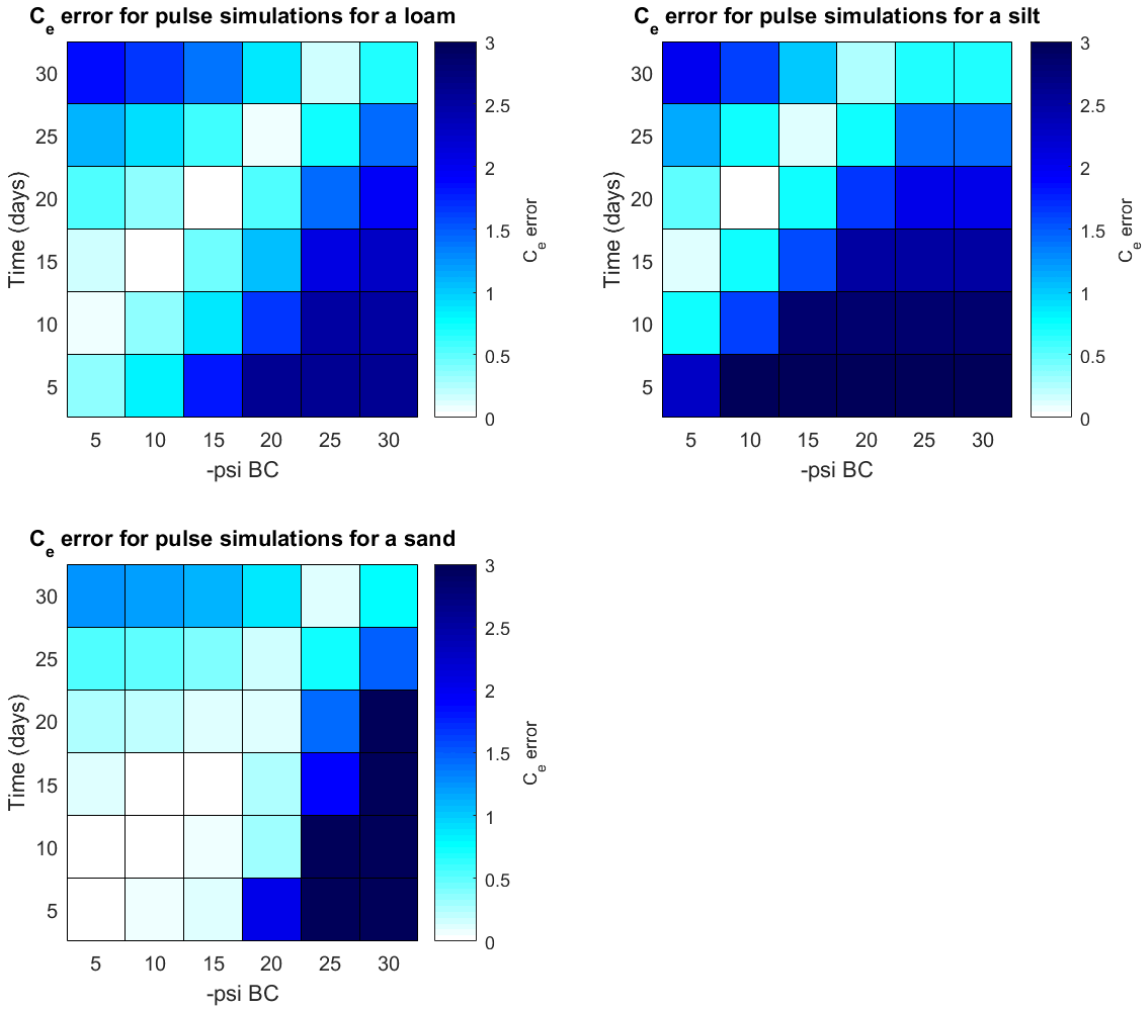


Figure 4.8. $C_e$ error for transient flux pulses for a loam, silt and sand at fluxes equal to unsaturated conductivity at pressure heads at -5, -10, -15, -20, -25, and -30 cm for infiltration durations of 5, 10, 15, 20, 25, and 30 days. Error is calculated as the difference between the steady-state $C_e$ and the $C_e$ from the transient pulse simulations.

## 4.5 CAPTURE EFFICIENCY LOOKUP TRIANGLES

Capture efficiency is dependent on the precipitation event and the soil type based on the results shown for the previous investigations (Figures 4.1, 4.2, 4.5, and 4.7). The fourth investigation explores the idea of determining the flux required to produce a specific capture efficiency, given a pulse duration and soil type. A lookup triangle that shows the flux required for a capture efficiency of 1.0 with a 4-day pulse is produced (Figure 4.9) as a starting point in the investigation.

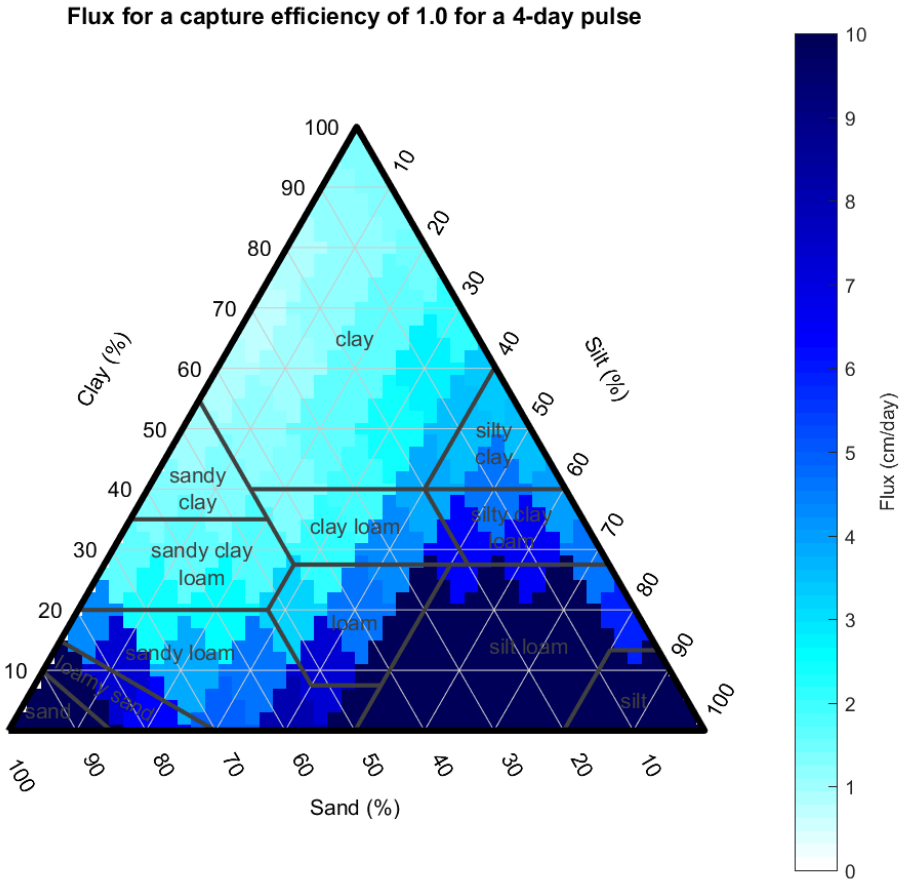


Figure 4.9. Flux lookup triangle for a $C_e$ of 1.0 for a 4-day pulse.

The fluxes plotted on the texture triangle can be used as reference fluxes for that specific soil assuming a 4-day flux duration. Any flux greater than the reference flux would result in

overestimation. Fluxes less than the reference flux would lead to underestimation. Siltier soils appear to require the largest fluxes to acquire a capture efficiency of one. To get near a capture efficiency of one, the fluxes for the soil need to be close to the unsaturated hydraulic conductivities between -20 and -30 cm of pressure head. This is because of the -30 cm pressure head boundary condition at the PCAP. Silt has the highest hydraulic conductivity at pressure heads in the in the range of -20 to -30 cm, by about an order of magnitude, compared to sand and clay (Figure 2.5).

Lookup triangles for capture efficiencies of 0.5, 1, 1.5, and 2.0 are each reproduced for the pulse durations of 2, 4, and 6 days (Figures 4.10, 4.11, and 4.12). The selected sets of capture efficiencies and pulse durations are representative of more typical precipitation events. The color axis for flux was limited up to a maximum of 10 cm/day to show the variation across the triangles. Some of the larger fluxes actually exceed 10 cm/day, reaching almost 100 cm/day.

The lookup triangles reveal several consistent trends that build upon the previous investigations with respect to flux and soil type. The first is that larger target capture efficiencies require larger fluxes. This is shown by the increasing presence of darker cells within each triangle with the same pulse duration (panels a through d on Figures 4.10, 4.11, and 4.12). Second, the shorter the pulse, the larger the required flux to reach a given capture efficiency. This is also shown by the increasing number of darker cells when comparing a triangle to another with the same target capture efficiency (Figures 4.10, 4.11, and 4.12). The resulting set of lookup triangles encompasses the all of the analyses performed in this study. Additional lookup triangles could be produced to represent site-specific conditions.

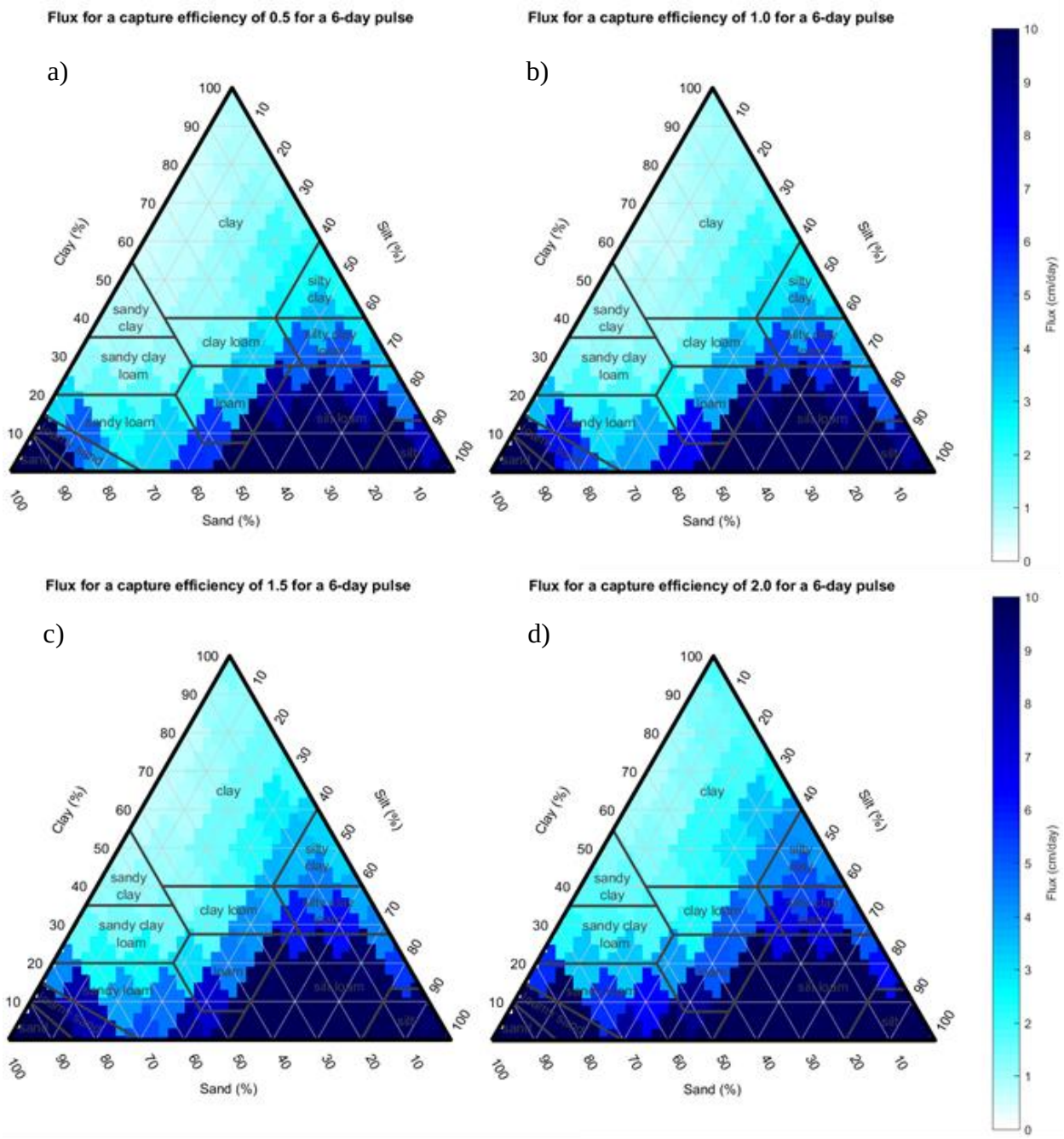


Figure 4.10. Lookup triangles for a 6-day pulse for $C_e$ of a) 0.5, b) 1.0, c) 1.5, and d) 2.0.

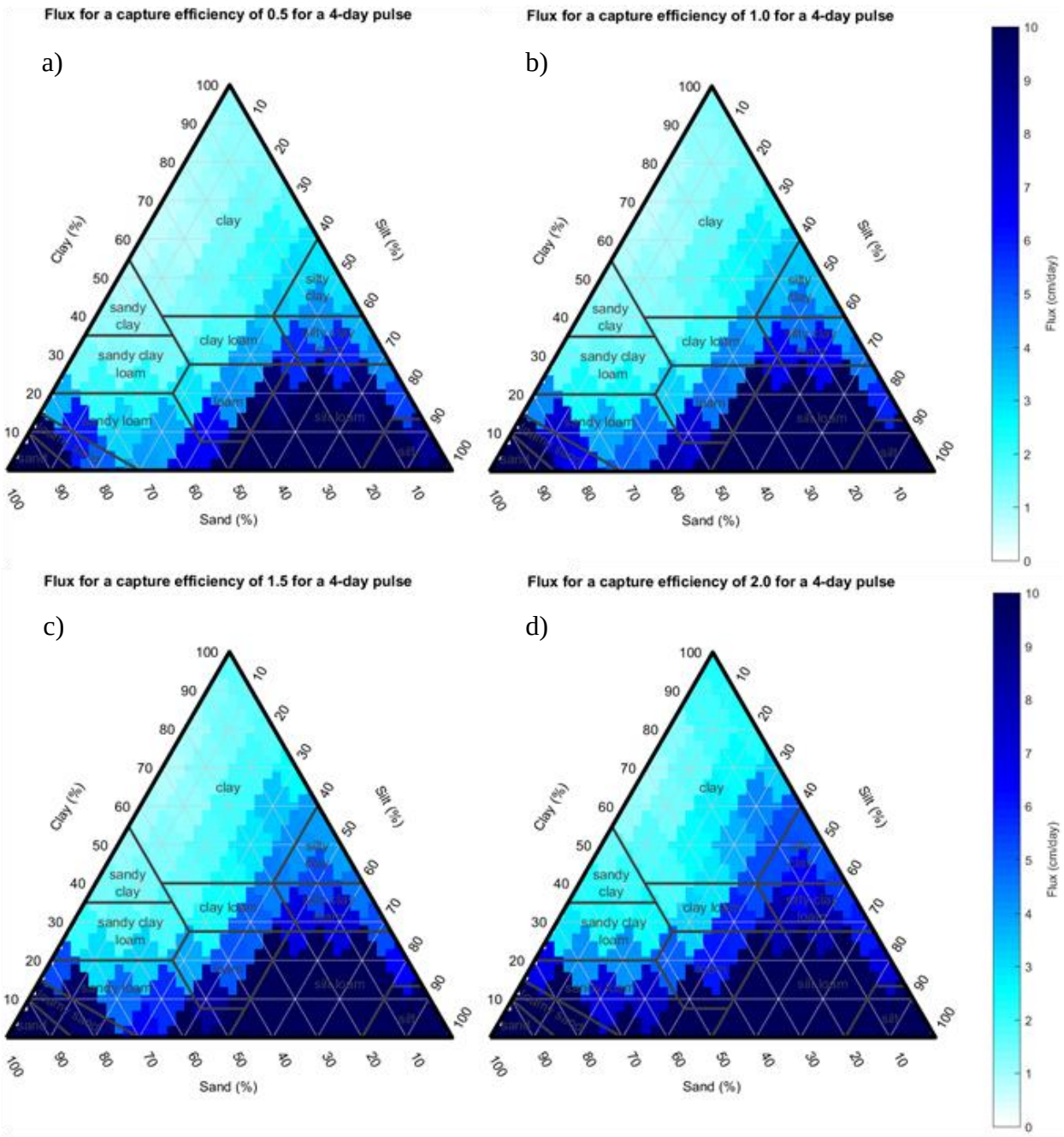


Figure 4.11. Lookup triangles for a 4-day pulse for $C_e$ of a) 0.5, b) 1.0, c) 1.5, and d) 2.0.

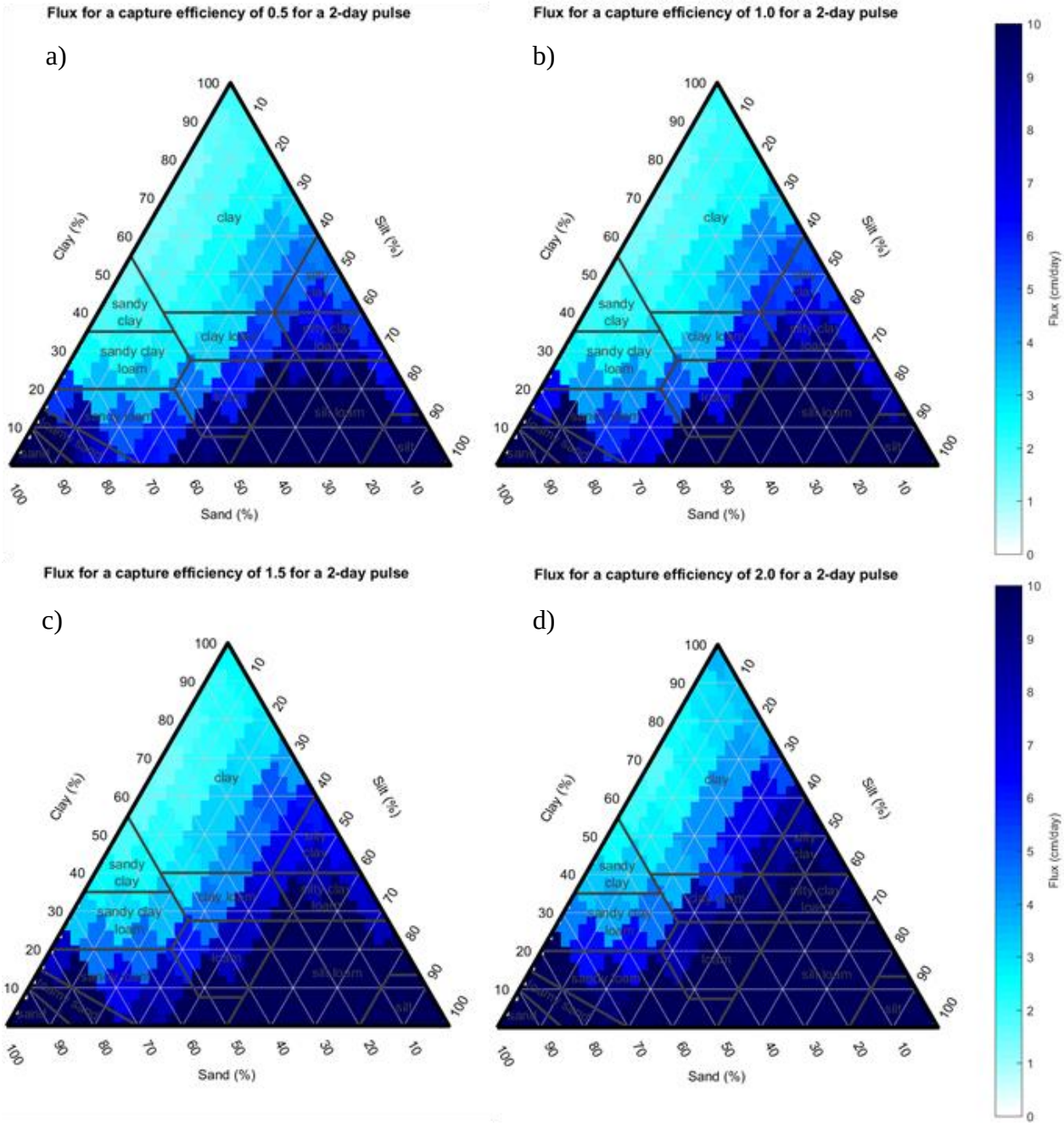


Figure 4.12. Lookup triangles for a 2-day pulse for $C_e$ of a) 0.5, b) 1.0, c) 1.5, and d) 2.0.

## 4.6 CAPTURE EFFICIENCY INTERPOLATION

The 12 lookup triangles generated (Figures 4.10, 4.11, 4.12) provide a dataset that can be used to estimate capture efficiency for other conditions. Capture efficiency can be estimated using Delaunay triangulation interpolation with a given flux rate, pulse duration, and soil type. The performance of the interpolation method is tested by comparing the estimated capture efficiency to a simulated capture efficiency of the same conditions. For this study, four sets of conditions are tested to see how the interpolation performs across the soil texture triangle. Fluxes of 2, 4, 6, and 10 cm/day for a pulse duration of 4 days are used as conditions for interpolation in addition to using all the soils in the texture triangle in 10% increments. This results in the production of error triangles representing the difference of capture efficiencies between interpolation and simulation (Figure 4.13).

Query points for interpolation are formed by flux rates and durations. Query points that fall within a triangulation surface for a soil should result in a small amount of error. For a 4-day pulse duration, the fluxes of 2, 4, 6, and 10 cm/day form the query points (4, 2), (4, 4), (4, 6), and (4, 8). Those query points have 15, 14, 10, and 8 triangulation surfaces, respectively, that encompass them (Figure 3.11). The overall error increases when looking at the error triangles (panels a through d on Figure 4.13). This is expected because the number of surfaces that encompass each query point decreases. The flux rate of 2 cm/day for the 4-day pulse (2, 4) yields the lowest error, while the flux rate of 10 cm/day for the 4-day pulse (10, 4) yields the highest error.

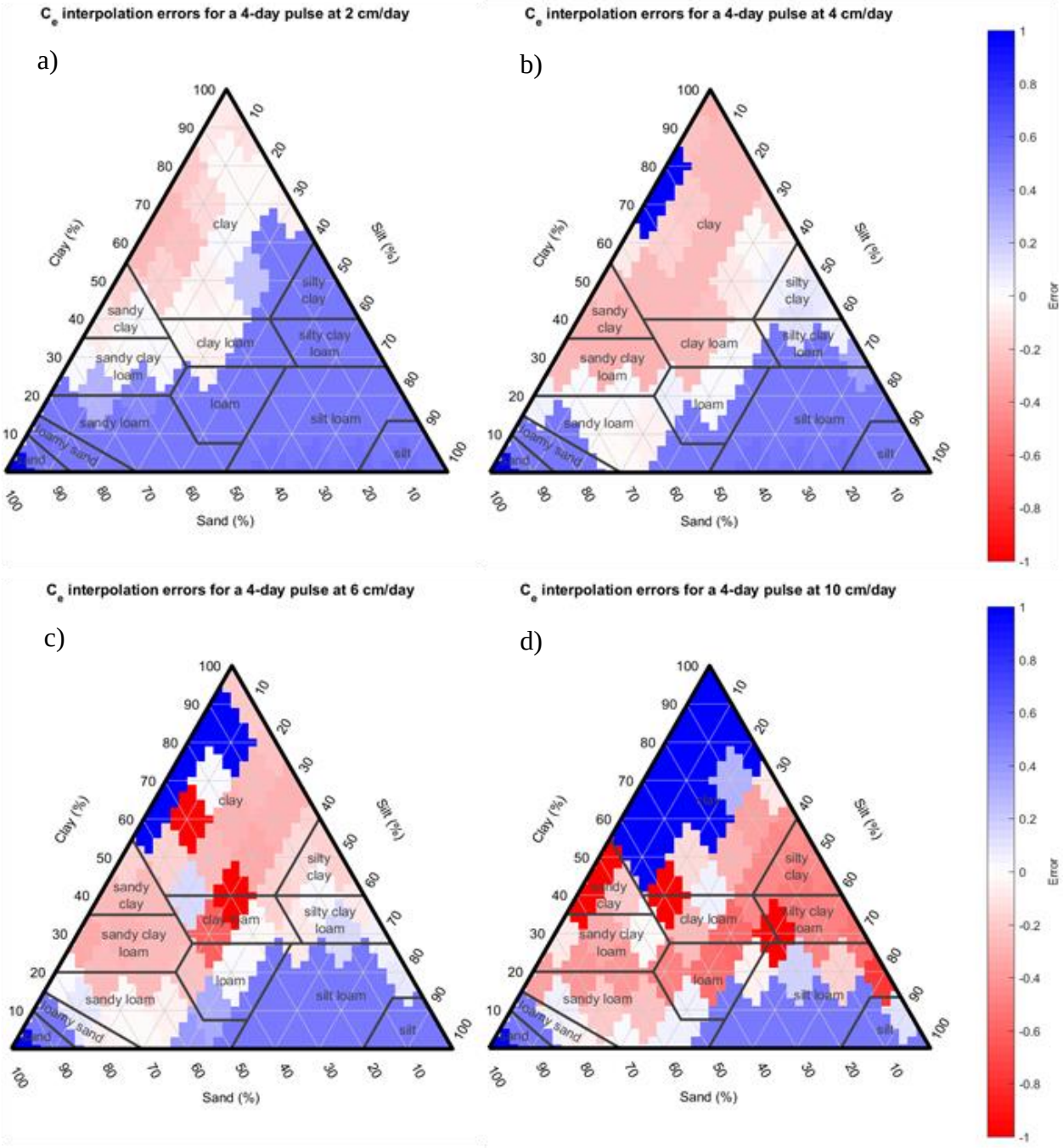


Figure 4.13. $C_e$ interpolation errors for simulations at a) 2, b) 4, c) 6, and d) 10 cm/day for a pulse duration of 4 days.

The specific case for a flux rate of 6 cm/day for a duration of 4 days was examined for the soil compositions of silty clay (10% sand, 50% silt, 40% clay), sandy (90% sand, 0% silt, 10% clay), and sandy clay (30% sand, 10% silt, 60% clay) soils. The query point formed (4, 6) falls within the triangulation surface for the silty clay soil, but falls outside the minimum and maximum points on the sandy and sandy clay soil surfaces (Figures 3.8, 3.9, 3.10). The interpolation is expected to have the least error on the silty clay soil. This is confirmed by the error triangle for the 4-day pulse at 6 cm/day (Figure 4.13, c)) because the silty clay soil is shown to have the smallest error compared to the sandy clay and sandy soil compositions.

Based on the analysis performed, the reliability of the interpolation method for capture efficiency depends on soil type, flux, and pulse duration. However, the lookup triangle dataset only covers pulse lengths in the range of 2 to 6 days with capture efficiencies of 0.5, 1.0, 1.5, and 2.0. The interpolation could be improved by producing more data to cover a larger range of capture efficiencies and pulse durations. The lookup triangle dataset was also formed at a specific depth of 38 cm below the surface. The data set would change if the depth was relocated closer to or farther from the surface under transient conditions. Capture efficiency may decrease at deeper depths because of the longer time period needed for flux to reach the PCAP. Transient simulations would require longer pulse durations to achieve the same capture efficiencies at depths deeper than 38 cm. Further investigation is needed to appropriately quantify the effects of the PCAP depth has on capture efficiency. Alternatively, site-specific models can be constructed to estimate capture efficiency for other conditions.

## 4.7 FIELD ANALYSIS

The capture efficiency of PCAPs in the model-based analyses ranged from 0.5 to 2.5 depending on the conditions simulated. This range of values can be qualitatively compared to the capture efficiencies in the Jemez River Basin CZO field site. Field measurements of interest are from six soil pits located within a 0.15 $km^2$ mixed conifer forest zero order basin (MCZOB) at the field site (Figure 4.14). Each pit has three PCAPs at various depths to collect soil water volumes. Capture efficiencies can be estimated with precipitation from the meteorological station (Papuga et al., 2016) and captured volumes from the soil pit data (Chorover et al., 2015). Snow and rain can be separated from precipitation

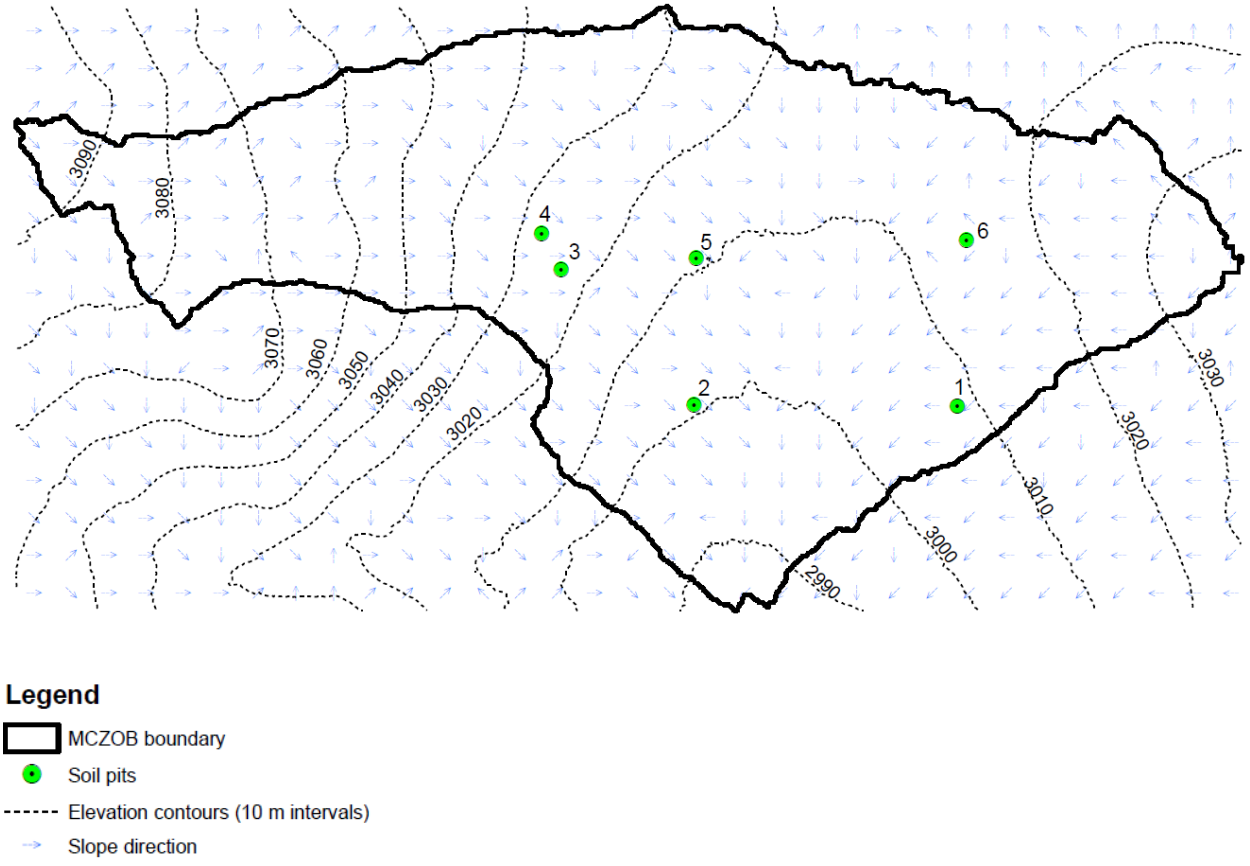


Figure 4.14. MCZOB boundary (Durcik, 2014) with soil pit locations, elevation contours (Guo et al., 2010), and slope direction vectors

using the Pipes and Quick method (1977), which is a piece-wise linear function dependent on the mean daily air temperature near ground level. Capture volumes are converted to fluxes by dividing the captured volume by the cross-sectional area of a PCAP (900 $cm^2$). The average flux across all PCAPs in the pit is used as the captured flux in the pit. The expected infiltration flux at the PCAP is the difference between precipitation and evapotranspiration. Evapotranspiration is taken from processed AmeriFlux flux data for the MCZOB (Litvak, 2016).

Consider the cumulative precipitation, evapotranspiration, and capture for soil pit 5 for the year 2012 at MCZOB (Figure 4.15). The year 2012 was selected because it has the most

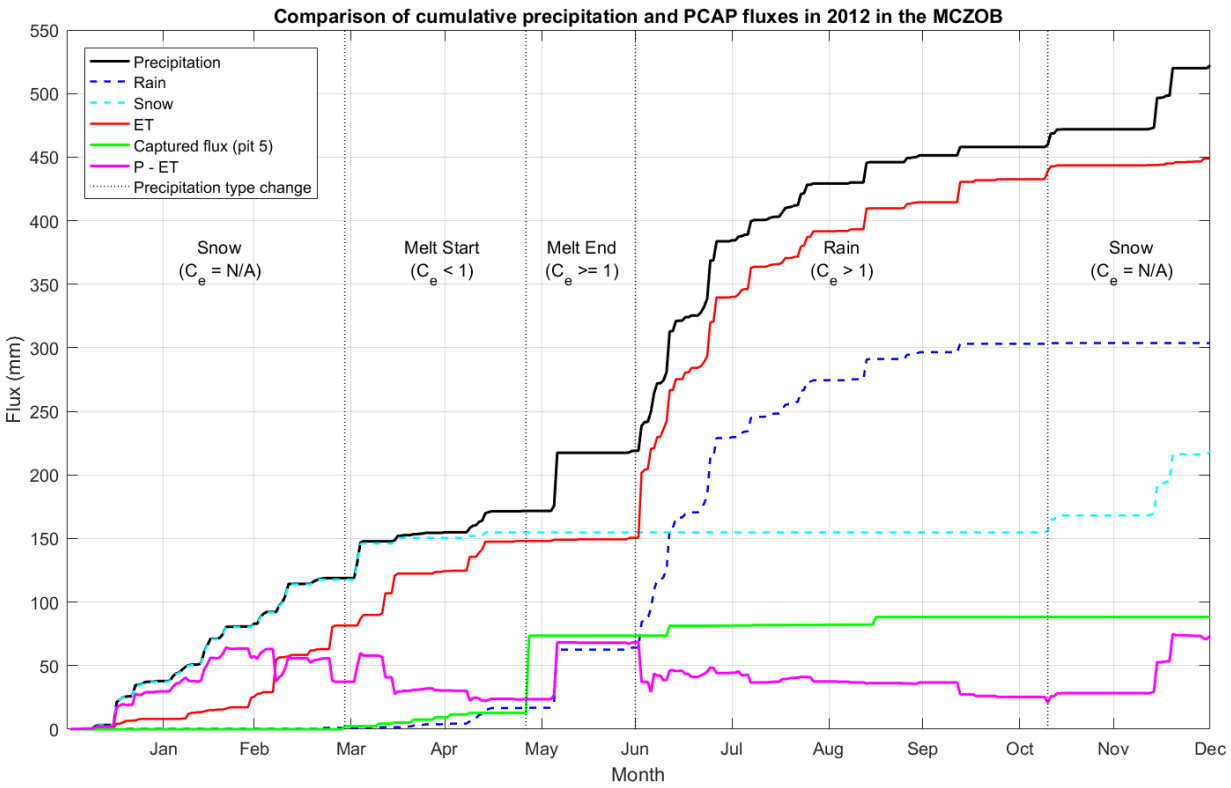


Figure 4.15. Cumulative precipitation and captured flux for the MC ZOB in 2012. Listed month represents the end of that month

complete temperature data for rain and snow separation from precipitation and pit 5 captured the most flux out of all the soil pits. The winter months of January, February, and March all have little to no capture with precipitation mainly consisting of snow. This is likely because the water is either frozen below the surface or present as snow above the surface. Capture starts when the snow begins to melt in March. Snowmelt continues such that the soil surrounding the PCAP is constantly saturated which causes a large increase in capture. The PCAP continues to capture more flux at a lower rate when precipitation switches to purely rainfall. This is likely due to the lower applied flux from rainfall compared to the snowmelt pulse.

Cumulative capture efficiency can be visualized as the ratio of cumulative capture and the expected infiltration, which is difference between precipitation and evapotranspiration fluxes (Figure 4.16). Capture efficiency in this study is an instantaneous value from singular precipitation events, so the cumulative capture efficiency cannot be used as a direct quantitative comparison. However, the cumulative capture efficiency plot does validate that the PCAP is inaccurate at different seasons throughout the year at the field site. The PCAP yields a cumulative capture efficiency less than 1 when the snow begins to melt. The snowmelt pulse causes the PCAP to overestimate flux with a cumulative capture efficiency of approximately 3. Finally, the PCAP continues to overestimate flux with cumulative capture efficiencies ranging from 1 to around 4 throughout the rest of the year when rain is the dominant form of precipitation. This is consistent with the concepts of PCAP capture under different conditions analyzed in this study; the PCAP water flux is not representative of the true flux. However, the annual cumulative capture efficiency for 2012 is only 1.18, which implies an 18% overestimation for annual cumulative capture. The PCAP is, on average, overestimating capture throughout the year (Figure 4.16).

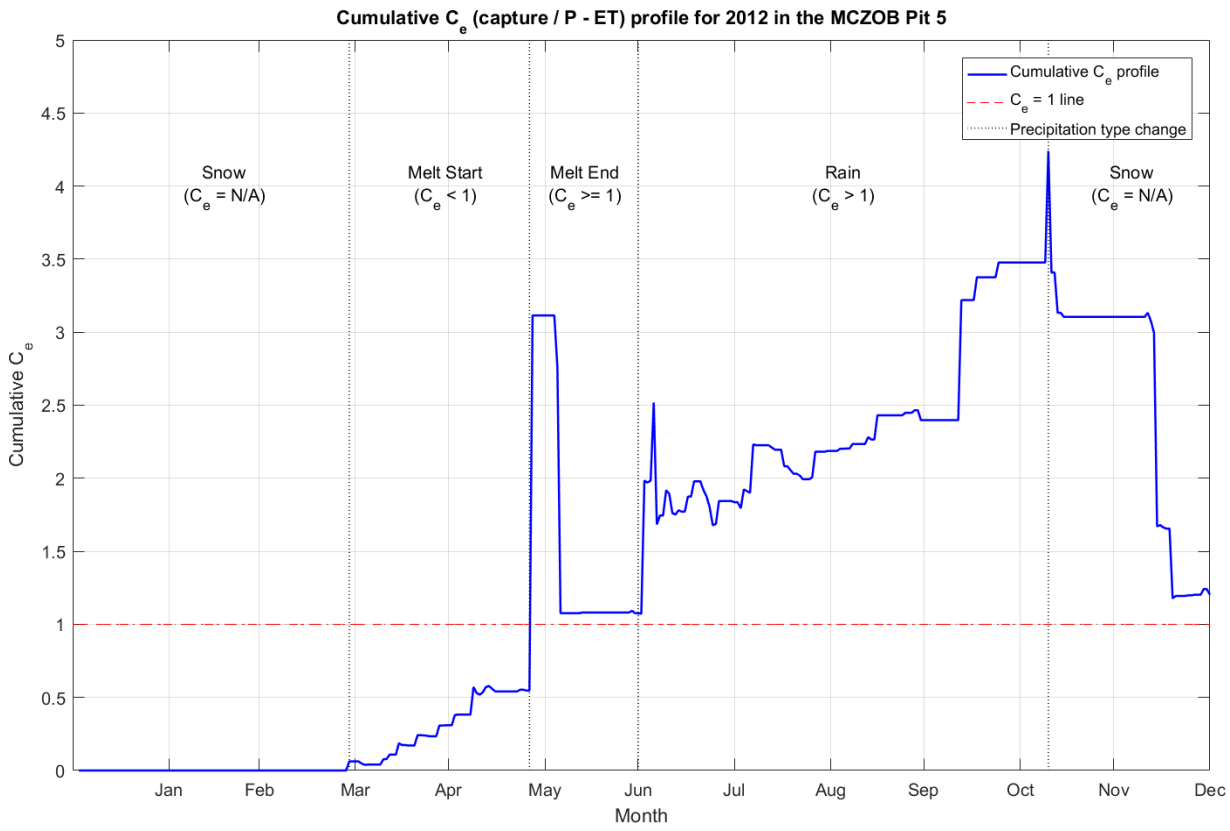


Figure 4.16. Cumulative $C_e$ profile for pit 5 in the MCZOB in 2012. Listed month represents the end of that month.

Initial field analysis of one soil pit shows that PCAP measurements are consistent with the numerical analysis performed in this study. However, the numerical analysis did not consider the effects of spatial and landscape positioning. Consider the comparison of cumulative fluxes and capture efficiencies across all six soil pits (Figure 4.17 and 4.18). The pits that captured the most flux, in descending order, are pit 5, 2, 6, 3, 1 and 4. Pits 2 and 5 are the closest to the convergent zone in the ZOB (Figure 4.14) and have the most capture. Pits 1, 3 and 4 have much smaller captured volumes because their surrounding slope vectors have a more horizontal orientation instead of an orientation towards the convergence zone of the ZOB (Figure 4.14). The higher positioning of pit 6 in the ZOB results in slightly less capture than pit 2 or 5 (Figure 4.14).

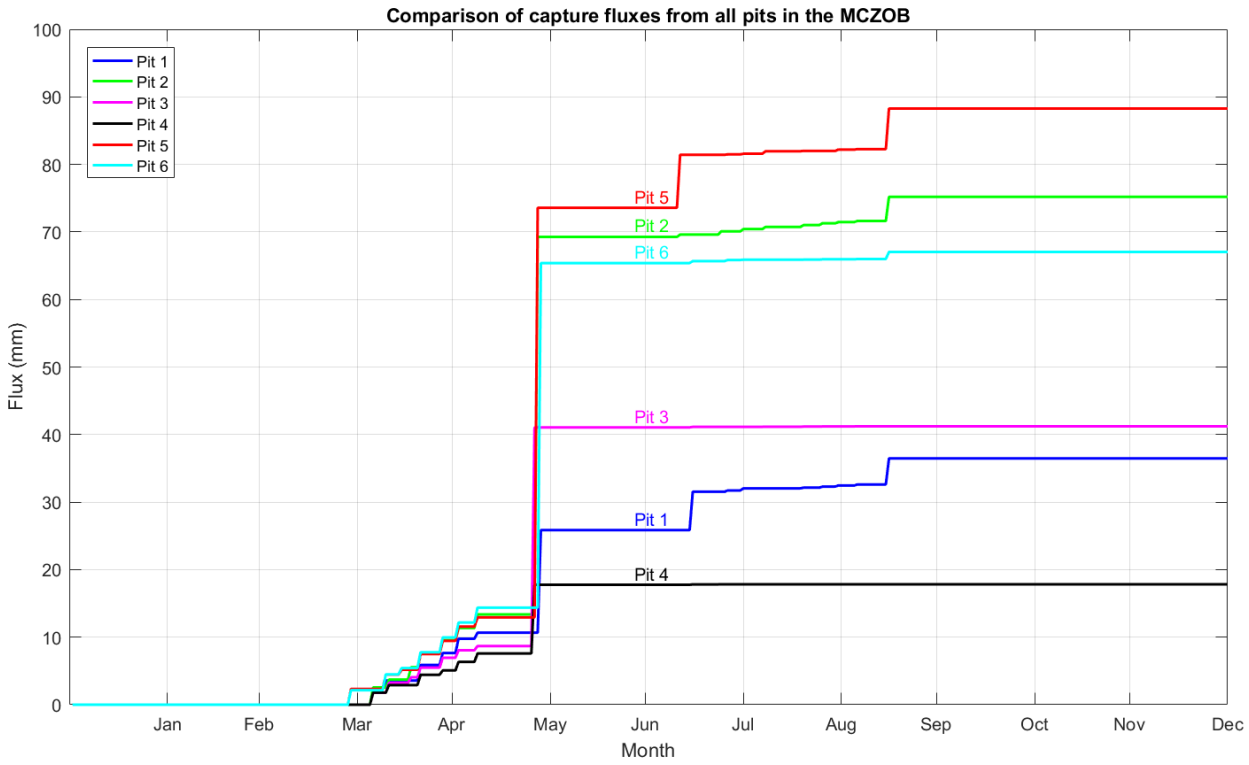


Figure 4.17. Cumulative captured flux for all soil pits in the MCZOB. Listed month represents the end of that month.

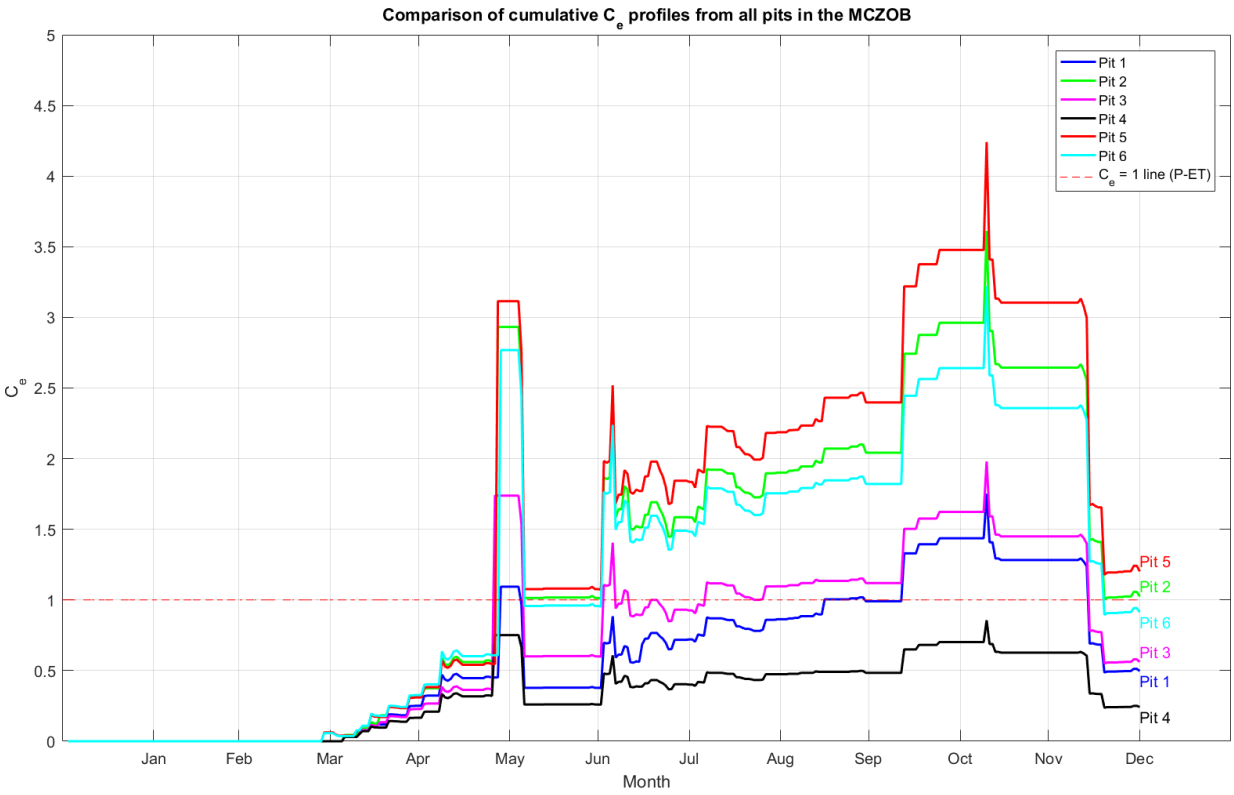


Figure 4.18. Cumulative $C_e$ profiles for all soil pits in the MCZOB. Listed month represents the end of that month.

The effects of landscape position on PCAP capture can be examined more quantitatively through the parameters of topographic wetness index (TWI) and landscape curvature. TWI is a measure of steady-state wetness and is a function of the upslope contributing area and the local slope (Beven and Kirkby, 1979). The combined landscape curvature can be computed by taking the second derivative of the surface elevation between a cell and its neighboring cells. It is the overall curvature combination of profile and plan curvature. Profile curvature is in the direction of the slope while plan curvature is orthogonal to the slope. Plan curvature determines the degree of convergence/divergence of flow across a surface (Zevenbergen and Thorne, 1987; Moore et al., 1991) and is the curvature of interest for this analysis. A positive plan curvature represents an upwardly convex shape (divergent), while a negative value represents an upwardly concave

(convergent). A previous study at the same site calculated TWI and curvatures at all the soil pits with 10 m LIDAR resolution dataset (Guo et al., 2010) to analyze hillslope effects on the redistribution of rare earth elements (Vázquez-Ortega et al., 2016).

Consider the comparison of average TWI and average plan curvature to the flux captured for each pit for 2012 at the MCZOB (Figure 4.19). TWI has a direct relationship to the plan curvature such that a higher TWI represents a more concave curvature, which should result in more convergence of flux. However, capture is not necessarily higher for more concave pits.

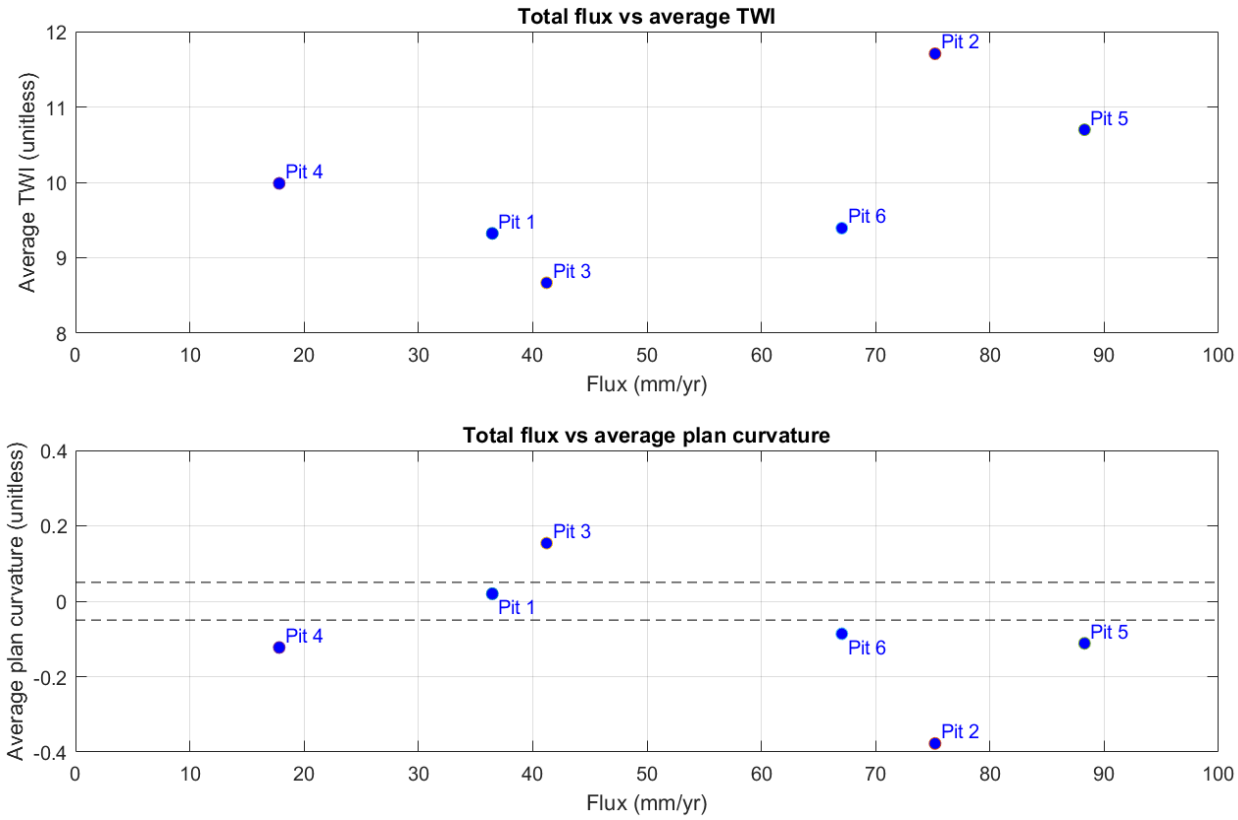


Figure 4.19. Average TWI and plan curvature compared to captured flux for each soil pit in 2012.

Pit 2 is the most concave and has the highest TWI, but pit 5 captured more water. Pit 3 is the most convex, but it still had more capture than pit 1 and pit 4 which were planar and concave,

respectively. The expected order of capture, in descending order, just from factoring TWI and plan curvature should be pit 2, 4, 5, 6, 1, 3, but this is not the case based on the data; the actual order is pit 5, 2, 6, 3, 1, 4. TWI and plan curvature are parameters that help quantify some of the local variables for capture surrounding a soil pit, but they do not account for the regional curvature that affects the general direction of flow in the MCZOB.

Field analysis in this study has only considered the average captured flux in each pit. Consider the cumulative capture profiles for each PCAP in every pit (Figure 4.20).

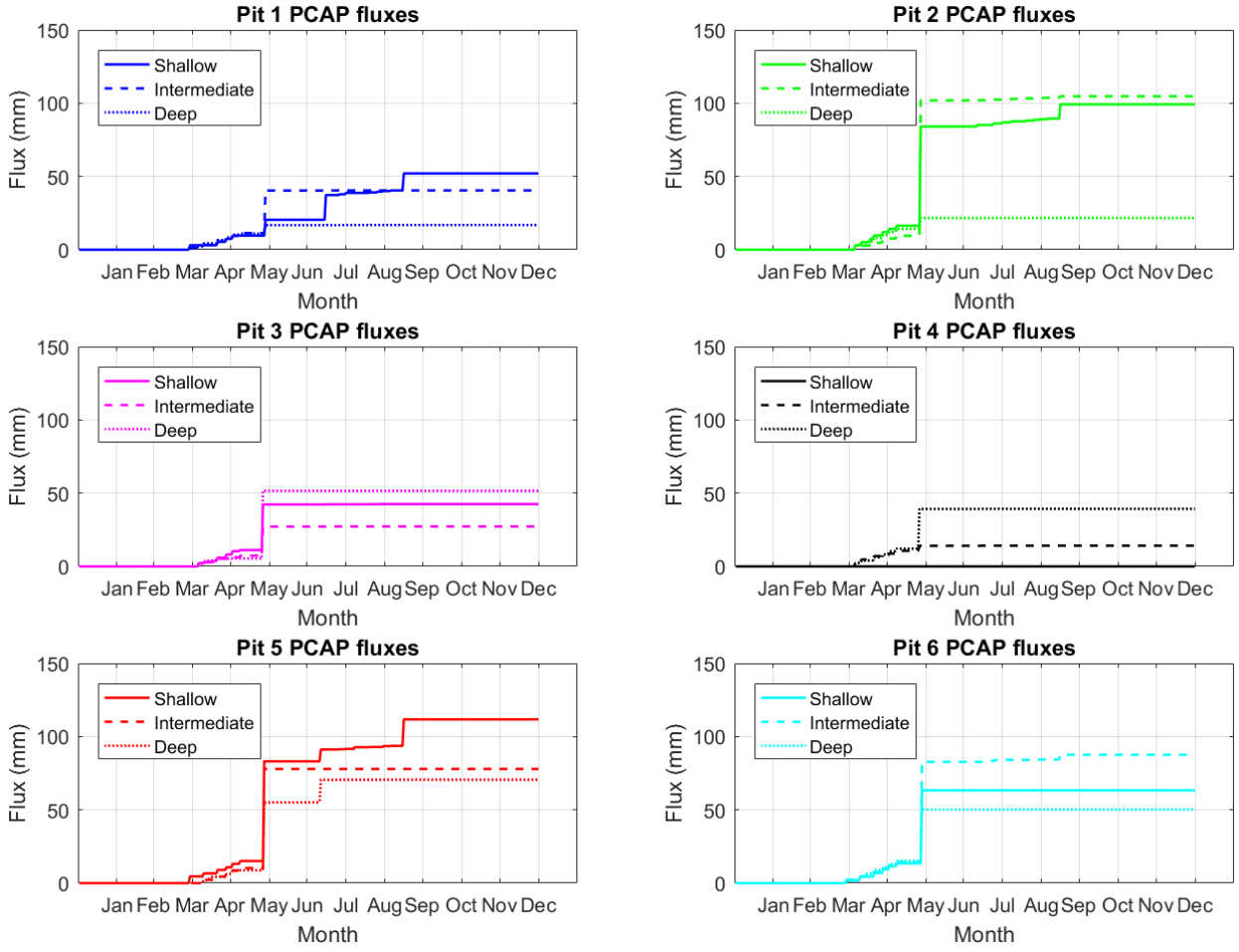


Figure 4.20. Cumulative capture profiles for all PCAPs in all soil pits placed at shallow (under 15 cm), intermediate (16 to 40 cm), and deep (over 40 cm) depths. Listed month indicates end of that month.

Each pit has PCAPs placed at shallow (under 15 cm), intermediate (16 to 40 cm), and deep (over 40 cm) depths below the surface. The deepest PCAP is the largest contributor of capture for the pits that are furthest from the convergent zone of the MCZOB (pits 3 and 4). This indicates the possibility of lateral flows in that area of the MCZOB. Pits 1 and 5 have the most capture at the shallowest PCAP. This is expected if flow happens more vertically with the shapes of pit 1 (planar) and pit 5 (concave). However, pit 2 and pit 6 are both more concave than pits 1 and 5, respectively. Pit 2 may have had a shallower water table during the end of the snowmelt process, which could be why the intermediate PCAP captured more flux. A shallower water table would slow the drainage process, extending the duration in which the soil surrounding the deeper PCAPs would be saturated. Pit 6 may have a coarse-to-fine soil texture break between the shallow and intermediate PCAPs. The intermediate PCAP would be more susceptible to convergence due to the finer soil having a lower hydraulic conductivity. Lateral flows could cause higher capture at lower depths if it occurred below shallower PCAPs. Vegetation would cause some infiltration to be pulled up due to root water uptake, which could lead to higher capture at shallow depths.

Lateral flow occurrence can be determined by looking at data from co-located water content and pressure head sensors near the PCAPs in each pit (Schaap et al., 2017). Each soil pit has three Decagon 5TE sensors installed within 10 cm from each PCAP that measure volumetric water content. Each pit also has a Decagon MPS-1 pressure head sensor installed near the shallow (under 15 cm) PCAP depths and another located in between the intermediate and deep (16 cm and over) PCAPs. The Decagon MPS-1 sensors record a voltage in millivolts (mV). The calibration equation from Decagon Devices, Inc. to convert the voltage into a pressure head reading in kilopascals (kPa) is:

$$\Psi = -e^{(0.000048 * mV^2 - 0.0846 * mV + 39.45)} \quad (4.1)$$

Pressure head readings in kPa is converted to cm of water by multiplying by 10.2. Higher pressure head and water content readings at deeper locations would infer lateral presence of lateral flow.

Consider the pressure head profiles (Figure 4.21) and the water content profiles (Figure 4.22) for the MCZOB in 2012.

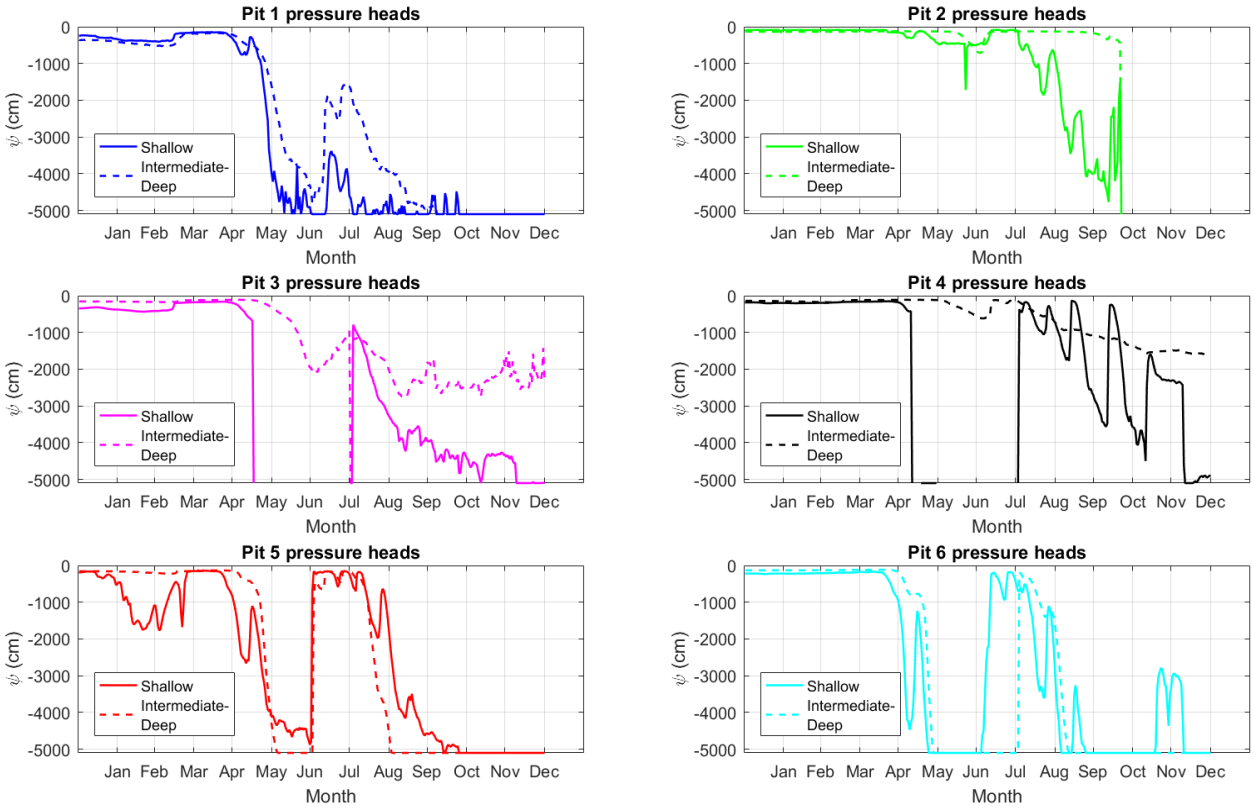


Figure 4.21. Pressure head profiles in all soil pits Decagon MPS-1 sensors placed at shallow (under 15 cm) and intermediate-deep (16 to over 40 cm) depths. Listed month indicates end of that month.

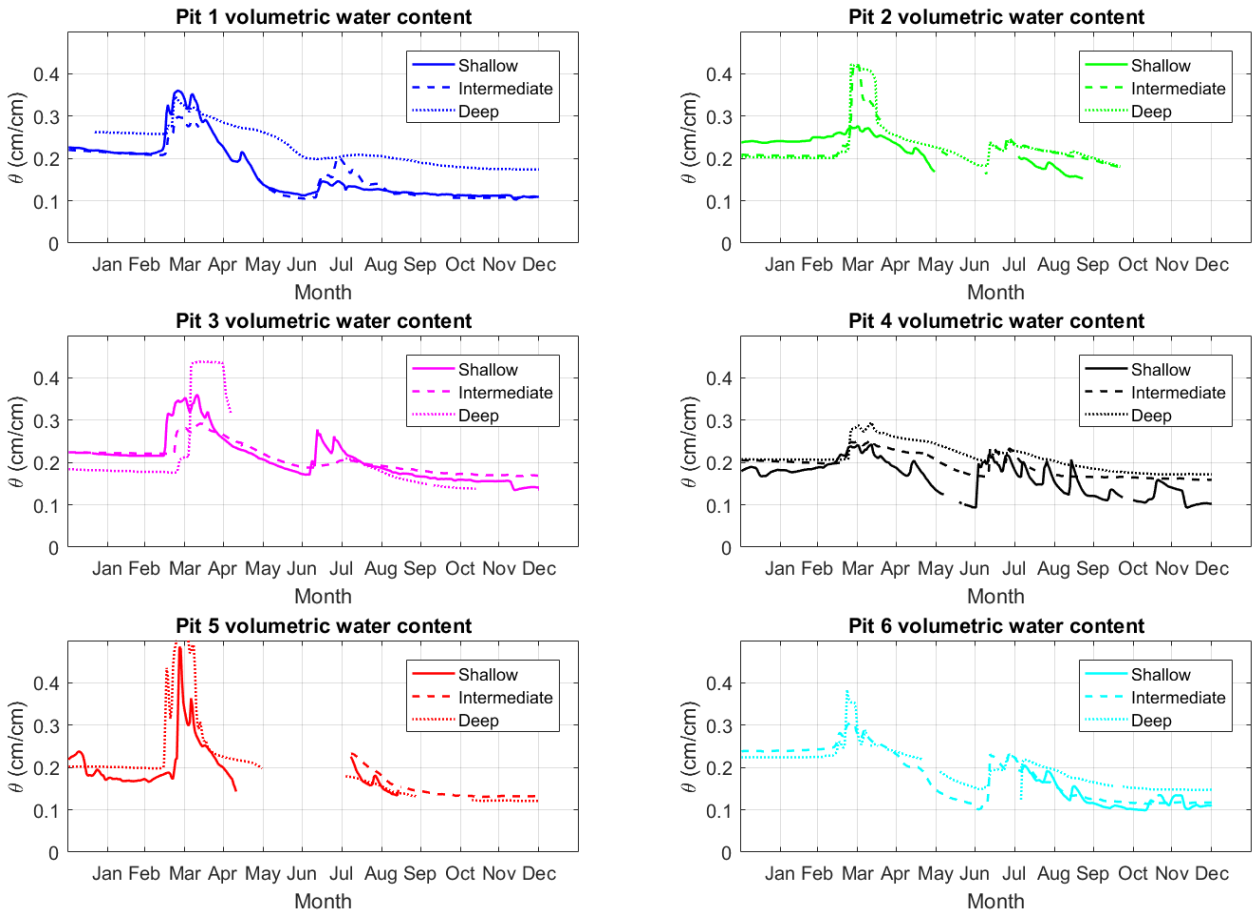


Figure 4.22. Water content profiles in all soil pits from Decagon ET5 sensors placed within 10 cm at shallow (under 15 cm), intermediate (16 to 40 cm), and deep (over 40 cm) depths. Listed month indicates end of that month. Missing data or erroneous data is not visualized.

Pits 3 and 4 have the largest pressure heads and water contents located at the deeper sensors, inferring the presence of lateral flow (Figures 4.21 and 4.22). This corresponds to pits 3 and 4 having the most capture at the deepest PCAP. Pits 2 and 6 experienced lateral flow because the intermediate PCAP captured the most flux, which is reflected in the intermediate water content and pressure head sensors yielding the largest values (Figures 4.21 and 4.22). The shallowest PCAP in pits 1 and 5 captured the most flux, while the shallowest pressure head sensors generally recorded the largest readings (Figure 4.21). However, water content sensors for pits 1

and 5 show the deepest water content sensors as having the largest values. The soil composition for pits 1 and 5 may have a higher hydraulic conductivity at their corresponding water contents at the shallow depths compared to the deeper sensors. Pits 1 and 5 also have higher overall pressure head throughout the year at the intermediate-deep sensors. The patterns we see in both the pressure head and the water content sensors remain consistent with those of the cumulative capture profiles for each PCAP.

The magnitudes reported by the Decagon MPS-1 pressure head sensors are inconsistent with the pressure head ranges focused on this study. This is because the inherent range of the sensors are only from -10 kPa to -500 kPa (-102 cm of water to -5100 cm of water), which are much drier conditions. Ideally pressure head sensors would be co-located at the same depth as each PCAP and pressure heads measured to be greater or less than the -30 cm of pressure head at the plate would infer lateral flow into or away, respectively, from the PCAP. The current magnitudes imply that the PCAP is constantly rejecting flow because the maximum possible pressure head recording of -102 cm is much smaller than the assumed -30 cm of pressure at the plate. In this study, the magnitudes of the pressure head measurements can't be appropriately used, but the overall patterns of the readings relative to each sensor at depth are consistent for each pit.

# 5 DISCUSSION

PCAPs are used at the field site to measure water flux. The issues with PCAP capture complicate the representability of the measured flux. Water flux in the vadose zone is directly affected because of convergence or divergence. Consider PCAP capture for a loam soil

undergoing a precipitation profile consisting of a two flux pulses of the same duration, but with different magnitudes such that the first pulse is larger than the second (Figure 5.1). The behavior of flow particles can be visualized with snapshots in time for each day (Figure 5.2). The flow particles proceed towards the PCAP during the first 2-day pulse and the next 2 days of drainage

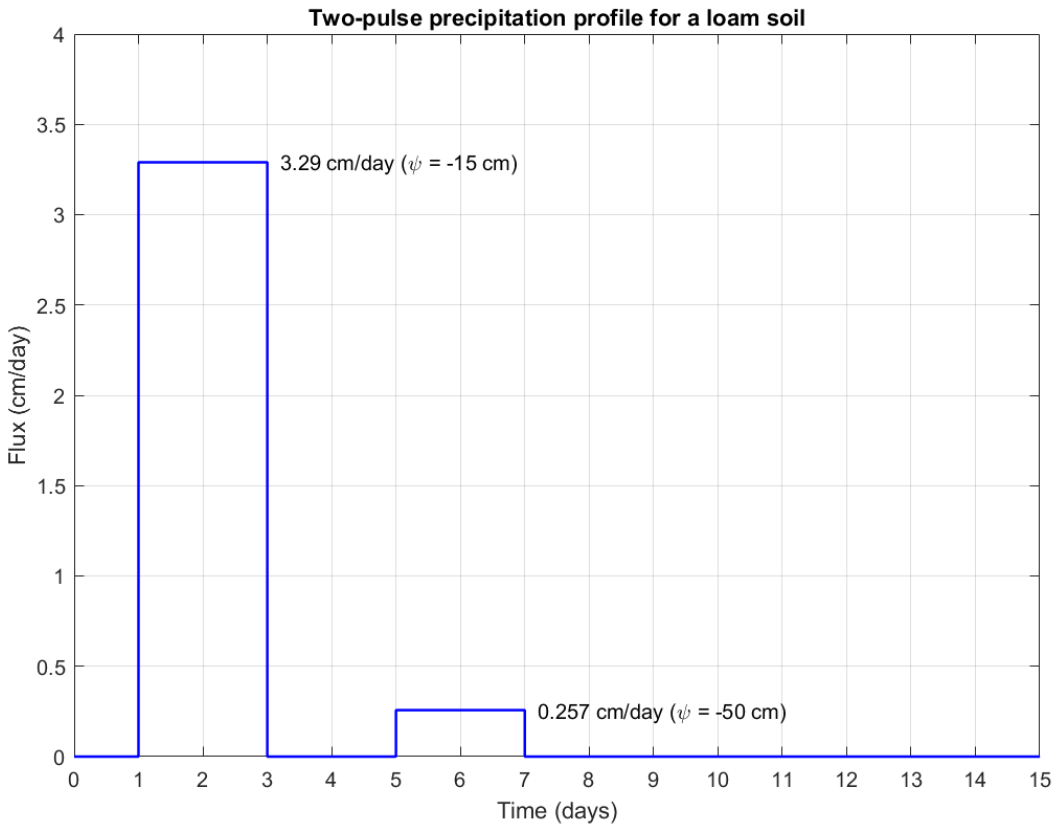


Figure 5.1. A precipitation profile for a loam soil consisting of 1 day of hydrostatic, followed by 2 days at a rate of 3.29 cm/day (ψ = -15 cm), then 2 days of drainage, followed by a 2-day pulse at a rate of 0.257 cm/day (ψ = -50 cm), and then 8 days of drainage.

as shown in the snapshots for days 1 through 5 in Figure 5.2. The pressure head profile from the first pulse is large enough to produce a gradient towards the PCAP to drive the flow particles downward. However, the remaining particles are progressively rejected once the seconds pulse is

introduced on day 5. This is due to the smaller pressure head profile introduced by the weaker pulse as shown in the snapshots for days 6 through 15 in Figure 5.2. The remaining flow particles would have drained into the PCAP if the weaker second pulse was not introduced. This shows that the initial conditions resulting from one precipitation event also affects what fluxes are captured in the next precipitation event. The degree of how much the initial conditions affect capture has not been explored in this study, but this example does show the added uncertainty with respect to the representability of the captured flux.

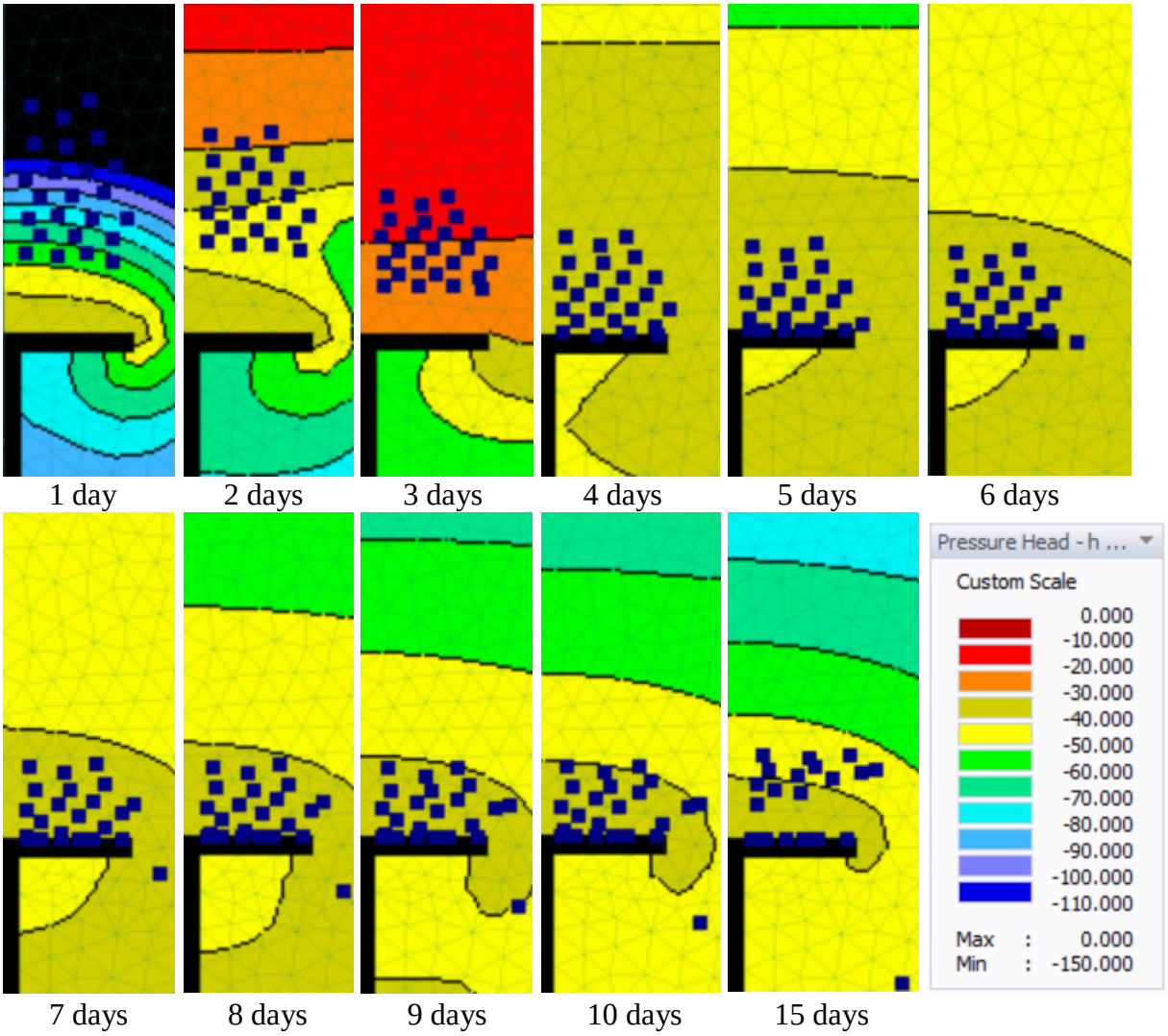


Figure 5.2. HYDRUS (2D/3D) particle and pressure head results of PCAP capture for a loam soil undergoing a two-pulse precipitation profile represented by Figure 5.1.

Using PCAP data from the field site for flux measurements would be difficult due to uncertainty from various conditions. Numerical analysis has shown that different soil type and flux conditions affects the accuracy of PCAPs because of convergence or divergence. Analysis of field measurements imply that landscape positioning on the local and regional scale influences the amount of infiltration in the soil pit. PCAPs closer to the convergent zone in the middle of the MCZOB generally captured more flux. Soil pits with convergent landscape parameters (concave curvatures and high TWI values) should have captured the most flux. However, this isn't always true because some pits with more divergent landscape parameters captured more flux. This behavior is shown in some pits that had more capture at deeper PCAPs than the shallower PCAPs in the same pit. Factors that may result in more capture at deeper PCAPs include shallow water tables from snowmelt, texture breaks in the soil medium, capillary rise, lateral flows, or loss from root water uptake. Deeper PCAPs may spend more time under saturated conditions from snowmelt, which will result in more convergence. A soil texture break from coarser to finer textures between two PCAPs would also increase convergence at the deeper PCAP. This is due to the less pronounced effects of gravity on water flow on finer textures. For example, Clay is a low hydraulic conductivity boundary that requires more water pressure to force water through it. If a clay layer exists just below the PCAP plate, pressure will build up close to the PCAP plate, which could result in convergence towards the plate. Water below the PCAPs could also be affected by capillary rise depending on the soil texture distribution in the pit. Lateral flows may pass below shallower PCAPs, but may be captured by deeper PCAPs. Soil pits located near vegetation could also gain water from plant roots. Preferential flow paths from geology, fractures, or roots disrupt infiltration of water from the surface. This was not considered in the study because of the added complexity that would require three-dimensional numerical

model. Under wet conditions such as snowmelt, preferential flow wouldn't affect capture as much because the PCAP would be undergoing convergence. However, preferential flow could carry infiltrating water away from the PCAP under drier conditions. Most PCAP capture in the MCZOB occurs in wet conditions during snowmelt so preferential flow is usually not a large factor in capture.

The numerical and field analysis performed in this study allows for a better understanding of PCAP capture under different flux conditions and landscape positioning, but there are still other variables that have not been accounted for. For the PCAP model, a maximum hydraulic conductivity was not assigned at the plate, which means that water was allowed to pass through indefinitely. The model ran simulations under steady-state conditions for extended periods, so the amount of water captured may be higher than it should be. In reality, the plate pulls in water at the hydraulic conductivity of the wicks, which is already very high. The carboy also has a limited volume and shouldn't take in more water if full. However, these problems do not detract from the analysis because the model is primarily meant to estimate capture efficiency and identify what conditions give rise to convergence and divergence. A more specialized three-dimensional HYDRUS model would be needed to accurately represent the environment in which a PCAP is in. Site-specific models of PCAPs can be developed if vegetation, soil distribution, landscape parameters, evapotranspiration, and snowmelt are accounted for.

Variables not addressed in the field analysis include the landscape distribution of vegetation, uniformity of precipitation and evapotranspiration, soil distribution surrounding the pits, lateral flow, regional curvature and TWI distribution in the MCZOB, and field measurement error. Geospatial data of vegetation distribution and average root depth would help to understand why certain pits capture more water at deeper PCAPs. This would also help determine potential

evapotranspiration sources in the vicinity of the soil pits. This study currently assumes a uniform distribution of precipitation and evapotranspiration, which is not necessarily true depending on the vegetation cover. However, it is difficult to come up with an area-weighted distribution of precipitation or evapotranspiration without additional instrumentation at the field site. Soil profile characterization of each pit would help determine depths prone to convergence and lateral flow from texture breaks. A map of curvature and TWI distribution throughout the MCZOB with the slope vectors would help identify convergent and divergent zones. Field instrumentation error may also be factor when interpreting results. For example, pit 4 in the MCZOB did not have any capture in the shallowest PCAP despite its convergent landscape parameters (Figure 4.20). The shallowest PCAP was usually a large contributor of capture for all soil pits. The lack of capture at pit 4 may indicate collection issues during sampling, which would explain some of the unexpected results in the field analysis among the pits (Figure 4.19).

# 6 CONCLUSION

PCAPs provide a convenient, non-destructive, and reasonable method to measure total infiltration at a given depth. Fiberglass wicks form a hanging water column that acts as a constant negative pressure head boundary condition at the plate of the PCAP. Tension at the plate is equal to the length of the hanging water column. This boundary condition influences flow through the medium in which the PCAP is placed because of convergence or divergence. Numerical analysis was performed to understand what conditions lead to inaccuracies and to see if capture efficiencies can be estimated. Field measurement data were then interpreted using behavioral knowledge of PCAPs from the simulations. Additional field data related to PCAP placement and landscape positioning was also examined to see how capture is affected by factors not addressed by the numerical analysis.

A simple HYDRUS (2D/3D) model was used to simulate water flow through the vadose zone with and without a PCAP present. Capture efficiencies are used as the primary metric for comparisons and were calculated as a ratio between the flux through the PCAP plate and flux through the same observation point without a PCAP. Various boundary conditions were simulated to represent short-term intense rainfall events, long duration steady-state conditions, and time-varying infiltration across different homogeneous soil types. The PCAP under/oversamples water flowing at a rate lower/higher than the hydraulic conductivity of the medium at a pressure head equal to the pressure applied to the plate. This means that water will diverge from the PCAP without being captured at low flow rates. At higher infiltration, the flow rate into the PCAP converges at a rate higher than the rate past the same depth had there been no PCAP or at some distance from the PCAP. The applied flux needed to yield specific capture efficiencies for a given range of soil types and flux profiles can be iteratively determined. This can be performed many times to produce a known dataset of flux rates with corresponding capture efficiencies, flux durations, and soil types specific to the modeled PCAP. Capture efficiencies can then be interpolated for the modeled PCAP. Site-specific models of PCAPs can be developed if parameters such as vegetation, landscape positioning, evapotranspiration, and snowmelt are accounted for within the model.

Numerical analysis suggests that PCAP capture may have seasonal biases that could lead to undersampling from shorter duration, high intensity rain events and long duration, low intensity precipitation events or oversampling from longer duration high intensity infiltration from snowmelt. This is reflected by the consistent sudden spike of capture during snowmelt from analyzing the cumulative precipitation profiles of the PCAPs at all the soil pits in the MCZOB. Post snowmelt, the amount of capture largely decreases during the smaller infiltration events the

rest of the year. With the assumption that the expected infiltration is only 10% of the precipitation, the PCAPs seem overestimate capture for most of the year. The amount of capture also varies throughout all the pits. Pits located closer to the convergent zone of the MCZOB generally had more capture. However, some this is not true for all the pits, suggesting additional influence from landscape positioning. Pits with more convergent landscape positioning (high TWI and concave curvatures) should yield the most capture, but the data suggests that this isn't necessarily true, indicating additional factors not accounted for in the analysis.

Capture at every pit for each PCAP at shallow, intermediate, and deep depths were examined individually to see which depths had the most capture. It is expected for the shallowest PCAP to capture the most flux because they would most easily capture infiltration from weaker precipitation events. Infiltration from low flux rates are unlikely to reach deeper PCAPs due to lower pressure build up. However, two pits yielded the most capture at the shallowest PCAP, two at the intermediate PCAP, and two at the deepest PCAP. This suggests the presence of other mechanisms that affect capture that have not been accounted for, which is confirmed by the pressure head and water content sensors co-located near the PCAPs. Other variables that could contribute to this behavior are shallow water tables from snowmelt, soil texture breaks that affect convergence/divergence, capture loss from root water uptake or evapotranspiration sources, lateral flows, preferential flows, and field instrumentation error. On an annual average, PCAPs in the MCZOB overestimate flux.

PCAP capture biases shown by both numerical and field analysis impart errors in measurements of infiltrating water. Further uncertainty is added when considering the number of additional factors not addressed in this study. Site-specific models of PCAPs can be developed to help understand potential site-specific behavior and to optimize PCAP placement. PCAPs still

provide a reasonable and more convenient approach to measure water flux in the vadose zone compared to other methods, but interpretations of PCAP measurements must be evaluated carefully before constructing further hypotheses.

**REFERENCES**


Beven, K.J., Kirkby, M.J., 1979. A physically based, variable contributing area model of basin hydrology. Hydrological Science Bulletin. 24, 43-69.

Boll, J., Steenhuis, T.S., Selker, J.S., 1992. Fiberglass wicks for sampling of water and solutes in the vadose zone. SOIL SCIENCE SOCIETY OF AMERICA JOURNAL, VOL. 56, NO. 3.

Brahy, V., Henao-Toro, M-C., Goor, F., Ledent, J-F., Delvaux, B., 2002. Assessing passive capillary-wick samplers for monitoring resident nitrate concentration in real field. SOIL USE AND MANAGEMENT, VOL. 18, NO. 1.

Brandi-Dohrn, F.M., Dick, R.P., Hess, M., Selker, M., 1996. Field evaluation of passive capillary samplers. SOIL SCIENCE SOCIETY OF AMERICA JOURNAL, VOL. 60, NO. 6.

Chorover, J., Perdrial, J., McIntosh, J., Troch, P., Amistadi, M.K., Losleben, M., Condon, K., Pedron, S.A., 2015. CZO Dataset: Jemez River Basin – Soil Chemistry (2011-2015)." Retrieved 09 Jun 2017, from http://criticalzone.org/catalina-jemez/data/dataset/4109/

Davis, R.O.E., Bennet, H.H., 1927. Grouping of soils on the basis of mechanical analysis. UNITED STATES DEPARTMENT OF AGRICULTURE DEPARTMENTAL, CIRCULATION NO. 419

Durcik, M., 2014. CZO Dataset: Catalina-Jemez – GIS/Map Data (2010-2014). Retrieved 09 Jun 2017, from http://criticalzone.org/catalina-jemez/data/dataset/3896

England, C.B., Comment on "A technique using porous cups for water sampling at any depth in the unsaturated zone" by Warren W. Wood. WATER RESOURCES RESEARCH, VOL. 10, NO. 5.

Freeze, R.A., Cherry, J.A., 1979. Groundwater. Prentice Hall, Englewood Cliffs NJ.

Gee, G.W., Ward, A.L., Caldwell, T.G., Ritter, J.C., 2002. A vadose zone water fluxmeter with divergence control. WATER RESOURCES RESEARCH, VOL. 38, NO. 8.

Gee, G.W., Zhang, Z.F., Ward, A.L., Keller, J.M., 2004. Passive-wick water fluxmeters: theory and practice. In SuperSoil 2004: Australian New Zealand Soils Conference, 3rd, Sydney, Australia. 5–9 Dec. 2004 [CD-ROM]. Univ. of Sydney, Australia.

Guo, Q., Pelleter, J., Parmenter, R., Allen, C., Judy, B., Durcik, M., 2010. CZO Dataset: Jemez River Basin – LiDAR (2010) – Snow-off. Retrieved 09 Jun2017, from http://criticalzone.org/catalina-jemez/data/dataset/2613

Holder, M., Brown, K.W., Thomas, J.C., Zabcik, D., Murry, H.E., 1991. Capillary wick unsaturated zone soil pore water sampler. SOIL SCIENCE SOCIETY OF AMERICA JOURNAL, VOL. 55, NO.5.

Hursh, C.R., Brater, E.F., 1941. Separating storm-hydrographs from small drainage-areas into surface- and subsurface-flow. TRANSACTIONS, AMERICAN GEOPHYSICAL UNION, VOL. 22.

Jabro, J.D., Kim, Y., Evans, R.G., Iversen, W.M., Stevens, W.B., 2008. Passive capillary sampler for measuring soil water drainage and flux in the vadose zone: design, performance, and enhancement. APPLIED ENGINEERING IN AGRICULTURE, VOL. 24, NO. 4.

Knutson, J.H., Selker, J.S., 1996. Fiberglass wick sampler effects on measurements of solute transport in the vadose zone. SOIL SCIENCE OF AMERICA JOURNAYL, VOL. 60, NO. 2.

Lee, D.T., Schachter, B.J., 1980. Two algorithms for constructing a Delaunay triangulation. INTERNATIONAL JOURNAL OF COMPUTER AND INFORMATION SCIENCES, VOL 9, NO. 3.

Litvak, M., 2016. AmeriFlux US-Vcm Valles Caldera Mixed Conifer. Web. DOI: 10.17190/AMF/1246121.

Louie, M.J., Shelby, P.M., Smesrud, J.S., Gatchell, L.O., Selker, J.S., 2000. Field evaluation of passive capillary samplers for estimating groundwater recharge. WATER RESOURCES RESEARCH, VOL. 36, NO 9.

Masarik, K.C., Norman, J.M., Brye, K.R., Baker, J.M., 2004. Improvements to measuring water flux in the vadose zone. JOURNAL OF ENVIORNMENTAL QUALITY, VOL. 33.

MATLAB Release R2016a. The MathWorks, Inc., Natick, Massachusetts, United States.

Mertens, J., Diels, J., Vanderborght, J., Feyen, J., 2007. Numerical analysis of passive capillary wick samplers prior to field installation. SOIL SCIENCE SOCIETY OF AMERICA JOURNAL, VOL. 71, NO. 1.

Moore, I.D., Grayson, R.B., Ladson, A.R., 1991. Digital terrain modeling: a review of hydrological, geomorphological, and biological applications. Hydrological Processes. 5, 3-30.

Mualem, Y., 1976. New model for predicting hydraulic conductivity of unsaturated porous media. WATER RESOURCES RESEARCH, VOL. 12, NO. 3.

Nandagiri, L., Prasad, R., 1996. Field evaluation of unsaturated hydraulic conductivity models and parameter estimation from retention data. JOURNAL OF HYDROLOGY, VOL. 179, NO. 1.

Papuga, S., Compton, S., Nelson, K., Losleben, M., Swetish, J., Minor, R., Wilcox, D., Harders, S., 2016. CZO Dataset: Jemez 2013 Burned ZOB – Meteorology (2010-2016) – South-East Site. Retrieved 09 Jun 2017, from http://criticalzone.org/catalina-jemez/data/dataset/2475/

Pipes, A., Quick, M.C., 1997. UBC Watershed Model Users Guide. Department of Civil Engineering, University of British Columbia. Vancouver, British Columbia, Canada.

Poletika, N.N., Ruth, K., Jury, W.A., 1992. Interpretation of solute transport data obtain with fiberglass wick solution samplers. SOIL SCIENCE SOCIETY OF AMERICA JOURNAL, VOL. 56, NO. 6.

Rimmer, A., Steenhuis, T.S., Selker, J.S., 1995. One-dimensional model to evaluate the performance of wick samplers in soils. SOIL SCIENCE SOCIETY OF AMERICA JOURNAL, VOL. 59, NO. 1.

Schaap, M.G., Leij, F.J., van Genuchten, M.T., 2001. ROSETTA: a computer program for estimating soil hydraulic parameters with hierarchical pedotransfer functions. JOURNAL OF HYDROLOGY, VOL. 251.

Schaap, M.G., Condon, K., Durcik, M., Losleben, M., 2017. CZO Dataset: Jemez 2013 Burned ZOB – Soil Moisture, Soil Temperature, Electrical Conductivity, Water Potential (2010 – 2017). Retrieved 17 Oct 2017, from http://criticalzone.org/catalina-jemez/data/dataset/3739/

Simunek, J., Sejna, M., Saito, H., Sakai, M., van Genuchten, M.T., 2009. The HYDRUS-1D software package for simulating the movement of water, heat, and multiple solutes in variably-saturated media, version 4.09. HYDRUS software series 3, Department of Environmental Sciences, University of California Riverside, Riverside, California, United States.

Simunek, J., van Genuchten, M.T., Sejna, M., 2012. The HYDRUS software package for simulating the two- and three-dimensional movement of water, heat, and multiple solutes in variably-saturated media, technical manual, version 2.00. PC Progress, Prague, Czech Republic.

Twarakavi, N.K.C., Simunek, J., Schaap, M.G., 2010. Can texture-based classification optimally classify soils with respect to soil hydraulics? WATER RESOURCES RESEARCH, VOL. 46, NO. 1.

van Genuchten, M.T., 1980. A closed-form equation for predicting the hydraulic conductivity of unsaturated soils. SOIL SCIENCE SOCIETY OF AMERICA JOURNAL, VOL. 44, NO. 5.

Vázquez-Ortega, A., Huckle, D., Perdrial, J., Amistadi, M. K., Durcik, M., Rasmussen, C., McIntosh, J., Chorover, J. (2016). Solid-phase redistribution of rare earth elements in hillslope pedons subjected to different hydrologic fluxes. Chemical Geology, 426, 1-18.

Zevenbergen, L.W., Thorne, C.R., 1987. Quantitative analysis of land surface topography. Earth Surface Processes and Landforms. 12, 47-56.

Zhu, Y., Fox, R.H., Toth, J.D., 2002. Leachate collection efficiency of zero-tension pan and passive capillary fiberglass wick lysimeters. SOIL SCIENCE SOCIETY OF AMERICA JOURNAL, VOL.66.